A COMPARATIVE ANALYSIS OF MATCHED FIELD PROCESSORS FOR UNDERWATER ACOUSTIC SOURCE LOCALIZATION

A THESIS SUBMITTED TO
THE GRADUATE SCHOOL OF NATURAL AND APPLIED SCIENCES
OF
MIDDLE EAST TECHNICAL UNIVERSITY

BY

TEVFİK BAHADIR SARIKAYA

IN PARTIAL FULFILLMENT OF THE REQUIREMENTS
FOR
THE DEGREE OF MASTER OF SCIENCE
IN
ELECTRICAL AND ELECTRONICS ENGINEERING

SEPTEMBER 2010

Approval of the thesis:

A COMPARATIVE ANALYSIS OF MATCHED FIELD PROCESSORS FOR UNDERWATER ACOUSTIC SOURCE LOCALIZATION

submitted by **TEVFİK BAHADIR SARIKAYA** in partial fulfillment of the requirements for the degree of
Master of Science in Electrical and Electronics Engineering Department, Middle East Technical University by,

Prof. Dr. Canan Özgen
Dean, Graduate School of **Natural and Applied Sciences** _____

Prof. Dr. İsmet Erkmen
Head of Department, **Electrical and Electronics Engineering** _____

Assoc. Prof. Dr. Tolga Çiloğlu
Supervisor, **Electrical and Electronics Engineering Department, METU** _____

Examining Committee Members:

Prof. Dr. Mustafa Kuzuoğlu
Electrical and Electronics Engineering, METU _____

Assoc. Prof. Dr. Tolga Çiloğlu
Electrical and Electronics Engineering, METU _____

Prof. Dr. Mübeccel Demirekler
Electrical and Electronics Engineering, METU _____

Assoc. Prof. Dr. Çağatay Candan
Electrical and Electronics Engineering, METU _____

Serkan Özgün, M.Sc.
Manager, Sonar Systems Department, ASELSAN _____

Date: _____

I hereby declare that all information in this document has been obtained and presented in accordance with academic rules and ethical conduct. I also declare that, as required by these rules and conduct, I have fully cited and referenced all material and results that are not original to this work.

Name, Last Name: TEVFİK BAHADIR SARIKAYA

Signature :

ABSTRACT

A COMPARATIVE ANALYSIS OF MATCHED FIELD PROCESSORS FOR UNDERWATER ACOUSTIC SOURCE LOCALIZATION

Sarıkaya, Tevfik Bahadır

M.S., Department of Electrical and Electronics Engineering

Supervisor : Assoc. Prof. Dr. Tolga Çiloğlu

September 2010, 86 pages

In this thesis, localization of the underwater sound sources using matched field processing technique is considered. Localization of the underwater sound sources is one of the most important problems encountered in underwater acoustics and signal processing. Many techniques were developed to localize sources in range, depth and bearing angle. However, most of these techniques do not consider or only slightly takes into account the environmental factors that dramatically effect the propagation of underwater sound. Matched field processing has been developed as a technique that fully considers the environmental factors. Matched field processing has proven to be successful in many applications such as localization of sources in range and depth, the determination of environmental parameters, and the evaluation of model accuracies. In this study, first a comparative analysis of narrowband matched field processors is given. Namely four main processors: Bartlett processor, Minimum Variance Distortionless Response (MVDR) processor, MVDR with neighboring location constraints and MVDR with environmental perturbation constraints are compared in terms of their probability of correct localization under certain environmental conditions. Sec-

ondly, a performance assesment for the most common broadband matched field processors is made. The correct localization performances for incoherent broadband matched field processor, Tolstoy/Michalopoulo's coherent matched field processor and broadband matched field processor with environmental perturbation constraints is given for certain environmental conditions. Finally, a new weighting approach to combine data for broadband matched field processing is introduced. The fact that information from different frequencies may have different reliability depending on the environmental conditions is considered to develop a weighting scheme. It is shown that a performance gain compared to existing processors can be achieved by using the weighting scheme introduced in this study.

Keywords: Localization of Underwater Sources, Narrowband Matched Field Processing, Broadband Matched Field Processing.

ÖZ

SUALTI AKUSTİK KAYNAK KONUMLANDIRMASI İÇİN EŞLENEN ALAN İŞLEYİCİLERİN KARŞILAŞTIRMALI ANALİZİ

Sarıkaya, Tevfik Bahadır
Yüksek Lisans, Elektrik ve Elektronik Mühendisliği Bölümü
Tez Yöneticisi : Doç. Dr. Tolga Çiloğlu

Eylül 2010, 86 sayfa

Bu tezde, sualtı ses kaynaklarının eşlenen alan işleme tekniği ile konumlandırılması ele alınmıştır. Sualtı ses kaynaklarının konumlandırılması problemi sualtı akustiği ve sinyal işlemede karşılaşılan en önemli problemlerden biridir. Kaynakları mesafe, derinlik ve kerteriz açısı olarak konumlandırmak için birçok teknik geliştirilmiştir. Ne var ki, bu tekniklerin birçoğu sualtında sesin yayılımını önemli bir şekilde etkileyen çevresel faktörleri dikkate almamakta ya da çok az dikkate almaktadır. Çevresel faktörleri tamamen dikkate alan bir tekniğin geliştirilmesi ihtiyacı sonunda eşlenen alan işleme tekniği geliştirilmiştir. Eşlenen alan işleme tekniği kaynakların mesafe ve derinlik olarak bulunması, çevresel parametrelerin tespit edilmesi ve modellerin doğruluğunun değerlendirilmesi gibi uygulamalarda oldukça başarılı olmuştur. Bu çalışmada, öncelikle darbant eşlenen alan işleyicilerin karşılaştırmalı analizi verilmiştir. Dört ana işleyici: Bartlett işleyicisi, MVDR işleyicisi, komşu kısıtlı MVDR işleyicisi ve çevresel bozulma kısıtlı MVDR işleyicisi doğru konumlandırma olasılığı açısından belli çevresel koşullar altında karşılaştırılmıştır. İkinci olarak, en çok kullanılan genişbant işleyicilerin performans değerlendirmesi yapılmıştır. Eşevresiz genişbant eşlenen alan

işleyici, Tolstoy/Michalopoulo'nun eşevreli işleyicisi ve çevresel bozulma kısıtlı eşevreli genişbant eşlenen alan işleyicinin belli çevresel koşullar altında doğru konumlandırma olasılıkları verilmiştir. Son olarak, genişbant eşlenen alan işleyicide verilerin birleştirilmesi için yeni bir ağırlıklandırma yaklaşımı getirilmiştir. Farklı frekanslardan gelen bilgilerin farklı güvenilirlikte olduğu gerçeği göz önünde bulundurularak bir ağırlıklandırma yaklaşımı geliştirilmiştir. Bu çalışmada öne sürülen ağırlıklandırma yaklaşımı ile, mevcut eşlenen alan işleyicilere kıyasla bir performans kazancı elde edilebildiği gösterilmiştir.

Anahtar Kelimeler: Sualtı kaynaklarının konumlandırılması, darbant eşlenen alan işleme, genişbant eşlenen alan işleme

To my family

ACKNOWLEDGMENTS

I would like to express my gratitude to my supervisor Assoc. Prof. Dr. Tolga Çiloğlu for his invaluable comments, guidance, encouragement and endless patience during my research activities. I would also like to express my special thanks to the jury members Prof. Dr. Mübeccel Demirekler, Prof. Dr. Mustafa Kuzuoğlu and Assoc. Prof. Dr. Çağatay Candan for evaluating my thesis.

I would like to thank to ASELSAN for supporting my research. I especially would like to thank to Dr. Hüseyin Yavuz who has encouraged me to work in the underwater acoustics area. I also would like to thank to my manager Serkan Özgün for his support and patience during my thesis.

I wish to express my deepest gratitude to my family who had endlessly and unconditionally supported me throughout my life. I also would like to thank to my all teachers, instructors and mentors to whom I owe all my knowledge today.

I would also like to thank to Türkiye Bilimsel ve Teknolojik Araştırma Kurumu (TÜBİTAK) for their contribution to my Master of Science education with the scholarship.

TABLE OF CONTENTS

LIST OF TABLES

TABLES

LIST OF FIGURES

FIGURES

CHAPTER 1

INTRODUCTION

1.1 Localization of Underwater Sound Sources

Localization of the underwater sound sources is one of the most important problems encountered in underwater acoustics and signal processing.

Let us consider the problem of locating a radiating underwater source using m passive hydrophones (underwater acoustic sensors). An acoustic wave field propagating from the source is sampled in both space and time by the array. Our aim is to combine the spatial and temporal signal information at the array with the geometry of the array in such a way that we can predict the location of the source accurately.

We first review some classical approaches to localization problem, such as beamforming and Minimum Variance Distortionless Response (MVDR) method. Then we introduce the basics of the matched field processing.

1.2 Classical Localization Techniques

In this section, we follow the signal model developed in [1], and also summarize beamforming and Minimum Variance Distortionless Response (MVDR) based on the derivations given in [1].

Let us consider the problem of locating a sound emitting source by using m hydrophones. The wave field generated by the source is sampled in both space and time by the sensor array.

We first make some assumptions to develop a model for the output signal at the sensor array. We assume that source is situated in the far field of the array and also the propagation medium is homogenous, therefore the waves arriving at the array is considered to be planar. Under these assumptions, the source location is characterized by the direction of arrival since waves follow a linear path from source to receivers.

Next we develop a model for the output signal. Let $s(t)$ be the value of the signal waveform at some reference point. Let τ_k be the time needed to travel from that reference point to sensor k, $(k = 1...m)$. Then the output of the sensor k can be written as:

$$y_k(t) = s(t - \tau_k) + n_k(t) \tag{1.1}$$

where $n_k(t)$ is the additive noise. Here $s(t)$ and τ_k are unknown source parameters. The source location information enters the equation via τ_k. So source location estimation problem is equivalent to the time-delay estimation problem.

Let $S(\omega)$ denote the Fourier transform of the continuous signal $s(t)$:

$$S(w) = \int_{-\infty}^{+\infty} s(t)e^{-iwt}dt \tag{1.2}$$

Similarly, $Y_k(w)$ and $N_k(w)$ denote the Fourier transform of the signals $y_k(t)$ and $n_k(t)$. Assuming that the received signal is narrowband and has a known frequency of ω, we can write,

$$Y_k(\omega) = S(\omega)e^{-i\omega\tau_k} + N_k(\omega) \tag{1.3}$$

In time domain,

$$y_k(t) = s(t)e^{-i\omega\tau_k} + n_k(t) \tag{1.4}$$

Next we define the array transfer function as follows:

$$\mathbf{a}(\theta) = [e^{-i\omega\tau_1}...e^{-i\omega\tau_m}]^T \tag{1.5}$$

In this expression θ denotes the direction of arrival of the source which is the parameter to be found. In closed form we can write:

$$\mathbf{y}(t) = \mathbf{a}(\theta)\mathbf{s}(t) + \mathbf{n}(t) \tag{1.6}$$

where

$$\mathbf{y}(t) = [y_1(t).....y_m(t)]^T \tag{1.7}$$

$$\mathbf{n}(t) = [n_1(t).....n_m(t)]^T \tag{1.8}$$

are the array output vector and the additive noise vector. We can simplify array transfer function as follows, assuming the signal arrives at time 0 to the first sensor:

$$\mathbf{a}(\theta) = [1\ e^{-i\omega\tau_2}...e^{-i\omega\tau_m}]^T \tag{1.9}$$

Next we consider the case of a uniform line array. A uniform line array consists of m identical sensors uniformly spaced on a line. Let d denote the distance between two sensors, and let θ denote the DOA of the signal arriving at the array. Using simple trigonometry, we can write τ_k as:

$$\tau_k = (k-1)\frac{d\sin\theta}{c} \text{ for } \theta\epsilon[-90^o,90^o] \tag{1.10}$$

where c is the velocity of the wave (sound velocity). $\mathbf{a}(\theta)$ now takes the form:

$$\mathbf{a}(\theta) = [1\ e^{-i\frac{\omega d\sin\theta}{c}}...e^{-i(m-1)\frac{\omega d\sin\theta}{c}}] \tag{1.11}$$

Now we can express direction of arrival problem as the problem of estimating parameters for θ. We assume that the positions of sensors are known and using this information, the functional form of $\mathbf{a}(\theta)$ is known.

Our aim is to use a spatial filter $\mathbf{w}$ such that when $\mathbf{y}(t)$ is filtered, it enables us to find the direction of arrival of the signal. If $\mathbf{w}$ is a spatial filter with weights w_k, $k = 1...m$, we can define the output of the filter as follows:

$$y_F(t) = \mathbf{w}^+\mathbf{y}(t) \tag{1.12}$$

where

$$\mathbf{y}(t) = [y_1(t).....y_m(t)]^T \tag{1.13}$$

and + denotes Hermitian operator.

For a noise free case, we can write:

$$y_F(t) = [\mathbf{w}^+\mathbf{a}(\theta)]s(t) \tag{1.14}$$

In order to find the direction of arrival, the filter we have designed should enhance signals from the direction θ whereas attenuate all other direction of arrivals different from θ. Next we review two different approaches to this design problem: beamforming and MVDR method. Our review is based on the derivations given in [1].

1.2.1 Beamforming

To design a filter that enhances signals from the direction θ, we first put the constraint that the signal coming from direction θ should not be distorted.

In formal terms;

$$\mathbf{w}^{+}\mathbf{a}(\theta) = 1 \tag{1.15}$$

We also want the filter to attenuate all other direction of arrivals than θ.

In this case, the power of the spatially filtered signal can be given as:

$$E\{|y_F(t)|^2\} = \mathbf{w}^{+}\mathbf{R}\mathbf{w} \text{ where } \mathbf{R} = E\{\mathbf{y}(t)\mathbf{y}^{+}(t)\} \tag{1.16}$$

If $\mathbf{y}(t)$ were spatially white with $\mathbf{R} = \mathbf{I}$, the power of filtered signal would be:

$$E\{|y_F(t)|^2\} = \mathbf{w}^{+}\mathbf{w} \tag{1.17}$$

Considering our filter design condition that we want all other direction of arrivals to be attenuated, we observe that we require a weight vector $\mathbf{w}$ that minimizes $E\{|y_F(t)|^2\}$ (filtered signal power). Hence the design problem can be stated as:

$$\min_{\mathbf{w}} \mathbf{w}^{+}\mathbf{w} \text{ subject to } \mathbf{w}^{+}\mathbf{a}(\theta) = 1 \tag{1.18}$$

The solution of this optimization problem is given by

$$\mathbf{w} = \mathbf{a}(\theta) \tag{1.19}$$

assuming that transfer vector $a(\theta)$ is normalized to 1.

In the optimization problem, we assumed $\mathbf{R} = \mathbf{I}$ to attenuate all other direction of arrivals than the actual one. However, if the signal is present, $\mathbf{R}$ is not equal to identity, which yields the power of filtered signal as:

$$E\{|y_F(t)|^2\} = \mathbf{a}^{+}(\theta)\mathbf{R}\mathbf{a}(\theta) \tag{1.20}$$

Finally we state that beamforming direction of arrival estimates are given by the highest peak of the function

$$\mathbf{a}^{+}(\theta)\mathbf{R}\mathbf{a}(\theta) \tag{1.21}$$

The theoretical covariance matrix R can be replaced by an estimate as follows:

$$\hat{\mathbf{R}} = \frac{1}{N}\sum_{t=1}^{N}\mathbf{y}(t)\mathbf{y}^{+}(t) \tag{1.22}$$

1.2.2 Minimum Variance Distortionless Response (MVDR) Method

One of the objectives in beamforming approach is to attenuate all other direction of arrivals different from θ as much as possible. However, the beamforming filter pays same attention to all direction of arrivals different from θ even if there is no signal present for many of the direction of arrivals [1].

In MVDR approach, a data-dependent model is developed to attenuate all other direction of arrivals other than θ. The aim is to attenuate the signals arriving to the array from a direction of arrival other than θ. Hence the minimization given in equation (1.18) takes the following form:

$$\min_{\mathbf{w}} \mathbf{w}^{+}\mathbf{R}\mathbf{w} \text{ subject to } \mathbf{w}^{+}\mathbf{a}(\theta) = 1 \tag{1.23}$$

The solution to this minimization problem is given by:

$$\mathbf{w} = \frac{\mathbf{R}^{-1}\mathbf{a}(\theta)}{\mathbf{a}^{+}(\theta)\mathbf{R}^{-1}\mathbf{a}(\theta)} \tag{1.24}$$

which yields the following output power:

$$E\{|y_F(t)|^2\} = \frac{1}{\mathbf{a}^{+}(\theta)\mathbf{R}^{-1}\mathbf{a}(\theta)} \tag{1.25}$$

The peak of the output power function given in equation 1.25 are the MVDR estimates for direction of arrivals.

1.3 Matched Field Processing

The localization methods mentioned so far works well under the assumption that propagation medium is homogenous and the propagation path is linear. However,

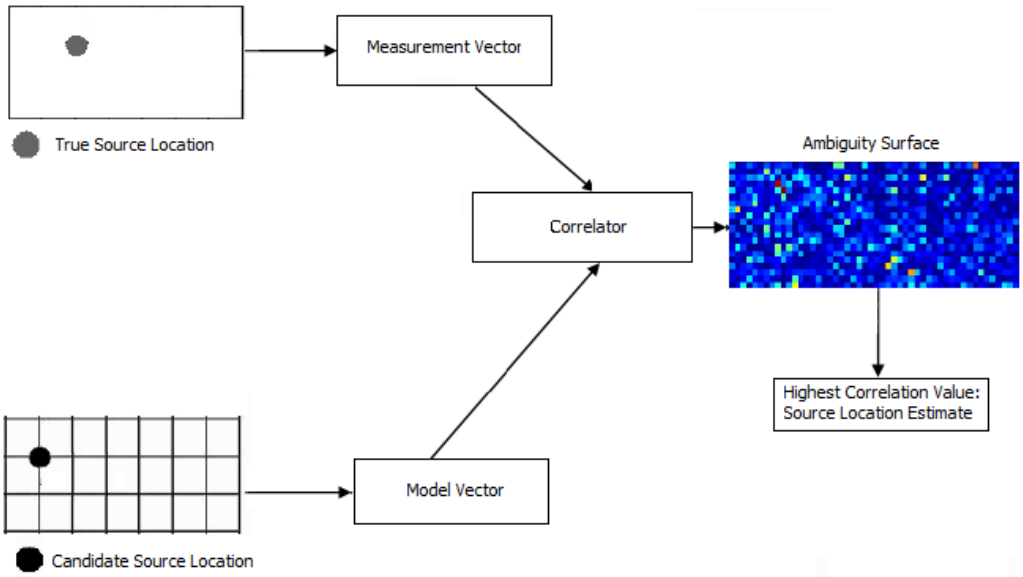

Figure 1.1: The generalized flow chart for Matched Field Processing

underwater environment is almost never a homogenous propagation medium.

Matched Field Processing was introduced as a technique which considers the effects of environmental factors that creates a nonlinear propagation of acoustic waves in an inhomogenous medium. The idea behind matched field processing is to compare the measured data at the array with modeled data for some candidate source locations [2].

The application of Matched Field Processing starts with measurement of acoustic data coming from an unknown location at the receiver array of m hydrophones. Then a search space (or grid) consisting of candidate source locations is defined. By using a propagation model, the acoustics fields that would be generated at the array for these candidate locations are calculated. Following this, the modeled data for the candidate source location and measured data is cross-correlated. The candidate source location that gives the highest correlation is suggested as the estimate of source's depth and range [2]. A graphical representation of this process is given in Figure 1.1.

The surface consisting of the correlation values for candidate locations is called the ambiguity surface. The high correlation areas not in the neighborhood of the true source location are called "sidelobes" [2].

Note that MFP can also be used to determine unknown environmental parameters for a known source location, and also to evaluate the accuracy of propagation models [2]. However, these problems are out of the scope of this thesis.

It is important to observe that MFP is closely related to frequency domain plane wave beamforming. In frequency domain,

$$G(\omega) = \sum_{k=1}^{m} w_k S_k(\omega) e^{-i\omega_k \tau_k} \tag{1.26}$$

where $S(\omega)$ is the Fourier transform of s_k. It can be observed that this is also equivalent to cross-correlating the measured frequency domain fields $S_k(\omega)$ with simple plane wave fields $e^{i\omega t_k}$. Thus beamforming steered in the direction of θ is simply creating a model data for the possible source at θ (without taking propagation effects into account) and correlating that data with the received signal. Repeating same procedure for different θs correspond to searching over candidate source locations. This allows us to interpret frequency domain simple plane beamforming as a special case (i.e. isovelocity, unbounded underwater environment) of matched field processing. In other words, matched field processing is equivalent to traditional beamforming where w_k, τ_k can be selected considering the criteria such as propagation effects and noise minimization.

1.4 Thesis Outline

The thesis outline is as follows: In Chapter 1 (Introduction), we make a brief introduction to the localization methods. In Chapter 2 (Modeling of Underwater Acoustics Wave Propagation), we summarize the modeling method that we use for this thesis. In Chapter 3 (Narrowband Matched Field Processing), we overview the narrowband matched field processors and give a comparative analysis of the most commonly used narrowband matched field processors. In Chapter 4 (Broadband Matched Field Processing), we give an overview of broadband matched field processors and make a comparative analysis. In Chapter 5 (Weighting Approach to Broadband Matched

Field Processing), we summarize our weighting approach to broadband matched field processors. In Conclusion, we conclude our thesis summarizing our work and giving our ideas on future work.

CHAPTER 2

MODELING OF UNDERWATER ACOUSTICS WAVE PROPAGATION

2.1 Overview of Acoustic Propagation Modeling

The inhomogeneous characteristics of the sea and dependence of underwater acoustic parameters (e.g. sound velocity) on depth, range and bearing makes the modeling of the acoustic propagation a very complex issue. In order to model acoustic propagation of sound, many different acoustic propagation models have been developed. Among these, the most important ones are the ray theory and the normal mode model. We briefly explain these models, and then give some more detail about the normal mode model which is chosen as the propagation model in this thesis.

Ray theory solves the wave equation under the key assumptions of infinite frequency and smaller variability of sound compared to the signal wavelength [4]. The seabody is divided into layers of very small size and Snell's law is used to compute the trajectory followed by the sound waves (or rays). Ray theory has the advantages of smaller computation time and provides more understandable visualization. However, it is usually not preferred for the low frequency applications due to the high level of inaccuracy.

The Normal Mode method solves the Helmholtz equation using the separation of variables (range-independency) technique [3]. By separating the depth and range dependent expressions, the acoustic wave can be found as a sum of depth-dependent modes and modal eigenfunctions. These modes satisfy the boundary conditions. Some methods to extend normal mode methods to range dependent conditions have been developed as well [4]. The advantages of normal mode methods include very accu-

rate modeling of acoustic waves and fast computation for low frequencies. On the other hand, for higher frequencies normal mode methods are inapplicable due to poor computation time performance.

In this thesis, due to the nature of problems we deal, we restrict ourselves to low frequency applications, hence it is possible to model underwater acoustic waves accurately using the normal mode method.

2.2 Normal Mode Method

The normal mode method makes use of the separation of the Helmholtz equation to range and depth dependent parts. Then the depth and range dependent parts are solved independently. The depth dependent part of the equation has normal mode functions and horizontal wavenumbers as the solution. The acoustic field can be found by summing up all the contributions of modes considering the depth of source and also the depth and range of the point at which the acoustic field is of interest.

The derivation of normal-mode equations uses the separation of variables method as explained below. These derivations are based on [3] and [4].

2.2.1 Derivation of Normal Mode Representation

For simplicity, we consider the point source in a cylindrical geometry case. The range-independent (i.e. sound speed and density depends on depth z only) Helmholtz equation in two dimensions is given by [3]:

$$\frac{1}{r}\frac{\delta}{\delta r}(r\frac{\delta p}{\delta r}) + \rho(z)\frac{\delta}{\delta z}(\frac{1}{\rho(z)}\frac{\delta p}{\delta z}) + \frac{\omega^2}{c^2(z)}p = 0 \tag{2.1}$$

where r is range, p is acoustic pressure, ρ is density, c is the sound speed and ω is the frequency of source.

We want to find a solution whose depth and range parts can be written independently to use the separation of variables, i.e. we want to write acoustic field as $p(r, z) = \phi(r)\psi(z)$. If we substitute $p(r, z) = \phi(r)\psi(z)$ into the above equation and divide all

terms by $\phi(r)\psi(z)$, we find [3]

$$\frac{1}{\phi}[\frac{1}{r}\frac{d}{dr}(r\frac{d\phi}{dr})] + \frac{1}{\psi}[\rho(z)\frac{d}{dz}(\frac{1}{\rho(z)}\frac{d\psi}{dz}) + \frac{\omega^2}{c^2(z)}\psi] = 0 \tag{2.2}$$

The left hand side of the summation is a function of r and the right hand side is a function of z. Since both sides do not include the variable of the other side, the only way this equation is satisfied is that both sides are equal to a constant. Let us denote this constant as k_{rm}^2 to get:

$$\frac{1}{\psi}[\rho(z)\frac{d}{dz}(\frac{1}{\rho(z)}\frac{d\psi}{dz}) + \frac{\omega^2}{c^2(z)}\psi] = k_{rm}^2 \tag{2.3}$$

Rearranging terms we get:

$$\rho(z)\frac{d}{dz}[\frac{1}{\rho(z)}\frac{d\psi_m(z)}{dz}] + [\frac{w^2}{c^2(z)} - k_{rm}^2]\psi_m(z) = 0 \tag{2.4}$$

Here the $\psi_m(z)$ is the modal function for the separation constant k_{rm}.

We also need to satisfy the boundary conditions as:

$$\psi(0) = 0,\ \frac{d\psi}{dz}|_{z=D} = 0 \tag{2.5}$$

Our boundary conditions indicate that the surface is pressure-release ($z = 0$) and bottom is rigid $z = D$.

As given in [4], the modal equation is a Sturm-Liouville eigenvalue problem. Sturm-Liouville problems have important properties which we can make use of to find our solution [5]. First of all, modal equation has infinite number of solutions. Secondly, all horizontal propagation constants are distinct and they have a corresponding mode shape function $\psi_m(z)$. Moreover, the m-th mode has m zeroes in the interval $[0, D]$ and the corresponding eigenvalues k_{rm}^2 are all real and ordered as $k_{r1} > k_{r2}$.... Finally, all eigenvalues are less than $\frac{\omega}{c_{min}}$, where c_{min} is the lowest sound speed in the problem.

The modes of Sturm-Liouville problems are also known to be orthogonal such that [4]:

$$\int_0^D \frac{\psi_m(z)\psi_n(z)}{\rho(z)}dz = 0,\ \text{for } m \neq \text{n} \tag{2.6}$$

We also assume that the modes are normalized so that:

$$\int_0^D \frac{\psi_m(z)^2}{\rho(z)}dz = 1 \tag{2.7}$$

It is possible to express an arbitrary function as a sum of normal modes:

$$p(r,z) = \sum_{m=1}^{\infty} \phi_m(r)\psi_m(z) \tag{2.8}$$

Substituting this into equation (2.1) we get:

$$\sum_{m=1}^{\infty} \{\frac{1}{r}\frac{d}{dr}(r\frac{d\phi_m(r)}{dr})\psi_m(z) + \phi_m(r)[\rho(z)\frac{d}{dz}(\frac{1}{\rho(z)}\frac{d\psi_m(z)}{dz}) + \frac{\omega^2}{c^2(z)}\psi_m(z)]\} = 0 \tag{2.9}$$

Further simplifying this using modal equation we get:

$$\sum_{m=1}^{\infty} \{\frac{1}{r}\frac{d}{dr}(r\frac{d\phi_m(r)}{dr})\psi_m(z) + k_{rm}^2\phi_m(r)\psi_m(z)\} = 0 \tag{2.10}$$

Applying the operator $\int_0^D (.)\frac{\psi_n(z)}{\rho(z)}dz$ and using orthogonality property we only have the n-th term as:

$$\frac{1}{r}\frac{d}{dr}[r\frac{d\phi_n(r)}{dr}] + k_{rn}^2\phi_n(r) = 0 \tag{2.11}$$

The solution to this equation is given in terms of first kind Hankel function as [4]:

$$\phi_n(r) = \frac{i}{4\rho(z_s)}\psi_n(z_s)H_0^{(1)}(k_{rn}r) \tag{2.12}$$

This yields the acoustic field term as:

$$p(r,z) = \frac{i}{4\rho(z_s)}\sum_{m=1}^{\infty}\psi_m(z_s)\psi_m(z)H_0^{(1)}(k_{rm}r) \tag{2.13}$$

Using the asymptotical approximation to Hankel function, we get.

$$p(r,z) = \frac{i}{\rho(z_s)\sqrt{8\pi r}}e^{\frac{i\pi}{4}}\sum_{m=1}^{\infty}\psi_m(z_s)\psi_m(z)\frac{e^{ik_{rm}r}}{\sqrt{k_{rm}}} \tag{2.14}$$

Having found the expression for $p(r,z)$, we need to solve for the modes and horizontal wave numbers.

2.2.2 Numerical Solution to Normal Mode Equation

In order to find a numerical solution to the modal problem, the finite difference approach can be used as explained in [3]. We start by dividing the interval $0 \leq z \leq D$ into N equal intervals so that we have a mesh of equally spaced points, $z_j = jh$, where $h = D/N$. We also adopt the notation $\psi_j = \psi(z_j)$ as used in [3].

If we assume that density is constant, we have the modal problem:

$$\psi^{''}(z) + [\frac{\omega^2}{c^2(z)} - k_r^2]\psi(z) = 0 \tag{2.15}$$

where primes denote the differentiation with respect to z. Using Taylor expansion as explained in [3], we have the forward difference approximation for the first derivative as:

$$\psi_j^{'} = \frac{\psi_{j+1} - \psi_j}{h} - \psi_j^{''}\frac{h}{2} \tag{2.16}$$

Using the modal equation, the $O(h^2)$ approximation to first derivative is found as:

$$\psi_j^{'} \simeq \frac{\psi_{j+1} - \psi_j}{h} + [\frac{w^2}{c^2(z_j)} - k_r^2]\psi_j\frac{h}{2} \tag{2.17}$$

Similarly a backward approximation is found as:

$$\psi_j^{'} \simeq \frac{\psi_j - \psi_{j-1}}{h} - [\frac{w^2}{c^2(z_j)} - k_r^2]\psi_j\frac{h}{2} \tag{2.18}$$

A centered difference approximation to the second derivative can also be found as:

$$\psi_j^{''} = \frac{\psi_{j-1} - 2\psi_j + \psi_{j+1}}{h^2} + O(h^2) \tag{2.19}$$

Next we replace the continuous derivatives in modal problem with discrete ones. Recall from [3] that the continuous problem is given by:

$$\psi^{''}(z) + [\frac{\omega^2}{c^2(z)} - k_r^2]\psi(z) = 0 \tag{2.20}$$

$$f^T(k_r^2)\psi(0) + \frac{g^T(k_r^2)}{\rho}\frac{d\psi(0)}{dz} = 0 \tag{2.21}$$

$$f^B(k_r^2)\psi(D) + \frac{g^B(k_r^2)}{\rho}\frac{d\psi(0)}{dz} = 0 \tag{2.22}$$

where f and g functions are bottom and surface dependent functions and for general cases they can be found as explained in [4]. For pressure-release surface cases such as the ones dealt in this thesis, the ratio $\frac{f}{g}$ in the boundary condition is infinity and for the rigid bottom boundary case, $\frac{f}{g}$ goes to zero.

Using the centered, forward and backward difference approximations we obtain [4]:

$$\psi_{j-1} + \{-2 + h^2[\frac{\omega^2}{c^2(z_j)} - k_r^2]\}\psi_j + \psi_{j+1} = 0,\ j = 1, ...N-1 \tag{2.23}$$

$$\frac{f^T}{g^T}\psi_0 + \frac{1}{\rho}\{\frac{\psi_1 - \psi_0}{h} + [\frac{\omega^2}{c^2(0)} - k_r^2]\psi_0\frac{h}{2}\} = 0 \tag{2.24}$$

$$\frac{f^B}{g^B}\psi_N + \frac{1}{\rho}\{\frac{\psi_N - \psi_{N-1}}{h} + [\frac{\omega^2}{c^2(D)} - k_r^2]\psi_N \frac{h}{2}\} = 0 \tag{2.25}$$

The first equation can be written as:

$$\frac{1}{h\rho}\psi_{j-1} + \frac{-2 + h^2[\omega^2/c^2(z_j) - k_r^2]}{h\rho}\psi_j + \frac{1}{h\rho}\psi_{j+1} = 0 \tag{2.26}$$

Using the difference equations, an algebraic eigenvalue problem as the following can be obtained:

$$\mathbf{A}(k_r^2)\psi = 0 \tag{2.27}$$

where $\psi = [\psi_0\psi_1....\psi_N]$. $\mathbf{A}$ is a symmetric tridiagonal matrix of the form:

$$\mathbf{A} = \begin{pmatrix} d_0 & e_1 & 0 & 0 & 0 & 0 & 0 \\ e_1 & d_1 & e_2 & 0 & 0 & 0 & 0 \\ 0 & e_2 & d_2 & e_3 & 0 & 0 & 0 \\ . & . & . & . & . & . & . \\ 0 & 0 & 0 & e_{N-2} & d_{N-2} & e_{N-1} & 0 \\ 0 & 0 & 0 & 0 & e_{N-1} & d_{N-1} & e_N \\ 0 & 0 & 0 & 0 & 0 & e_N & d_N \end{pmatrix}$$

where coefficients d_j and e_j are defined by:

$$d_0 = \frac{-2 + h^2[\omega^2/c^2(z_0) - k_r^2]}{2h\rho} + \frac{f^T(k_r^2)}{g^T(k_r^2)} \tag{2.28}$$

$$d_j = \frac{-2 + h^2[\omega^2/c^2(z_j) - k_r^2]}{h\rho},\ j = 1...., N-1 \tag{2.29}$$

$$d_N = \frac{-2 + h^2[\omega^2/c^2(z_N) - k_r^2]}{2h\rho} - \frac{f^B(k_r^2)}{g^B(k_r^2)} \tag{2.30}$$

and $e_j = \frac{1}{h\rho}, j = 1....N$.

Next we explain how to find the root of this characteristic equation numerically as given in [3] and [4].

2.2.3 Rootfinding by Bisection

In order to find the roots of characteristic equation, four techniques were suggested in [3]: Bisection, Deflation, Brute-Force Search and Analytic Formulas for estimating

the eigenvalues. For a purely acoustic problem such as ours, we consider the bisection approach which is known to be the most efficient scheme [3]. The bisection algorithm relies on the property of Sturm-Liouville problem that the mth mode has m zeroes. When we use a shooting technique to calculate a trial eigenfunction, the number of zeroes in the calculated function increases monotonically as the trial eigenvalue k_r decreases [4].

The rootfinding scheme can be described as follows [3], [4]:

[1] As mentioned before, the lowest order eigenvalue is bounded above by $\frac{\omega}{c_{min}}$ (c_{min} is the lowest sound speed in the problem). This provides an upper bound for the mode search. A lower bound can be found by the user.

[2] After finding the lower and higher bounds, we take the midpoint of interval and compute the number of modes to the right of the midpoint. It is possible to determine if first eigenvalue lies to the left or to the right of the midpoint by checking the number of zero-crossings in the trial eigenfunction.

[3] The midpoint is then assigned as a new lower bound or upper bound for the eigenvalue. If the interval contains only one eigenvalue, the interval is found as the isolating interval for that eigenvalue. If there are more than one eigenvalue, interval is halved again.

[4] The same procedure is repeated for each mode.

[5] After finding all isolating intervals, it is possible to continue with bisection or a better root finder may be used. We use Brent's method [3] in our work which guarantees the convergence.

CHAPTER 3

NARROWBAND MATCHED FIELD PROCESSING

3.1 Overview of Narrowband Matched Field Processors

As we have seen in Section 1.3, matched field processing uses the idea to crosscorrelate the actual received data with the data modeled for candidate positions. Many techniques based on this idea have been proposed, each having its own advantages and disadvantages. In this section, we review some of the most widely used matched field processors: the Linear (Bartlett) processor, Minimum Variance Distortionless Response (MVDR) processor, MVDR with Neighboring Location Constraints (MVDR-NLC) and MVDR with Environmental Perturbation Constraints (MVDR-EPC).

3.2 Linear (Bartlett) Processor

Bartlett Processor is the simplest and easiest processor to understand and implement. We give an explanation of Bartlett processor as given in [2].

Let us assume that we have m hydrophones and we are trying to find the location of a sound emitting source. Let the position of the source given by $\mathbf{p} = (x, z)$ where x and z denotes the real range and the depth of the source respectively.

Let $s_k(\mathbf{p}, t)$ be the measured signal at hydrophone $k, k = 1...m$ and $S_k(\mathbf{p}, \omega)$ be the Fourier transform of that signal. Then we can define the measured data vector, $\mathbf{S}(\mathbf{p})$ as follows:

$$\mathbf{S}(\mathbf{p}) = [S_1(\mathbf{p}, \omega)...S_m(\mathbf{p}, \omega)] \tag{3.1}$$

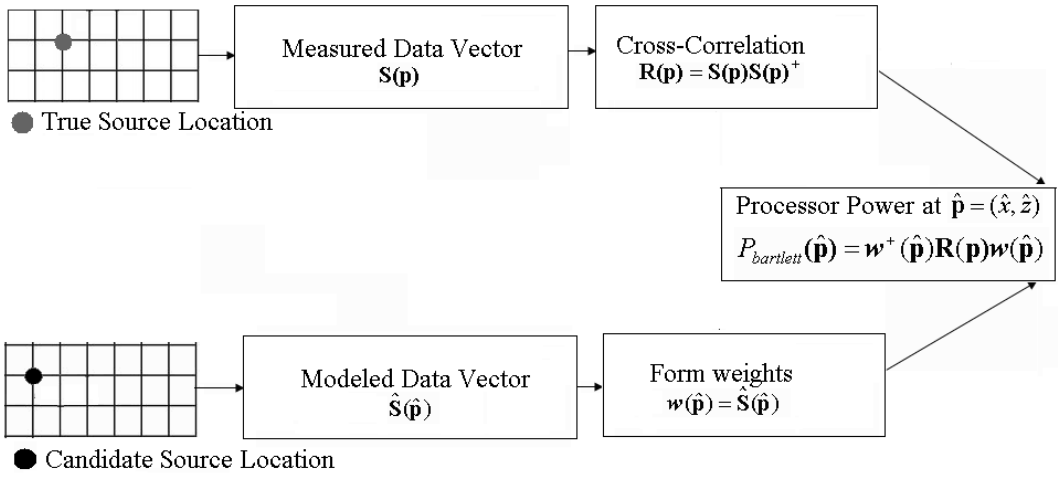

Figure 3.1: The flow chart for Bartlett Matched Field Processor

Next let us define $\hat{s}_k(\hat{\mathbf{p}}, t)$ as the modeled acoustic field for the candidate source position $\hat{\mathbf{p}} = (\hat{x}, \hat{z})$ as sensed at hydrophone $k, k = 1...m$. Let $\hat{S}_k(\hat{\mathbf{p}}, \omega)$ be the Fourier transform of that signal. We define the modeled data vector, $\hat{\mathbf{S}}(\hat{\mathbf{p}})$, as follows:

$$\hat{\mathbf{S}}(\hat{\mathbf{p}}) = [\hat{S}_1(\hat{\mathbf{p}}, \omega)...\hat{S}_m(\hat{\mathbf{p}}, \omega)] \tag{3.2}$$

We assume that $\mathbf{S}(\mathbf{p})$ and $\hat{\mathbf{S}}(\hat{\mathbf{p}})$ are normalized to 1 with respect to L_2 norm.

The direct correlation of $\mathbf{S}(\mathbf{p})$ and $\hat{\mathbf{S}}(\hat{\mathbf{p}})$ will give an idea on the similarity of the measured data and modeled data for the candidate position $\hat{\mathbf{p}}$. Linear Processor uses this idea to estimate a location for the source. The candidate position that results highest correlation value is suggested as the source position. The location of the source is estimated as the result of the following optimization problem [2]:

$$\arg\max_{\hat{\mathbf{p}}} \mathbf{w}^{+}(\hat{\mathbf{p}})\mathbf{R}(\mathbf{p})\mathbf{w}(\hat{\mathbf{p}}) \tag{3.3}$$

where $\mathbf{w}(\hat{\mathbf{p}}) = \hat{\mathbf{S}}(\hat{\mathbf{p}})$ and $+$ denotes conjugate transpose. $\mathbf{R}(\mathbf{p}) = \mathbf{S}(\mathbf{p})\mathbf{S}(\mathbf{p})^{+}$ is the cross spectral density matrix for the measured data. Note that the optimization is done over the cross-spectral matrices instead of individual samples of the fields. The reason doing so is to reduce the effect of phase and amplitude disturbances occurring coherently across the array due to the variation in the ocean. The flowchart for Bartlett processor can be seen in Figure 3.1.

Note that Linear Processor is closely related to the beamforming described in Introduction chapter. In beamforming, a signal model is developed such that the location of the signal is characterized only by its direction of arrival. Then for candidate direction of arrivals, the received signal is correlated with the modeled signal, and the candidate direction of arrival resulting highest correlation is found as the estimate of the source direction. This estimate is considerable under the assumption that propagation medium is homogenous. On the other hand, if propagation medium is not homogenous, the sound waves will not follow a straight path and direction of arrival will not be satisfactory to characterize source location. In linear matched field processor, the signal model is developed considering the environmental factors as well. For different candidate source locations, signals at the sensors are modeled and then correlated with the received signal. As in beamforming, the candidate source location that results higher correlation value is estimated to be the source location. Both beamforming and linear processor use the idea of correlation to find the source position. However, linear processor considers the environmental factors and also finds the location as a point, whereas beamforming considers a homogenous propagation medium and finds only the direction.

3.3 The Minimum Variance Processor (MVDR)

The minimum variance distortionless processor (MVDR) is a processor which minimizes the output noise power subject to the constraint that the signal be undistorted by the filter. This processor has been derived from the MVDR method that has been mentioned in Section 1.2. The derivation of MVDR given here is based on the derivation given in [2].

The filter design objective is to minimize the variance of the processor response to the noise field without distorting the signal,i.e. $\mathbf{w}^{+}(\hat{\mathbf{p}})\hat{\mathbf{S}}(\hat{\mathbf{p}}) = \mathbf{1}$. In more formal terms,

$$\mathbf{w}(\hat{\mathbf{p}}) = \arg\min_{\mathbf{w}} \mathbf{w}^{+}(\hat{\mathbf{p}})\mathbf{R}(\mathbf{p})\mathbf{w}(\hat{\mathbf{p}}) + \lambda Re(\mathbf{w}^{+}(\hat{\mathbf{p}})\hat{\mathbf{S}}(\hat{\mathbf{p}}) - \mathbf{1}) \tag{3.4}$$

Solving this minimization problem yields the following filter [2]:

$$\mathbf{w}(\hat{\mathbf{p}}) = \frac{\mathbf{R^{-1}}(\mathbf{p})\hat{\mathbf{S}}(\hat{\mathbf{p}})}{\hat{\mathbf{S}}^{+}(\hat{\mathbf{p}})\mathbf{R^{-1}}(\mathbf{p})\hat{\mathbf{S}}(\hat{\mathbf{p}})} \tag{3.5}$$

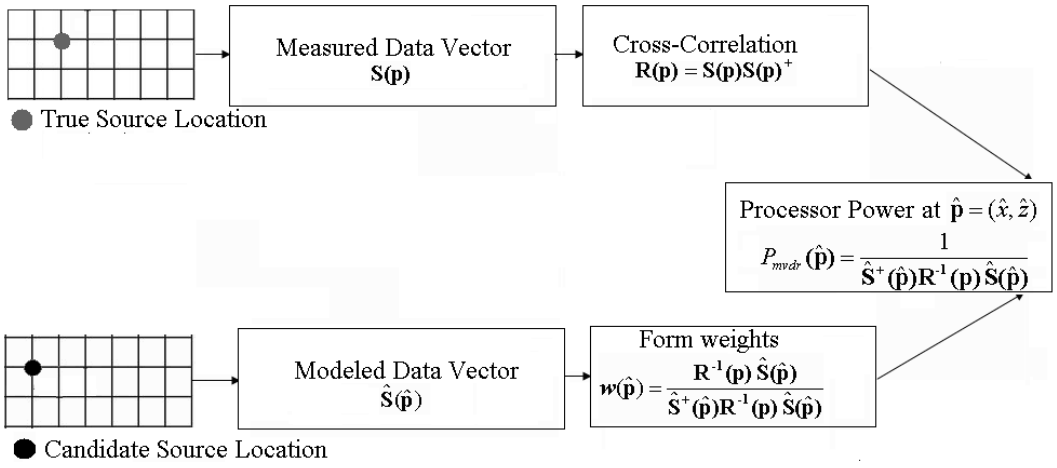

Figure 3.2: The flow chart for MVDR Matched Field Processor

Then the minimum variance processor is defined as:

$$P_{mvdr}(\hat{\mathbf{p}}) = \frac{\mathbf{1}}{\hat{\mathbf{S}}(\hat{\mathbf{p}})\mathbf{R}^{-1}\hat{\mathbf{S}}(\hat{\mathbf{p}})} \tag{3.6}$$

The source location estimate is given as the candidate source location $\hat{\mathbf{p}}$ that makes $P_{mvdr}(\hat{\mathbf{p}})$ maximum. The flowchart for MVDR processor can be seen in Figure 3.2.

Note that the processor needs inversion of the cross-spectral matrix $\mathbf{R}(\mathbf{p})$. Therefore to get a meaningful result in a reasonable time the matrix should not be too large and it must be assured to be of rank m.

As stated in [2] and as can be seen from Section 3.1.5 where we give examples of narrowband matched field processors, MVDR provides a higher resolution than Bartlett.

3.4 MVDR using Neighboring Location Constraints

As explained in the previous section, the Minimum Variance Distortionless Response processor provides better resolution compared to Bartlett's method. However, MVDR is highly sensitive to changes in environmental parameters on which acoustic fields depend on [9]. Inaccurate knowledge of the environment (e.g. lack of knowledge of the true sound speed profile) will result in a move of the peak from the correct position to some faulty position. Sensitivity to environmental parameters is something not desirable in underwater source estimation problems since it is very rare that the

complete knowledge of environment is available. The processors designed for the perfectly known environment usually suffer from the so called environmental mismatch which are the unknown deviations from the deterministic propogation models due to the natural phenomena such as internal waves.

In order to overcome the problems caused by high sensitivity in mismatch cases and to provide a more robust MVDR processor to random inhomogeneities, Schmidt and Baggeroer [9] have introduced a modification of MVDR which is called MVDR with Neighboring Locations Constraints MVDR-NLC. In this section we overview this processor as given in [9].

The idea is, by using a multiple constraint approach, it is possible to solve the sensitivity to mismatch problems of MVDR to some extent. So instead of using MVDR with the constraint of passing signal undistorted and suppress all signals coming from other directions, more constraints are defined around the source location, so that the move of the peak at the processor output caused by mismatch can be tolerated. This is achieved by designing a processor with a wider mainlobe similar to Bartlett but also having the sidelobe suppression properties of MVDR, as explained below.

The processor suggested by Schmidt and Baggeroer [9] consists of using multiple constraints to achieve a mainlobe response equal to the more robust Bartlett beamformer. The derivation of processor is very similar to the derivation of MVDR. However, instead of using one constraint to pass only signals coming from one point and suppress other directions, multiple constraints are used to pass signals coming from a certain spot (an area around a point) and to minimize sidelobe effects.

Recall that the Bartlett Processor is given by

$$P_{bartlett} = \mathbf{w}(\hat{\mathbf{p}})^{+}\mathbf{R}(\mathbf{p})\mathbf{w}(\hat{\mathbf{p}}) \tag{3.7}$$

If this ambiguity function is minimized with the single constraint that it passes only signals coming from a certain point and suppresses signals coming from all other directions, the MVDR processor is derived. However, this optimization of weights to a particular range and depth will create a very sharp peak and it will create a need of denser sampling [9].

Now consider using total N constraints such that signals coming from a certain spot

(an area around a point) are passed. In this case, if $\mathbf{w}$ is the weight vector and $\mathbf{e_n}$ is the replica vector for the constraint point n, the constraints can be expressed as[9]:

$$\mathbf{w}(\hat{\mathbf{p}})^{+}\mathbf{e_n}(\hat{\mathbf{p}}) = d_n \; n = 1, ..., N \tag{3.8}$$

where d_n, $n = 1, .., N$ are desired responses at the constraint points. Note that if $d_1 = 1$, and $\mathbf{e_1}(\hat{\mathbf{p}})$ is chosen such as the only constraint, the resultant processor is same as the MVDR processor.

To determine the weight vector, which has a minimum mean-square response to ambient field with covariance matrix $\mathbf{R}$ while satisfying the above constraints, the Lagrangian cost is written as follows [9]:

$$\Sigma^2 = \mathbf{w}(\hat{\mathbf{p}})^{+}\mathbf{R}(\mathbf{p})\mathbf{w}(\hat{\mathbf{p}}) + \sum_{n=1}^{N} Re[\lambda_n(\mathbf{w}(\hat{\mathbf{p}})^{+}\mathbf{e_n}(\hat{\mathbf{p}}) - d_n)] \tag{3.9}$$

The matrix derivative formulas for the real and imaginary parts can be written as[9]:

$$\frac{\delta\Sigma^2}{\delta\mathbf{w}(\hat{\mathbf{p}})_\mathbf{r}} 2Re[\mathbf{R}(\mathbf{p})\mathbf{w}(\hat{\mathbf{p}})] + \sum_{m=1}^{N} Re[\lambda_m \mathbf{e_m}(\hat{\mathbf{p}})] \tag{3.10}$$

$$\frac{\delta\Sigma^2}{\delta\mathbf{w}(\hat{\mathbf{p}})_\mathbf{i}} 2Im[\mathbf{R}(\mathbf{p})\mathbf{w}(\hat{\mathbf{p}})] + \sum_{m=1}^{N} Im[\lambda_m \mathbf{e_m}(\hat{\mathbf{p}})] \tag{3.11}$$

We define the replica matrix $\mathbf{E}(\hat{\mathbf{p}})$ as a matrix of the N replica vectors for the constraint points ($\mathbf{E}(\hat{\mathbf{p}})$ is an $M \times N$ complex matrix):

$$\mathbf{E}(\hat{\mathbf{p}}) = [\mathbf{e_1}(\hat{\mathbf{p}}); \mathbf{e_2}(\hat{\mathbf{p}}); ...\mathbf{e_N}(\hat{\mathbf{p}})] \tag{3.12}$$

Next we define the Lagrangian multiplier vector λ as:

$$\lambda = \begin{pmatrix} \lambda_1 \\ \lambda_2 \\ . \\ \lambda_N \end{pmatrix}$$

and the constraint column vector $\mathbf{d}$ as:

$$\mathbf{d} = [d_1; d_2; ...d_N] \tag{3.13}$$

If we set derivatives of Lagrangian to zero, we obtain:

$$\mathbf{2R}(\mathbf{p})\mathbf{w}(\hat{\mathbf{p}}) + \mathbf{E}(\hat{\mathbf{p}})\lambda = \mathbf{0} \tag{3.14}$$

Solving this yields, the Lagrangian vector, λ and weight vector $\mathbf{w}(\hat{\mathbf{p}})$ as:

$$\lambda = -\mathbf{2}[\mathbf{E}(\hat{\mathbf{p}})^{+}\mathbf{R}(\mathbf{p})^{-\mathbf{1}}\mathbf{E}(\hat{\mathbf{p}})]^{-\mathbf{1}}\mathbf{d}^{+} \tag{3.15}$$

and

$$\mathbf{w}(\hat{\mathbf{p}}) = \mathbf{R}(\mathbf{p})^{-\mathbf{1}}\mathbf{E}(\hat{\mathbf{p}})[\mathbf{E}(\hat{\mathbf{p}})^{+}\mathbf{R}(\mathbf{p})^{-\mathbf{1}}\mathbf{E}(\hat{\mathbf{p}})]^{-\mathbf{1}}\mathbf{d}^{+} \tag{3.16}$$

where $\mathbf{E}(\hat{\mathbf{p}}) = [\mathbf{e_1}(\hat{\mathbf{p}})...\mathbf{e_N}(\hat{\mathbf{p}})]$ and $\mathbf{d} = [d_1...d_N]$

Using these, the MVDR-NLC beamformer can be found as:

$$P_{mvdr-nlc} = \mathbf{d}[\mathbf{E}(\hat{\mathbf{p}})^{+}\mathbf{R}(\mathbf{p})^{-\mathbf{1}}\mathbf{E}(\hat{\mathbf{p}})]^{-\mathbf{1}}\mathbf{d}^{+} \tag{3.17}$$

The constraints are chosen such that the MVDR-NLC response is equal to that of the Bartlett beamformer in the actual direction and the closest neighbor mainlobe directions, but minimizes the response signals from anywhere else [9]. In order to avoid sidelobes of Bartlett beamformer and have a similar sidelobe response of MVDR, all constraint points are chosen in the Bartlett mainlobe. Since Bartlett weights are replicas of the field, the constraints are assigned the values:

$$d_m = \mathbf{e_1}(\hat{\mathbf{p}})^{+}\mathbf{e_m}(\hat{\mathbf{p}}) \tag{3.18}$$

which are the inner product of the center replica and the replica in the constraint point. The resulting weight vector for the MVDR-NLC processor is found as

$$\mathbf{w}_{mvdr-nlc}(\hat{\mathbf{p}}) = \mathbf{R}(\mathbf{p})^{-\mathbf{1}}\mathbf{E}(\hat{\mathbf{p}})(\mathbf{E}(\hat{\mathbf{p}})^{+}\mathbf{R}(\mathbf{p})^{-\mathbf{1}}\mathbf{E}(\hat{\mathbf{p}}))^{-\mathbf{1}}\mathbf{d} \tag{3.19}$$

By introducing additional constraints, we expand the set of wavefronts considered by the processor as coming from the candidate source location. So MVDR-NLC expands the signal set to include sources in neighboring locations as well. The flowchart for MVDR-NLC can be seen in Figure 3.3.

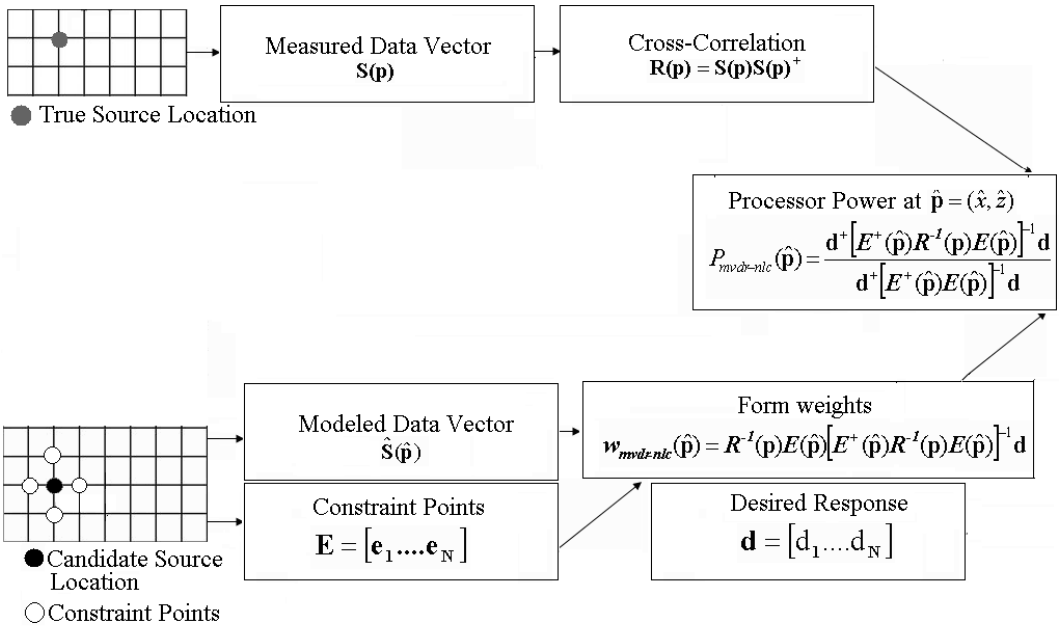

Figure 3.3: The flow chart for MVDR-NLC Matched Field Processor

3.5 MVDR using Environmental Perturbation Constraints

In a work by Krolik [16], a more direct approach is used to reduce the sensitivity of MVDR to sound speed perturbations. Multiple constraints are used to design a beamformer which tolerates acoustic fields resulted from perturbations at the sound speed profiles between source and the receiver. The idea is first to predict pressure fields using a set of perturbed sound speed profiles, and then use these fields to derive constraints to be used in MVDR optimization problem. We first review the perturbation model used by Krolik [16] to develop a model for acoustic wave propagation under environmental uncertainty.

3.5.1 Krolik's Perturbation Model

In order to develop a model for the perturbed pressure fields a normal mode based model is used. Recall that, for a range-independent underwater acoustic environment with deterministic sound velocity $\bar{c}(z)$, the complex pressure at a receiving depth z, generated by a source of frequency ω, and located at range r_s and depth z_s is:

$$p(z, z_s, r_s) = a\sqrt{(2\pi)} \sum_{n=1}^{N} \frac{\bar{\psi}_n(z)\bar{\psi}_n(z_s)}{\sqrt{\bar{k}_n r_s}} e^{j\bar{k}_n r_s} \tag{3.20}$$

where $\bar{\varphi}_n(z)$, $i = 1..N$ are modal eigenfunctions and $\bar{k}_n$, $i = 1..N$ are horizontal wave numbers. The overhead bar indicator is used in (3.20) to indicate that the eigenfunctions and wavenumbers are given for the deterministic channel, $\bar{c}(z)$. If the vertical array has M elements and s_m is the output of the m-th sensor located at depth z_m; the narrowband sensor outputs, $\mathbf{s} = [s_1, ..s_M]^T$ can be given as:

$$s_m = a\sqrt{(2\pi)} \sum_{n=1}^{N} \frac{\bar{\psi}_n(z_m)\bar{\psi}_n(z_s)}{\sqrt{\bar{k}_n r_s}} e^{j\bar{k}_n r_s} + \eta_m \tag{3.21}$$

The $\eta = [\eta_1 ... \eta_M]$ vector represents the random noise at the sensors.

Next a model for the perturbation is developed as given in [16]. Let $c(z, r) = \bar{c}(z) + \Delta c(z, r)$ be the random range dependent sound speed profile and $\Delta c(z, r) << c_0(z)$ is the zero-mean random sound-speed perturbation and $\bar{c}(z)$ is the mean profile, assumed to be known a priori. Under the adiabatic approximation of [12] as summarized in

Appendix 1, the random channel can be expressed as:

$$p(z; r_s, z_s) = a\sqrt{(2\pi)} \sum_{n=1}^{N} \frac{\psi_n(z;0)\psi_n(z_s; r_s)}{\sqrt{k_n(r_s)r_s}} \exp(j \int_0^{r_s} k_n(r)dr) \tag{3.22}$$

where $\psi_n(z;0)$ and $\psi_n(z_s, r_s)$ are range dependent modal eigenfunctions at source and receiver respectively. Furthermore, the local modal eigenfunctions $\psi_n(z;r)$ and horizontal wave numbers $k_n(r)$ satisfy the perturbed Helmholtz equation [16]:

$$\frac{d^2\psi_n}{dz^2} + \{[\bar{k}(z)^2 + \Delta k(z,r)^2] - k_n(r)^2\}\psi_n = 0 \tag{3.23}$$

where

$$\Delta k(z,r)^2 = [(1 + \frac{\Delta c(z,r)}{\bar{c}(z)})^{-2} - 1]\bar{k}(z)^2 \cong -2\frac{\Delta c(z,r)}{\bar{c}(z)}\bar{k}(z)^2 \tag{3.24}$$

The perturbed horizontal wave number can be given as:

$$k_n(r) \cong \bar{k}_n + \Delta k_n(r) \tag{3.25}$$

where

$$\Delta k_n(r) = \frac{-1}{\bar{k}_n} \int_0^{\infty} |\bar{\psi}_n(z)|^2 \frac{\Delta c(z,r)}{\bar{c}(z)} \bar{k}(z)^2 dz \tag{3.26}$$

This yields:

$$p(z; r, z_s) \cong a\sqrt{2\pi} \sum_{n=1}^{N} \frac{\psi_n(z;0)\bar{\psi}_n(z_s)}{\sqrt{\bar{k}_n r_s}} \exp(j\bar{k}_n r_s + j\Delta\theta_n(r_s)) \tag{3.27}$$

where

$$\Delta\theta_n(r_s) = \frac{-1}{\bar{k}_n} \int_0^{\infty} \frac{|\bar{\psi}_n(z)|^2[\bar{k}(z)]^2}{\bar{c}(z)} \bar{\Delta}c(z, r_s)dz \tag{3.28}$$

whereas

$$\tilde{\Delta}c(z, r_s) = \int_0^{r_s} \Delta c(z,r)dr \tag{3.29}$$

is the range integrated sound perturbation.

The expression above shows that the phase perturbations caused by random perturbations can be given as a function of variations in the sound speed profile integrated over range and depth.

As shown in Krolik [16], $\Delta c(z,r)$ can be written in terms of empirical orthogonal functions, $\varphi_l(z)$ so that

$$\Delta c(z,r) = \sum_{l=1}^{L} g_l(r)\varphi_l(z) \tag{3.30}$$

where the $g_l(r)$ are zero mean random processes that describes the range dependence of the perturbation. $\varphi_l(z)$ are empirical orthogonal functions that can be derived from real data statistics. The range dependent perturbation can be written as a range integrated term as follows [16]:

$$\tilde{\Delta}c(z,r) = \sum_{l=1}^{L} \tilde{g}_l(r)\varphi_l(z) \tag{3.31}$$

where range dependency is included in the integrated term:

$$\tilde{g}_l(r_s) = \int_0^{r_s} g_l(r)dr \tag{3.32}$$

Note that $\tilde{g}_l(r_s)$ has approximately a Gaussian distribution independent of the distribution of $g_l(r)$ if the source range is large.

3.5.2 Derivation of MVDR-EPC

Using this model for the uncertainty in acoustic waveguide, instead of MVDR-Neighboring Location Constraints Processor, a processor that uses a more direct approach for reducing sensitivity to mismatch of MVDR can be developed. Here we summarize the derivation of MVDR-EPC as given in [16].

Let $\bar{\mathbf{g}}(\xi, r_s) = [\bar{g}_1(\xi, r_s)...\bar{g}_L(\xi, r_s)]$ be the vector of sound speed perturbation coefficients, where the outcome of ξ results in a realization of $\tilde{\Delta}c(z, r_s)$. Using different outcomes, it is possible to model approximately all set of possible signal wave-front vectors for a candidate source location. Let this set be $\mathbf{g}(\xi_1, r_s), ..., \mathbf{g}(\xi_K, r_s)$. Using a similar approach to the one in MVDR-NLC, a constraint matrix based on sound-speed perturbations can be given by

$$\mathbf{P} = [\hat{\mathbf{S}}(\hat{\mathbf{p}}, \mathbf{g}(\xi_\mathbf{1}))...\hat{\mathbf{S}}(\hat{\mathbf{p}}, \mathbf{g}(\xi_\mathbf{K}))] \tag{3.33}$$

The set of constraint equations for the MVDR method with sound speed perturbation constraints can be expressed as:

$$\mathbf{P}(\hat{\mathbf{p}})^{+}\mathbf{w}(\hat{\mathbf{p}}) = \mathbf{q} \tag{3.34}$$

where the elements of $\mathbf{q}$ are the desired response at each constraint point.

It is shown in [16] that the random signal wavefronts created by the perturbations in sound speed profile are highly correlated. This correlation of random signal wavefront

makes the columns of $\mathbf{P}(\hat{\mathbf{p}})$ very nearly dependent and it makes it possible to decrease the number of constraints and increase the degree of freedom.

This dependency of the columns of $\mathbf{P}(\hat{\mathbf{p}})$ brings the advantage that instead of introducing K constraints, by using a singular value decomposition number of constraints can be reduced. In other words, by selecting the minimum J vectors that span the column space of $\mathbf{P}(\hat{\mathbf{p}})$, the number of degrees of freedom can be increased.

The approximate singular value decomposition (best rank J approximation) of $\mathbf{P}(\hat{\mathbf{p}})$ can be given as:

$$\mathbf{P}(\hat{\mathbf{p}}) = \mathbf{H}(\hat{\mathbf{p}})\mathbf{\Lambda}(\hat{\mathbf{p}})\mathbf{\Gamma}(\hat{\mathbf{p}})^{+} \tag{3.35}$$

where $\mathbf{H}(\hat{\mathbf{p}})$ is a $M \times J$ matrix whose columns are the largest left singular vectors of $\mathbf{P}(\hat{\mathbf{p}})$, $\mathbf{\Lambda}(\hat{\mathbf{p}})$ is a $J \times J$ diagonal matrix of the largest singular values of $\mathbf{P}(\hat{\mathbf{p}})$ and $\mathbf{\Gamma}(\hat{\mathbf{p}})$ is a $K \times J$ matrix whose columns are the largest right singular vectors of $\mathbf{P}(\hat{\mathbf{p}})$. Using this decomposition, we can write the constraints as:

$$\mathbf{H}(\hat{\mathbf{p}})^{+}\mathbf{w}(\hat{\mathbf{p}}) = \mathbf{\Lambda}(\hat{\mathbf{p}})^{-\mathbf{1}}\mathbf{\Gamma}(\hat{\mathbf{p}})^{+}\mathbf{q} \tag{3.36}$$

Recall that the weight vector for MVDR-NLC for multiconstraints is given as:

$$\mathbf{w}_{mvdr-nlc}(\hat{\mathbf{p}}) = \mathbf{R}(\mathbf{p})^{-\mathbf{1}}\mathbf{E}(\hat{\mathbf{p}})[\mathbf{E}(\hat{\mathbf{p}})^{+}\mathbf{R}(\mathbf{p})^{-\mathbf{1}}\mathbf{E}(\hat{\mathbf{p}})]^{-\mathbf{1}}\mathbf{d}^{+} \tag{3.37}$$

where $\mathbf{E}(\hat{\mathbf{p}})$ are the set of constraints and $\mathbf{d}$ are the desired response at each constraint point. Similar to this, the beamformer weight vector for the MVDR method with environmental perturbation constraints is given by [16]:

$$\mathbf{w}_{mvdr-epc}(\hat{\mathbf{p}}) = \mathbf{R}(\mathbf{p})^{-\mathbf{1}}\mathbf{H}(\hat{\mathbf{p}})(\mathbf{H}(\hat{\mathbf{p}})^{+}\mathbf{R}(\mathbf{p})^{-\mathbf{1}}\mathbf{H}(\hat{\mathbf{p}}))^{-\mathbf{1}}\mathbf{\Lambda}(\hat{\mathbf{p}})^{-\mathbf{1}}\mathbf{\Gamma}(\hat{\mathbf{p}})^{+}\mathbf{q} \tag{3.38}$$

Here it is important to observe the similarities and differences between the MVDR-NLC and MVDR-EPC processors. The both processors are multiconstraint processors and the idea to use multiconstraints comes from the desire to tolerate the environmental mismatches. MVDR-NLC uses neighboring points to form the wave fields that forms the constraint matrix in the way that wave fields are formed as if the signal is coming from a neighboring point. On the other hand, MVDR-EPC uses the possible sound speed perturbations and the resultant wave fields to form the constraint matrix.

Next we find the desired response at each constraint point. Note that the desired response and the beamformer weight vector which results for the spatially uncorrelated noise only situation (the quiescent weight vector, $\mathbf{w^q_{mvdr-epc}}$) are related by:

$$\mathbf{P}(\hat{\mathbf{p}})^{+}\mathbf{w^q_{mvdr-epc}}(\hat{\mathbf{p}}) = \mathbf{q} \text{ and } \mathbf{w^q_{mvdr-epc}}(\hat{\mathbf{p}}) = \mathbf{P}(\hat{\mathbf{p}})(\mathbf{P}(\hat{\mathbf{p}})^{+}\mathbf{P}(\hat{\mathbf{p}}))^{-1}q \tag{3.39}$$

If $\mathbf{w^q_{mvdr-epc}}(\hat{p})$ is chosen to maximize average gain $G = \frac{\mathbf{w^{q^+}_{mvdr-epc}}(\hat{\mathbf{p}})\mathbf{R_s}(\mathbf{p})\mathbf{w^q_{mvdr-epc}}(\hat{\mathbf{p}})}{\mathbf{w^{q^+}_{mvdr-epc}}(\hat{\mathbf{p}})\mathbf{w^q_{mvdr-epc}}(\hat{\mathbf{p}})}$, where $\mathbf{R_s}$ is the expected cross-spectra matrix where the expectation is taken over perturbations, the desired response of the MVDR-EPC beamformer is given by

$$\mathbf{q} = \mathbf{P}(\hat{\mathbf{p}})^{+}\mathbf{h_1}(\hat{\mathbf{p}}) \tag{3.40}$$

where $\mathbf{h_1}(\hat{\mathbf{p}})$ is the first column of $\mathbf{H}(\hat{\mathbf{p}})$. Thus we can write:

$$\mathbf{H}(\hat{\mathbf{p}})^{+}\mathbf{w}(\hat{\mathbf{p}}) = \mathbf{H}(\hat{\mathbf{p}})^{+}\mathbf{h_1}(\hat{\mathbf{p}}) = \mathbf{e_1} \tag{3.41}$$

where $\mathbf{e_1} = [1, 0...0]^T$. This yields

$$\mathbf{w}_{mvdr-epc}(\hat{\mathbf{p}}) = \mathbf{R}(\mathbf{p})^{-1}\mathbf{H}(\hat{\mathbf{p}})(\mathbf{H}(\hat{\mathbf{p}})^{+}\mathbf{R}(\mathbf{p})^{-1}\mathbf{H}(\hat{\mathbf{p}}))^{-1}\mathbf{e_1} \tag{3.42}$$

The resulting ambiguity surface can be given by:

$$P_{mvdr-epc} = \mathbf{e_1^+}(\mathbf{H^+R^{-1}H})^{-1}\mathbf{e_1} \tag{3.43}$$

The flowchart for MVDR-EPC can be seen in Figure 3.4.

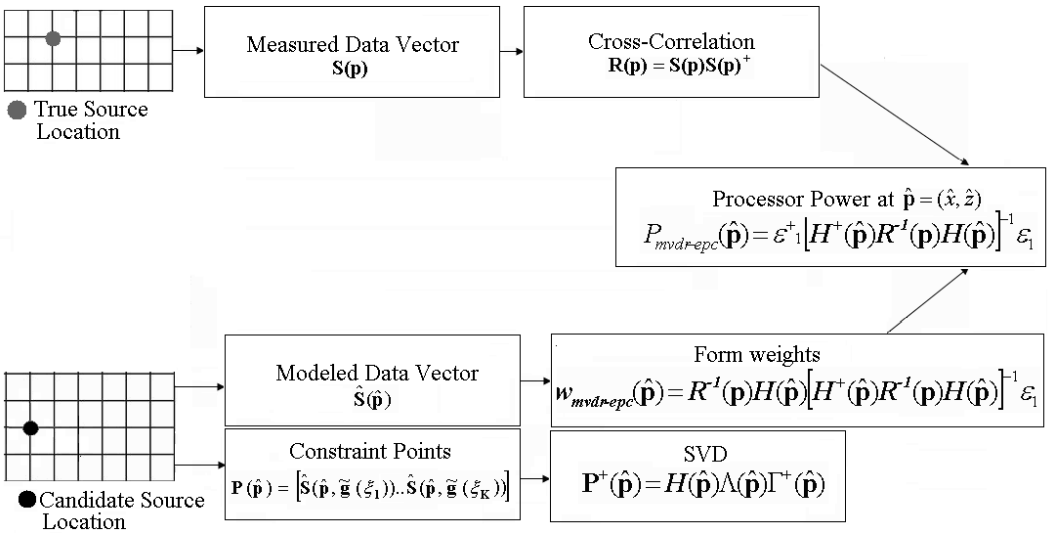

Figure 3.4: The flow chart for MVDR-EPC Matched Field Processor

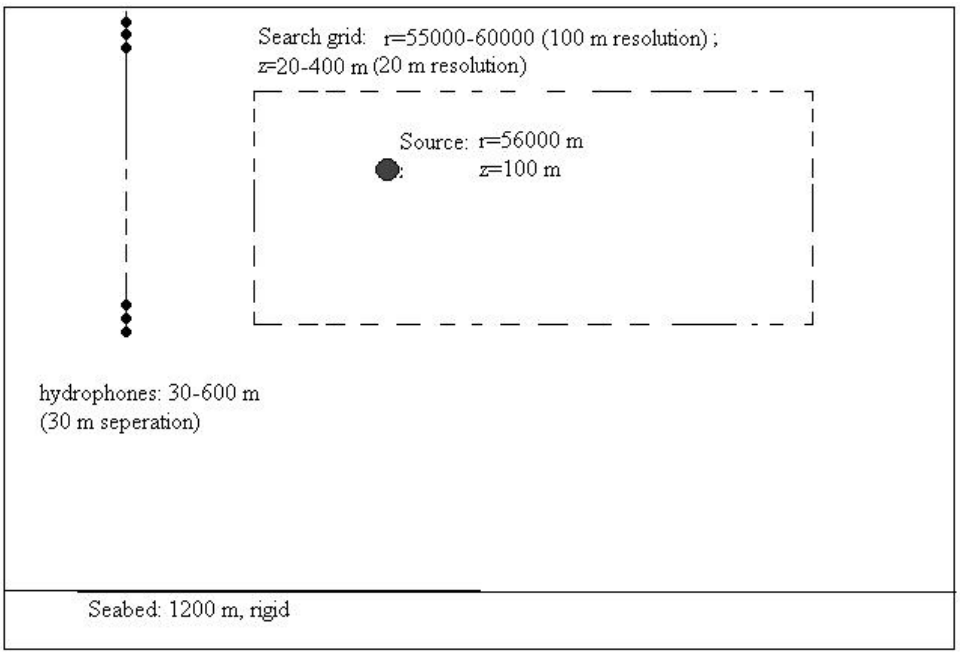

Figure 3.5: The scenario considered for the narrowband examples

3.6 Narrowband Examples

In order to illustrate and compare performances of narrowband matched field processors, a deep-water case is considered in the following simulation experiments. We give some examples of the applications of Matched Field Processing and observe some specific features of the most common Matched Field Processors: the Linear Processor, the Minimum Variance Distortionless Response Processor (MVDR), MVDR with Neighboring Location Constraints (MVDR-NLC), and MVDR with Environmental Perturbation Constraints (MVDR-EPC).

To begin with, let us consider the following scenario (Figure 3.5): A source with frequency 20 Hz and depth 100m is in a range-independent underwater environment of constant depth of 1200m. Let us also assume that at 56000 meters distance from the source, there is an array of 20 elements with an interelement distance of 30m.

We consider the sound speed profile as the Munk profile. The Munk profile is an idealized sound speed profile given by:

$$c(z) = 1500(1 + \epsilon(\bar{z} - 1 + e^{\bar{z}})) \tag{3.44}$$

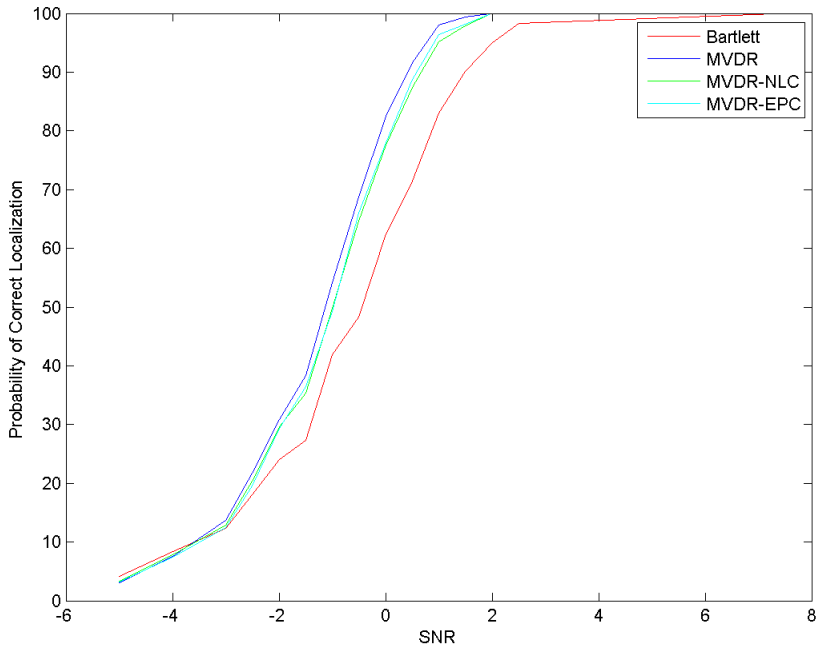

Figure 3.6: The probability of correct localizations for Bartlett, MVDR, MVDR-NLC and MVDR-EPC processors for no mismatch case

The quantity epsilon is given by

$$\epsilon = 0.00737 \tag{3.45}$$

whereas scaled depth is given by:

$$\bar{z} = \frac{2(z - 1300)}{1300} \tag{3.46}$$

The search grid is taken as between 55000 and 60000 meters for range with 100 meter resolution and between 20 and 400 meters with 20 meter resolution.

First, we evaluate the correct localization performances of the four processors for different ambient noise levels and for the case of perfectly known environment, i.e. there is no mismatch. The probability of correct localizations for different processors is given in Table 3.1 and in Figure 3.6. Also for a sample case of SNR 2 dB, ambiguity surfaces are given in Figures 3.7, 3.8, 3.9 and 3.10.

Table 3.1: The probability of correct localizations for Bartlett, MVDR, MVDR-NLC and MVDR-EPC processors for the no mismatch case

SNR	$Bartlett$	$MVDR$	$MVDR-NLC$	$MV-EPC$
7.5	100	100	100	100
2.5	98.3	100	100	100
2	95	100	100	100
1.5	90.1	99.4	97.9	98.2
1	83	98.0	95.1	96.4
0.5	71.4	91.6	87.4	88.8
0	62.4	82.5	77.6	78
-0.5	48.3	68.7	64.6	66
-1	41.9	54.2	49.8	49.3
-1.5	27.3	38.3	35.4	36.4
-2	24	30.9	29.6	29.3
-2.5	18.1	21.7	20.3	19.5
-3	12.3	13.7	12.9	12.4
-4	8.4	7.5	7.8	7.4
-5	4.1	3	3.4	3.2

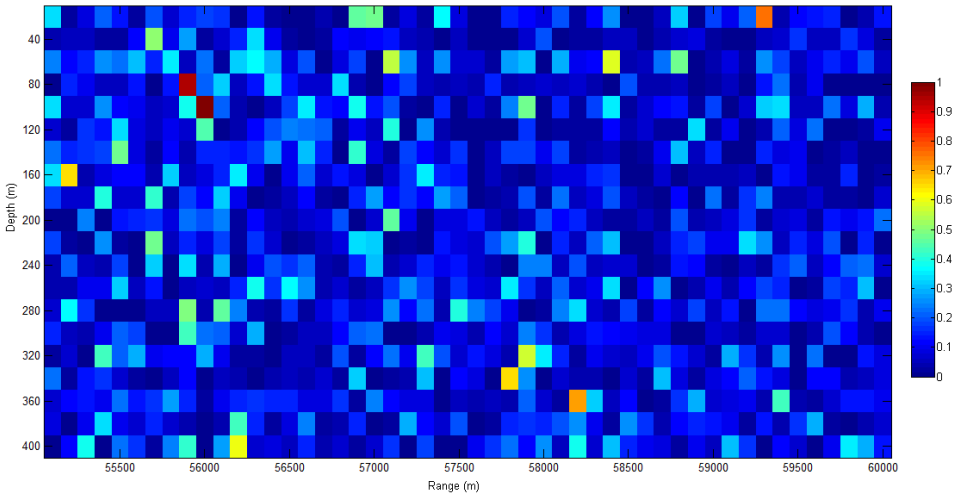

Figure 3.7: Ambiguity Surface for the Bartlett Processor, no mismatch, SNR 2 dB

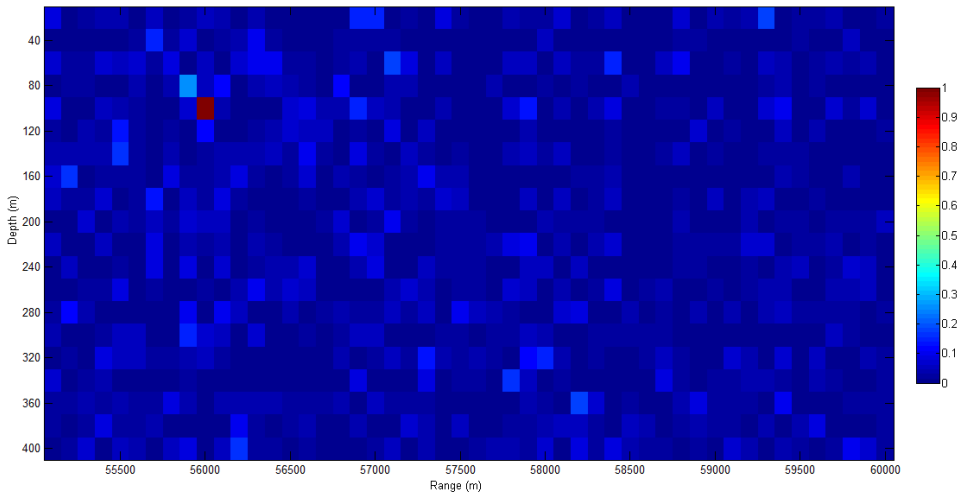

Figure 3.8: Ambiguity Surface for the MVDR Processor, no mismatch, SNR 2 dB

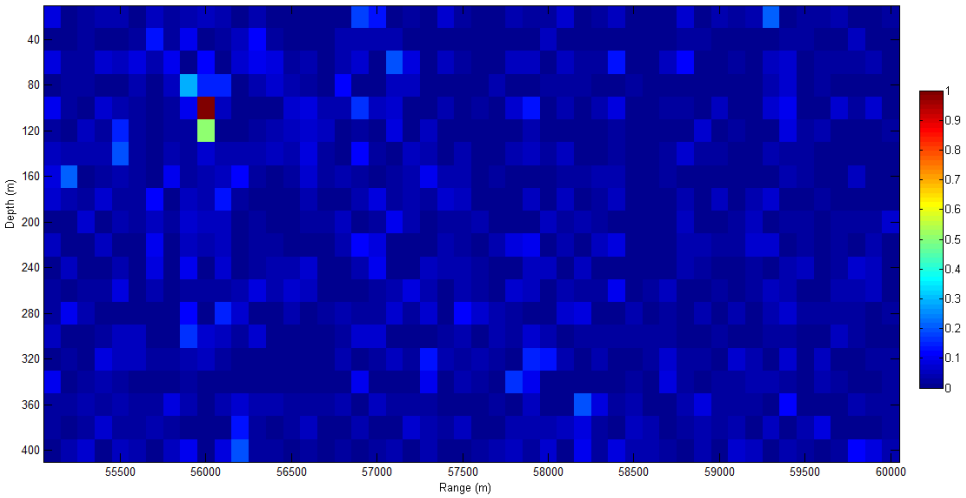

Figure 3.9: Ambiguity Surface for the MVDR-NLC Processor, no mismatch, SNR 2 dB

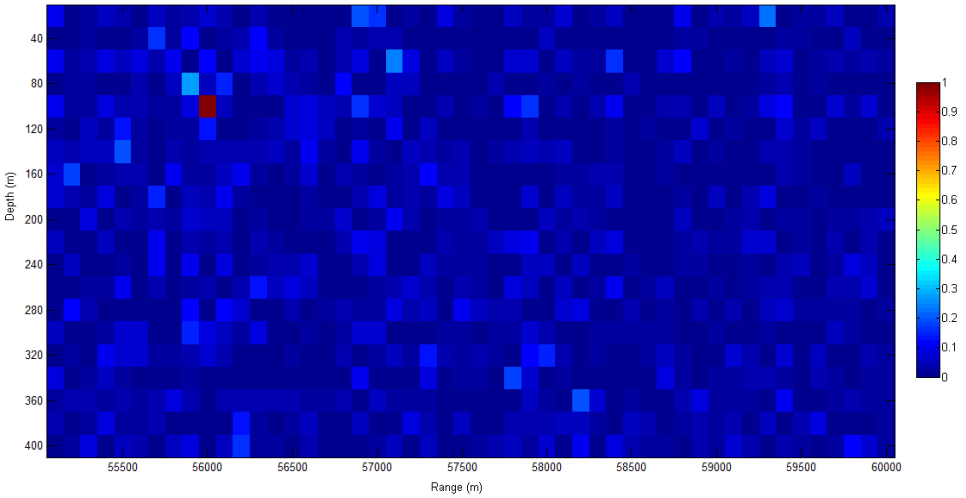

Figure 3.10: Ambiguity Surface for the MVDR-EPC Processor, no mismatch, SNR 2 dB

We see that among all processors, MVDR has the best performance for no perturbation case. This is as expected as MVDR has the highest resolution and best sidelobe suppression. As SNR level goes lower, the performance of Bartlett processors gets worse, because of the sidelobe problem. The MVDR-NLC and MV-EPC processors have a performance between Bartlett and MVDR processors. This is due to the fact that these processors are designed to have a wider mainlobe than MVDR (similar to Bartlett) and to have a MVDR type sidelobe suppression.

Next, we consider the perturbation case. As the perturbation model, we consider a very similar model to the model as given in [16]. The empirical orthogonal functions are given in Figure 3.11 which is taken from [16]. Corresponding $g_l(r)$ are chosen as uniformly distributed random variables on $(-\gamma_l, \gamma_l)$ where $\gamma_l = \sqrt{3}\sigma_l$ with $\sigma_1^2 = 376.8$ and $\sigma_2^2 = 56$ as in [16].

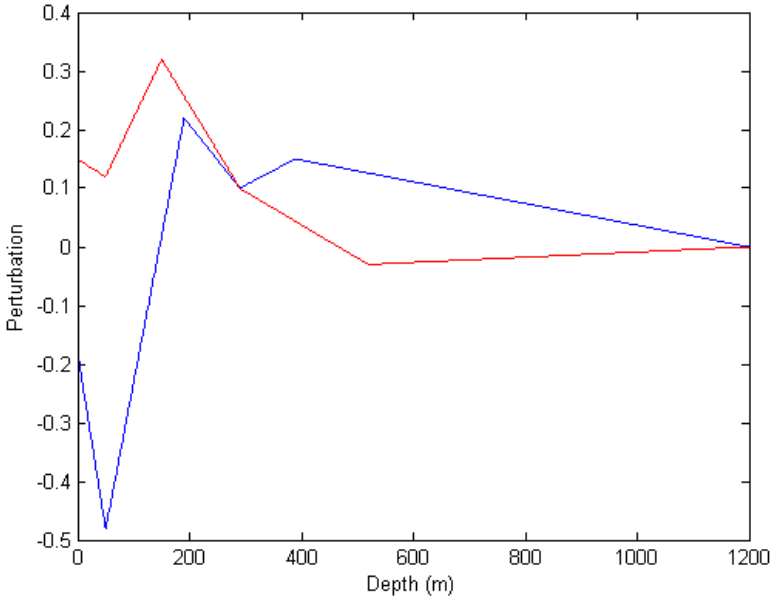

Figure 3.11: Empirical Orthogonal Functions to Create Perturbations

Table 3.2: The probability of correct localizations for Bartlett, MVDR, MVDR-NLC and MVDR-EPC processors under mismatch

SNR	$Bartlett$	$MVDR$	$MVDR-NLC$	$MV-EPC$
7.5	37.7	38	69.5	95.5
2.5	32.4	36	51.3	61.1
2	33.6	39.2	50.1	57.8
1.5	28.2	34.7	44.8	48.2
1	24.4	31.7	38.6	42.7
0.5	22.6	30.1	36.3	39.9
0	19	26	28.3	30.8
-0.5	15.7	19.7	22.4	22.9
-1	12.1	16.8	17.3	20
-1.5	10.2	12.7	13.5	13.7
-2	8.4	10.4	12	11.7
-2.5	5.6	5.8	6	6.2
-3	5.2	4.9	4.3	4.7
-4	3.2	3.2	3.1	3.4
-5	1.8	1.6	1.5	1.1

It is possible to observe the effect of random sound speed perturbations by analyzing the ambiguity surfaces give in Figures 3.13 to 3.16 and probability of correct localizations given in Table 3.2 and Figure 3.12 under mismatch. We see that the high resolution property of MVDR is now a disadvantage because it cannot tolerate the move of peak from correct position, and the processors with wider mainlobes, such as MVDR-NLC and MV-EPC, have better performances. It can be observed that MV-EPC has a better sidelobe suppression due to the fact that it directly considers the perturbations generating its constraints.

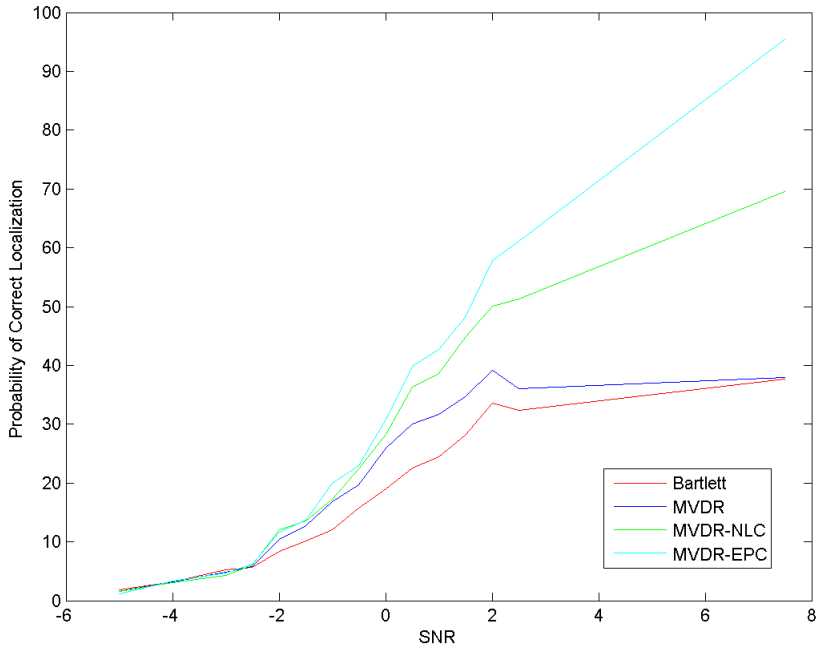

Figure 3.12: The probability of correct localizations for Bartlett, MVDR, MVDR-NLC and MVDR-EPC processors under mismatch

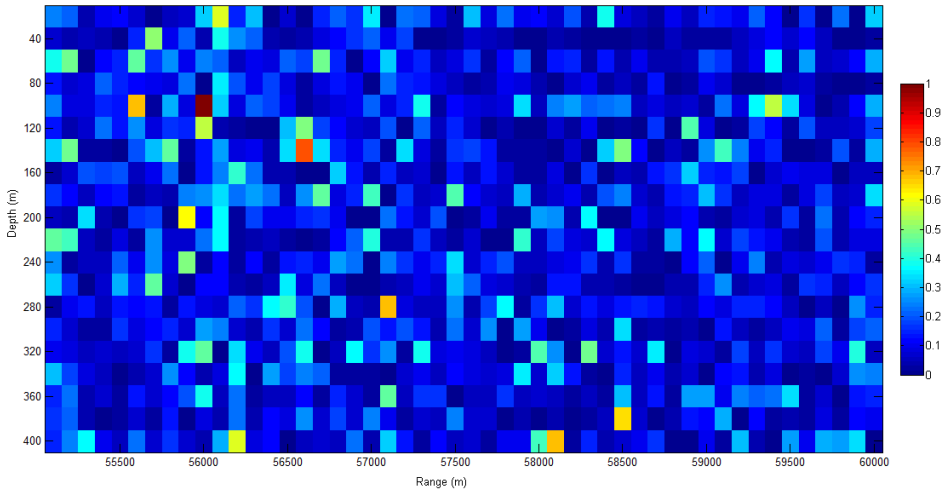

Figure 3.13: Ambiguity Surface for the Bartlett Processor, under mismatch, SNR 2 dB

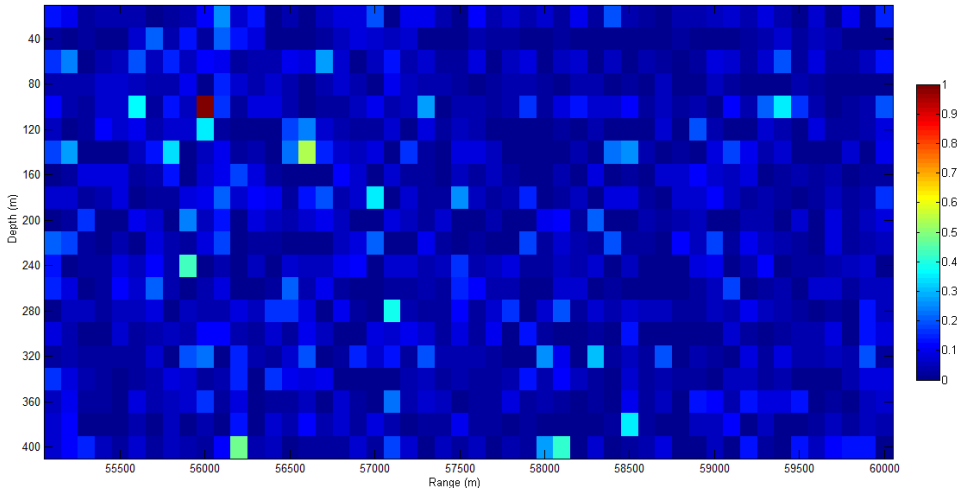

Figure 3.14: Ambiguity Surface for the MVDR Processor, under mismatch, SNR 2 dB

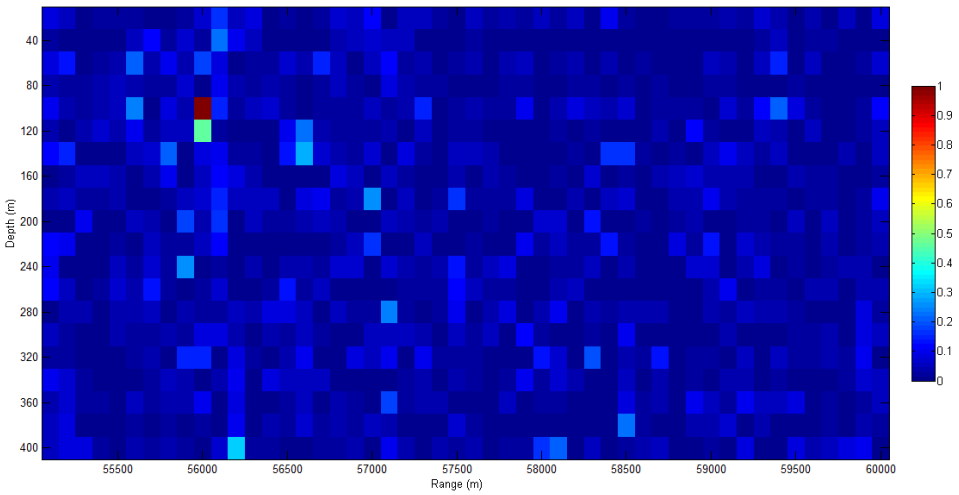

Figure 3.15: Ambiguity Surface for the MVDR-NLC Processor, under mismatch, SNR 2 dB

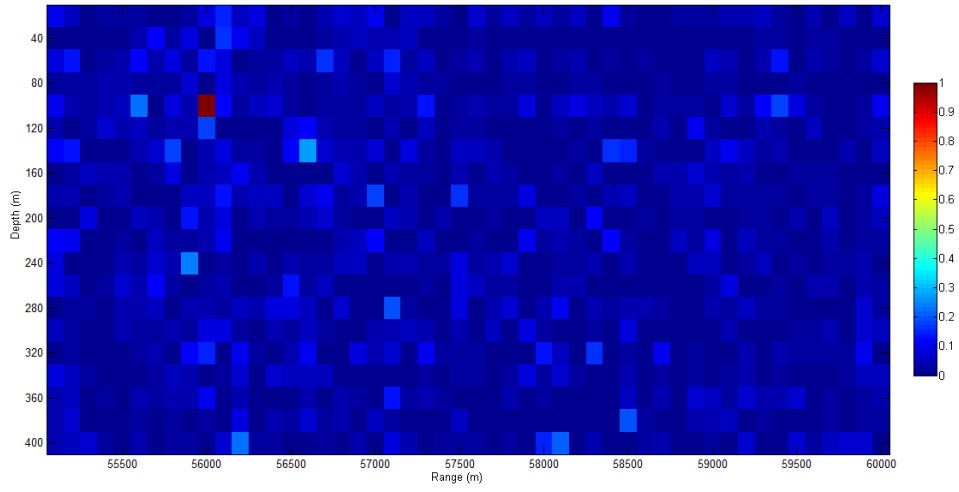

Figure 3.16: Ambiguity Surface for the MVDR-EPC Processor, under mismatch, SNR 2 dB

CHAPTER 4

BROADBAND MATCHED FIELD PROCESSING

4.1 Introduction to Broadband Matched Field Processing

Traditionally, matched field processing has been applied to problems involving single frequency (narrowband) sources. However, the shift of academic and commercial interest from deep water problems to shallow water problems has emerged an interest in broadband techniques. Shallow water scenarios have created the need of the usage of broadband techniques to increase the amount of information available. The usage of broadband techniques has increased the robustness by making use of multifrequency information.

There are two main approaches to broadband MFP methods. These are incoherent and coherent approaches. We briefly explain these methods.

4.2 Incoherent Broadband MFP

Incoherent Broadband MFP was first proposed by Baggeroer et al [8]. To apply the incoherent broadband processor of Baggeroer, for each frequency component of the source, ambiguity surfaces are separately generated and then these surfaces are averaged in a linear or logarithmic fashion. In mathematical terms, if $P(\hat{\mathbf{p}}, \mathbf{f})$ is the matched field processor (e.g. Bartlett, MVDR etc.) output for the frequency f, $f = 1, ..., K$, the linear incoherent broadband MFP output can be given by:

$$P_{incoherent.broadband}(\hat{\mathbf{p}}) = \sum_{f=1}^{K} P(\hat{\mathbf{p}}, f) \tag{4.1}$$

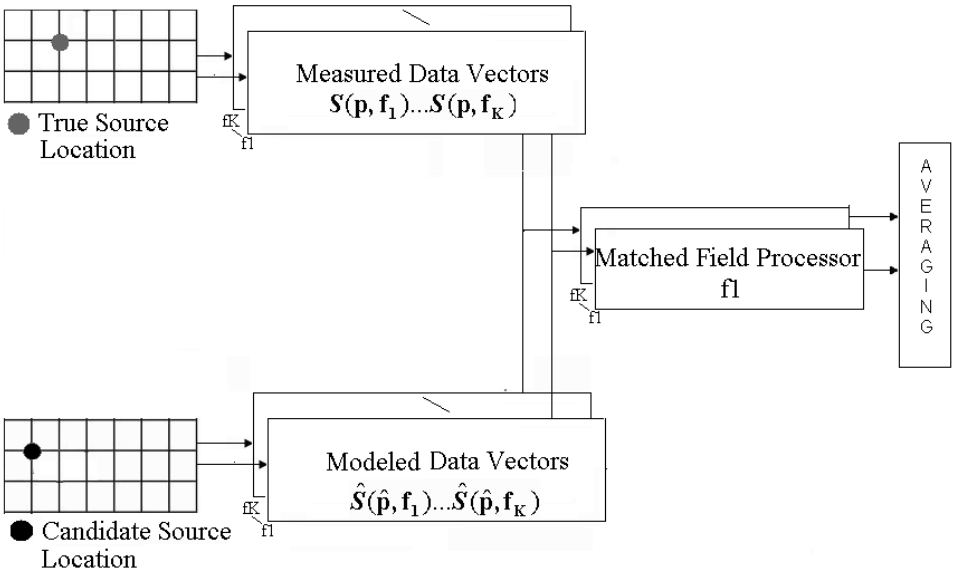

Figure 4.1: The flow chart for Incoherent Broadband Matched Field Processor

The idea behind incoherent MFP is to suppress random sidelobe energy while reinforcing the energy at the true source location. The flowchart for Incoherent Broadband Processor can be seen in Figure 4.1.

4.3 Tolstoy/Michalopoulo's Coherent Broadband MFP

Although the incoherent broadband MFP considers the spatial coherence of the acoustic field along the array of hydrophones, the averaging of the ambiguity surfaces is performed incoherently across the frequencies. However, it is known that spatial coherence exists across frequencies as well [14]. In order to exploit the information across frequency and space at the same time, coherent broadband matched field processors have been introduced.

A coherent approach to broadband matched field processing was first introduced by Tolstoy [13]. In coherent MFP, the measured data vectors at different frequencies are concatenated to form supervectors. If there are N hydrophones and K frequencies, a data vector of size $N \times K$ is formed. Similarly, modeled data vectors are concatenated to form supervectors. Then these supervectors of measured and modeled data are used in matched field processors such as Bartlett or MVDR to form the ambiguity

surfaces. In more formal terms; let $\mathbf{w}(\hat{\mathbf{p}}, f)$ be the weight vector for frequency f, then a super weight vector $\mathbf{w}_{super}(\hat{\mathbf{p}})$ can be formed as follows:

$$\mathbf{w_{super}}(\hat{\mathbf{p}}) = \begin{pmatrix} \mathbf{w}(\hat{\mathbf{p}}, 1) \\ \mathbf{w}(\hat{\mathbf{p}}, 2) \\ . \\ \mathbf{w}(\hat{\mathbf{p}}, K) \end{pmatrix}$$

Similarly, let $\mathbf{S}(\mathbf{p}, f)$ be the measurement vector for frequency f, then a super measurement vector $\mathbf{S}_{super}(\mathbf{p})$ can be formed as follows

$$\mathbf{S}(\mathbf{p}) = \begin{pmatrix} \mathbf{S}(\mathbf{p}, 1) \\ \mathbf{S}(\mathbf{p}, 2) \\ . \\ \mathbf{S}(\mathbf{p}, K) \end{pmatrix}$$

These vectors can be used in any type of processors as described in Narrowband Matched Field Processing section, such as Bartlett and MVDR processors. For example, if Bartlett MFP is used broadband coherent MFP can be expressed as:

$$P_{coherent.broadband}(\hat{\mathbf{p}}) = \mathbf{w}_{super}(\hat{\mathbf{p}})\mathbf{R}_{super}(\mathbf{p})\mathbf{w}_{super}(\hat{\mathbf{p}}) \tag{4.2}$$

where

$$\mathbf{R}_{super}(\mathbf{p}) = \mathbf{S}^{+}_{super}(\mathbf{p})\mathbf{S}_{super}(\mathbf{p}) \tag{4.3}$$

The flowchart for this processor can be seen in Figure 4.2.

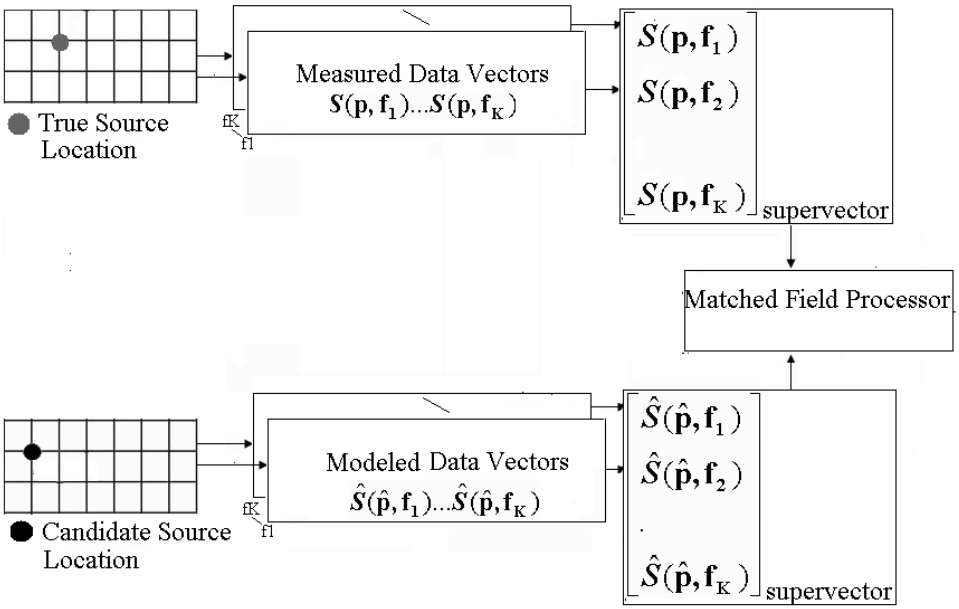

Figure 4.2: The flow chart for Tolstoy/Michalopoulou coherent Broadband Matched Field Processor

In order to get meaningful results using the processor described by Tolstoy the knowledge of the source spectrum, i.e. knowledge of the phase components of the signal, is required. To overcome this difficulty, Michalopoulo has suggested a coherent MFP that does not require source spectrum information [14].

To improve the estimation of the received signal term independent of the source spectrum, Michalopoulo suggested the normalization scheme that before the concatenation of the acoustic field vectors, all data vectors at individual frequencies are normalized with respect to an estimation for the phase at the first hydrophone. To estimate the phase at the first hydrophone, the exponentiated phases of the received vector measurements are averaged and the phase corresponding to the average value at the first hydrophone is extracted [14].

In Michalopoulo's work, comparison of incoherent and coherent Bartlett processors show that for relatively low SNR values, probability of correct localization is higher when coherent broadband MFP is used. Also it is seen that when fewer number of hydrophones are used, the benefit of using coherent MFP is more substantial. This can be explained by the fact that, coherent processor spatially interpolates the array and obtains more spatial samples than the incoherent processor [14].

To understand this issue further, let us consider the simplest case of two frequencies and two hydrophones:

The received signal at first hydrophone will have two components: $S_{11} = A_{11}e^{j(\phi_1+\phi_{11})}$ and $S_{12} = A_{12}e^{j(\phi_2+\phi_{12})}$. Similarly, the received signal at second hydrophone has two components: $S_{21} = A_{21}e^{j(\phi_1+\phi_{21})}$ and $S_{22} = A_{22}e^{j(\phi_2+\phi_{22})}$. Here S_{ij} denotes the signal corresponding to the i-th hydrophone and j-th frequency. ϕ_i is the initial phase for the first frequency and ϕ_{ij} is the phase introduced for the i-th frequency between source and the hydrophone j.

The modeled signal at first hydrophone will have the following components: $\hat{S_{11}} = \hat{A_{11}}e^{j(\hat{\phi_{11}})}$ and $\hat{S_{12}} = A_{12}e^{j(\hat{\phi_{12}})}$. In the same manner, the received signal at second hydrophone has two components: $\hat{S_{21}} = A_{21}e^{j(\hat{\phi_{21}})}$ and $\hat{S_{22}} = A_{22}e^{j(\hat{\phi_{22}})}$. Here, the hat denotes that the corresponding value has been found for a candidate source location.

Let us first consider the incoherent broadband MFP case. If the noise is ignorable,

the processor output for a candidate location will be:

$$P_{inc} = C_1 + C_2 e^{\phi_{21} - \hat{\phi_{21}} + \hat{\phi_{11}} - \phi_{11}} + C_3 e^{\phi_{11} - \hat{\phi_{11}} + \hat{\phi_{21}} - \phi_{21}} + C_4 e^{\phi_{22} - \hat{\phi_{22}} + \hat{\phi_{12}} - \phi_{12}} + C_5 e^{\phi_{12} - \hat{\phi_{12}} + \hat{\phi_{22}} - \phi_{22}}.$$

where C_i are coefficients.

Next we consider the coherent broadband MFP without normalization. The processor output is given by:

$$\begin{aligned} P_{coh} = C_1 &+ C_2 e^{\phi_{21} - \hat{\phi_{21}} + \hat{\phi_{11}} - \phi_{11}} + C_3 e^{\phi_2 - \phi_1 + \phi_{12} - \hat{\phi_{12}} + \hat{\phi_{11}} - \phi_{11}} \\ &+ C_4 e^{\phi_2 - \phi_1 + \phi_{22} - \hat{\phi_{22}} + \hat{\phi_{11}} - \phi_{11}} + C_5 e^{\phi_{11} - \hat{\phi_{11}} + \hat{\phi_{21}} - \phi_{21}} \\ &+ C_6 e^{\phi_2 - \phi_1 + \phi_{12} - \hat{\phi_{12}} + \hat{\phi_{21}} - \phi_{21}} + C_7 e^{\phi_2 - \phi_1 + \phi_{22} - \hat{\phi_{22}} + \hat{\phi_{21}} - \phi_{21}} \\ &+ C_8 e^{\phi_1 - \phi_2 + \phi_{11} - \hat{\phi_{11}} + \hat{\phi_{12}} - \phi_{12}} + C_9 e^{\phi_1 - \phi_2 + \phi_{21} - \hat{\phi_{21}} + \hat{\phi_{12}} - \phi_{12}} \\ &+ C_{10} e^{\phi_{22} - \hat{\phi_{22}} + \hat{\phi_{12}} - \phi_{12}} + C_{11} e^{\phi_1 - \phi_2 + \phi_{11} - \hat{\phi_{11}} + \hat{\phi_{22}} - \phi_{22}} \\ &+ C_{12} e^{\phi_1 - \phi_2 + \phi_{21} - \hat{\phi_{21}} + \hat{\phi_{22}} - \phi_{22}} + C_{13} e^{\phi_{12} - \hat{\phi_{12}} + \hat{\phi_{22}} - \phi_{22}} \end{aligned}$$

If normalization is applied, the processor output takes the form:

$$\begin{aligned} P_{mcoh} = C_1 &+ C_2 e^{\phi_{21} - \hat{\phi_{21}} + \hat{\phi_{11}} - \phi_{11}} + C_3 e^{\phi_{22} - \hat{\phi_{22}} + \hat{\phi_{12}} - \phi_{12}} \\ &+ C_4 e^{\phi_{11} - \hat{\phi_{11}} + \hat{\phi_{21}} - \phi_{21}} + C_5 e^{\phi_{12} - \hat{\phi_{12}} + \hat{\phi_{21}} - \phi_{21}} \\ &+ C_6 e^{\phi_{22} - \hat{\phi_{22}} + \hat{\phi_{12}} - \phi_{12} + \hat{\phi_{21}} - \phi_{21} + \hat{\phi_{11}} - \phi_{11}} \\ &+ C_7 e^{\phi_{21} - \hat{\phi_{21}} + \hat{\phi_{11}} - \phi_{11}} + C_8 e^{\phi_{22} - \hat{\phi_{22}} + \hat{\phi_{12}} - \phi_{12}} \\ &+ C_9 e^{\phi_{12} - \hat{\phi_{12}} + \hat{\phi_{22}} - \phi_{22}} \\ &+ C_{10} e^{\phi_{21} - \hat{\phi_{21}} + \hat{\phi_{11}} - \phi_{11} + \hat{\phi_{22}} - \phi_{22} + \hat{\phi_{12}} - \phi_{12}} \\ &+ C_{11} e^{\phi_{12} - \hat{\phi_{12}} + \hat{\phi_{22}} - \phi_{22}} \end{aligned}$$

If the processor outputs for the incoherent case and the normalized coherent case are compared, it can be seen that the normalized coherent processor includes a larger number of terms to estimate the relevance between modeled and measured data. So a mismatch between modeled and measured data causes a lesser degradation in processor output which makes normalized coherent processor more robust [14].

On the other hand, when the number of hydrophones increases the performance of coherent processor degrades [14]. This degradation appears due to the problems in the estimation of the coherent cross-spectral density matrix [14].

4.4 Brodband MFP with Environmental Perturbation Constraints

In order to tolerate the environmental uncertainties, Czenszak and Krolik introduced another coherent broadband technique in [17]. This technique differs from the one suggested in Michalopoulou's work ([14]) in two senses. Firstly, it considers the localization of broadband random sources with uncorrelated frequency components. Secondly, instead of computing the similarity between measured data and modeled data, it matches the cross-spectral density matrix of the measured data with a weight matrix.

The signal and the perturbation model is the same as used in [16] generalized to multi-frequency cases. Again using an adiabatic normal mode solution to the wave equation (as explained in Appendix), the complex Fourier series coefficient at frequency ω_l of the field measured at depth z from a distant source at range r_s and depth z_s can be expressed as:

$$p(z; r_s, z_s, \omega_l) = a(\omega_l)\sqrt{2\pi} \sum_{n=1}^{N(\omega_l)} \frac{\phi_n(z,0)\phi_n(z_s)}{\sqrt{k_n r_s}} e^{-jk_n r_s} \tag{4.4}$$

where $k_n = (1/r_s)\int_0^{r_s} k_n(r)dr$, for $n = 1....N(\omega_l)$ are the range dependent modal horizontal wave numbers, while $\phi_n(z_s)$ and $\phi_n(z,0)$ are the modal depth eigenfunctions at the source and receiver, respectively. The parameter $N(\omega_l)$ is the number of modes and the complex scalar, $a(\omega_l)$, is the source amplitude and phase at frequency ω_l. Here there is the key assumption that the source and noise considered are broadband zero mean random processes, i.e. the $a(\omega_l)$ and n_l are uncorrelated across frequency ($E\{a(\omega_l)a(\omega_j)^+\} = 0$ and $E\{n_l n_j^+\} = 0$ for $l \neq j$).

Having explained the signal model, let us review the incoherent broadband matched field processing. Recall that the ambiguity surface for incoherent Bartlett processor can be written as:

$$P_{inc}(\hat{\mathbf{p}}) = \sum_{l=1}^{L} |\mathbf{w_l}(\hat{\mathbf{p}})\mathbf{S_l}(\mathbf{p})|^{\mathbf{2}} \tag{4.5}$$

Next we derive the broadband MFP with environmental perturbation constraints as given in [17]. Let $\mathbf{w_l}(\hat{\mathbf{p}})$, $l = 1, .., L$ be the weight vector and $\mathbf{S_l}(\mathbf{p})$, $l = 1, ..., L$ be the measured signal vectors. We can rewrite

$$|\mathbf{w_l}(\hat{\mathbf{p}})^+\mathbf{S_l}(\mathbf{p})|^2 = \text{trace}(\mathbf{W_l}(\hat{\mathbf{p}})\mathbf{S_l}(\mathbf{p})\mathbf{S_l}(\mathbf{p})^+) = \text{vec}(\mathbf{W_l}(\hat{\mathbf{p}}))^+\text{vec}(\mathbf{S_l}(\mathbf{p})\mathbf{S_l}(\mathbf{p})^+) \quad (4.6)$$

where

$$\text{vec}(\mathbf{A}) = [a_{11}a_{21}a_{31}...a_{n1}a_{12}...a_{nm}]^T \quad (4.7)$$

is an $nm \times 1$ column vector for a general $n \times m$ matrix $\mathbf{A}$ and $\mathbf{W_l}(\hat{\mathbf{p}}) = \mathbf{w_l}(\hat{\mathbf{p}})\mathbf{w_l}(\hat{\mathbf{p}})^+$ is an $M \times M$ rank-one Hermitian weight matrix. The expression $\text{trace}(\mathbf{W_l}(\hat{\mathbf{p}})^+\mathbf{S_l}(\mathbf{p})\mathbf{S_l}(\mathbf{p})^+)$ is a complex-valued Frobenius inner product. The coherent broadband MVDR-EPC uses the squared magnitude of $\text{trace}(\mathbf{W_l}(\hat{\mathbf{p}})^+\mathbf{S_l}(\mathbf{p})\mathbf{S_l}(\mathbf{p})^+)$ as the norm to derive the processor [17].

Let us write the processor power as:

$$P_{coh-epc}(\hat{\mathbf{p}}) = |\sum_{l=1}^{L} \text{trace}(\mathbf{W_l}(\hat{\mathbf{p}})^+\mathbf{S_l}(\mathbf{p})\mathbf{S_l}(\mathbf{p})^+)|^2 = |\sum_{l=1}^{L} \text{vec}(\mathbf{W_l}(\hat{\mathbf{p}})^+)\text{vec}(\mathbf{S_l}(\mathbf{p})\mathbf{S_l}(\mathbf{p})^+)|^2 \quad (4.8)$$

Letting $\mathbf{W} = [\mathbf{W_1}\mathbf{W_2}.....\mathbf{W_L}]$ and $\mathbf{S} = [\mathbf{S_1}\mathbf{S_1^+}\mathbf{S_2}\mathbf{S_2^+}.....\mathbf{S_L}\mathbf{S_L^+}]$, equation 4.8 can be compactly expressed as:

$$P_{coh-epc}(\hat{p}) = |\text{trace}(\mathbf{W}(\hat{\mathbf{p}})^+\mathbf{S}(\mathbf{p}))|^2 = \bar{\mathbf{W}}(\hat{\mathbf{p}})^+\bar{\mathbf{R}}(\mathbf{p})\bar{\mathbf{W}}(\hat{\mathbf{p}}) \quad (4.9)$$

where $\bar{\mathbf{W}}(\hat{p}) = \text{vec}(\mathbf{W}(\hat{\mathbf{p}}))$ is the generalized weight vector, $\bar{\mathbf{S}}(\mathbf{p}) = \text{vec}(\mathbf{S}(\mathbf{p}))$ and $\bar{\mathbf{R}} = \bar{\mathbf{S}}(p)\bar{\mathbf{S}}(p)^+$.

Now consider a wideband weight vector defined by

$$\bar{\mathbf{W}}(\hat{\mathbf{p}}) = \text{vec}([\hat{\mathbf{R}}_\mathbf{1}(\hat{\mathbf{p}})\hat{\mathbf{R}}_\mathbf{2}(\hat{\mathbf{p}})...\hat{\mathbf{R}}_\mathbf{L}(\hat{\mathbf{p}})] = \text{vec}(\hat{\mathbf{R}}(\hat{\mathbf{p}})) \quad (4.10)$$

where $\hat{\mathbf{R}}_\mathbf{l}(\hat{\mathbf{p}})$ is the modeled cross-spectral density matrix at frequency ω_l.

Next consider using a MVDR approach such that:

$$\text{minimize } \bar{\mathbf{W}}(\hat{\mathbf{p}})^+\bar{\mathbf{R}}\bar{\mathbf{W}}(\hat{\mathbf{p}}) \text{ subject to } \text{vec}(\hat{\mathbf{R}}(\hat{\mathbf{p}}))^+\bar{\mathbf{W}}(\hat{\mathbf{p}})^+ = 1 \quad (4.11)$$

The minimization results in the following ambiguity surface:

$$P_{coh}(\hat{\mathbf{p}}) = \text{vec}(\hat{\mathbf{R}}(\hat{\mathbf{p}}))^+\bar{\mathbf{R}}^{-1}\text{vec}(\hat{\mathbf{R}}(\hat{\mathbf{p}}))^{-1} \quad (4.12)$$

The sensitivity to mismatch problem mentioned for narrowband cases will be also effective here [17]. So Czenszak et al. [17] suggests a coherent wideband MV-EPC approach which considers random environmental parameters that creates mismatch as well.

Let matrix $\mathbf{P}(\hat{\mathbf{p}})$ be defined such that, the columns of the matrix $\mathbf{P}(\hat{\mathbf{p}})$ are the signal field vectors corresponding to the different random realizations, ξ_k, of the environmental parameter vector ξ such as the perturbed sound profile:

$$\mathbf{P}(\hat{\mathbf{p}}) = [\text{vec}(\hat{\mathbf{R}}(\hat{\mathbf{p}}); \xi_1)\text{vec}(\hat{\mathbf{R}}(\hat{\mathbf{p}}); \xi_2)...\text{vec}(\hat{\mathbf{R}}(\hat{\mathbf{p}}); \xi_K)] \tag{4.13}$$

As in the narrowband MV-EPC, the column space of $\mathbf{P}(\hat{\mathbf{p}})$ is low rank, and dominant eigenvectors $\mathbf{H}(\hat{\mathbf{p}})$ of $\mathbf{P}(\hat{\mathbf{p}})$ can be obtained via singular value decomposition. Following the narrowband MV-EPC approach, the coherent wideband MV-EPC method can be obtained by selecting $\bar{\mathbf{W}}(\hat{\mathbf{p}})$ to

$$\text{minimize } \bar{\mathbf{W}}(\hat{\mathbf{p}})^{+}\bar{\mathbf{R}}\bar{\mathbf{W}}(\hat{\mathbf{p}}) \text{ subject to } \mathbf{H}(\hat{\mathbf{p}})^{+}\bar{\mathbf{W}}(\hat{p}) = \mathbf{H}(\hat{\mathbf{p}})^{+}\bar{\mathbf{W}}_q(\hat{\mathbf{p}}) \tag{4.14}$$

whereas the weight vector $\bar{\mathbf{W}}_q(\hat{\mathbf{p}})$ defines the desired response, and is chosen to maximize the output signal-to-noise ratio averaged over the ensemble of environmental realizations. The average output signal-to-noise ratio for a weight vector,$\bar{\mathbf{W}}_q(\hat{\mathbf{p}})$, is given by [17]:

$$SNR_0(r,z) = \frac{\bar{\mathbf{W}}_q(\hat{\mathbf{p}})\bar{\mathbf{R}}_P(\mathbf{p})\bar{\mathbf{W}}_{\mathbf{q}}(\hat{\mathbf{p}})}{\bar{\mathbf{W}}_q(\hat{\mathbf{p}})\bar{\mathbf{R}}_Q(\mathbf{p})\bar{\mathbf{W}}_{\mathbf{q}}(\hat{\mathbf{p}})} \tag{4.15}$$

where $\bar{\mathbf{R}}_P(\mathbf{p}) = \bar{\mathbf{R}}(\mathbf{p})\{\text{signal only}\}$ and $\bar{\mathbf{R}}_Q(\mathbf{p}) = \bar{\mathbf{R}}(\mathbf{p})\{\text{noise only}\}$ are the fourth order expectations of the date in the presence of signal only and noise only, respectively. The generalized weight vector which maximizes SNR_0 is given by

$$\bar{\mathbf{W}}_q(\hat{\mathbf{p}}) = \bar{\mathbf{R}}_G^{-1}(\mathbf{p})\widetilde{\mathbf{h}}_{\mathbf{1}}(\mathbf{p}) \tag{4.16}$$

where $\bar{\mathbf{R}}_Q(\mathbf{p}) = \bar{\mathbf{R}}_{\mathbf{G}}^{+}(\mathbf{p})\bar{\mathbf{R}}_{\mathbf{G}}(\mathbf{p})$ is obtained via Cholesky decomposition and $\widetilde{\mathbf{h_1}}(\mathbf{p})$ is the eigenvector corresponding to the largest eigenvalue of $\bar{\mathbf{R}}_G^{+}(\mathbf{p})\bar{\mathbf{R}}_{\mathbf{P}}(\mathbf{p})\bar{\mathbf{R}}_{\mathbf{G}}(\mathbf{p})$. Substituting $\bar{\mathbf{W}}_q(\hat{\mathbf{p}})$ into 4.14 the coherent wideband MV-EPC ambiguity surface is found as:

$$P_{epc}(\hat{\mathbf{p}}) = \frac{\widetilde{\mathbf{h_1}}(\mathbf{p})(\bar{\mathbf{R}}_{\mathbf{G}}^{+}(\mathbf{p}))^{-\mathbf{1}}\mathbf{H}(\hat{\mathbf{p}})(\mathbf{H}(\hat{\mathbf{p}})^{+}\bar{\mathbf{R}}^{-\mathbf{1}}(\mathbf{p})\mathbf{H}(\hat{\mathbf{p}}))^{-\mathbf{1}}\mathbf{H}(\hat{\mathbf{p}})^{+}\bar{\mathbf{R}}_{\mathbf{G}}^{-\mathbf{1}}(\mathbf{p})\widetilde{\mathbf{h_1}}(\mathbf{p})}{\widetilde{\mathbf{h_1}}(\mathbf{p})(\bar{\mathbf{R}}_{\mathbf{G}}^{+}(\mathbf{p}))^{-\mathbf{1}}\mathbf{H}(\hat{\mathbf{p}})(\mathbf{H}(\hat{\mathbf{p}})^{+}\bar{\mathbf{R}}_{\mathbf{Q}}^{-\mathbf{1}}(\mathbf{p})\mathbf{H}(\hat{\mathbf{p}}))^{-\mathbf{1}}\mathbf{H}(\hat{\mathbf{p}})^{+}\bar{\mathbf{R}}_{\mathbf{G}}^{-\mathbf{1}}(\mathbf{p})\widetilde{\mathbf{h_1}}(\mathbf{p})} \tag{4.17}$$

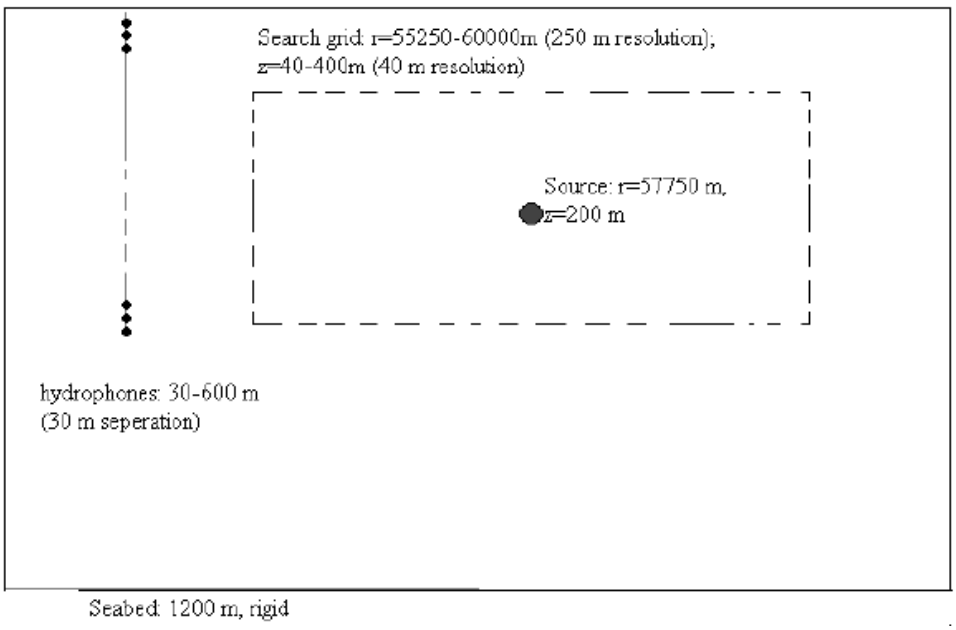

Figure 4.3: The scenario considered for the broadband examples

4.5 Broadband Examples

In order to illustrate and compare performances of broadband matched field processors, a deep-water case is considered in the following simulation experiments,. We give some examples of the applications of Matched Field Processing and observe some specific features of the broadband matched field processors considered upto now.

We consider the following scenario (Figure 4.3).

A source with frequency components of 10, 20 and 25 Hz and depth 200m is in a range-independent underwater environment of constant depth of 1200m. Let us also assume that at 57750 meters distance from the source, there is an array of 20 elements with an interelement distance of 30m.

We consider the sound speed profile as the Munk profile as we did in narrowband case.

The search is grid is taken as between 55000 and 60000 meters for range with 250 meter resolution and between 40 and 400 meters with 40 meter resolution.

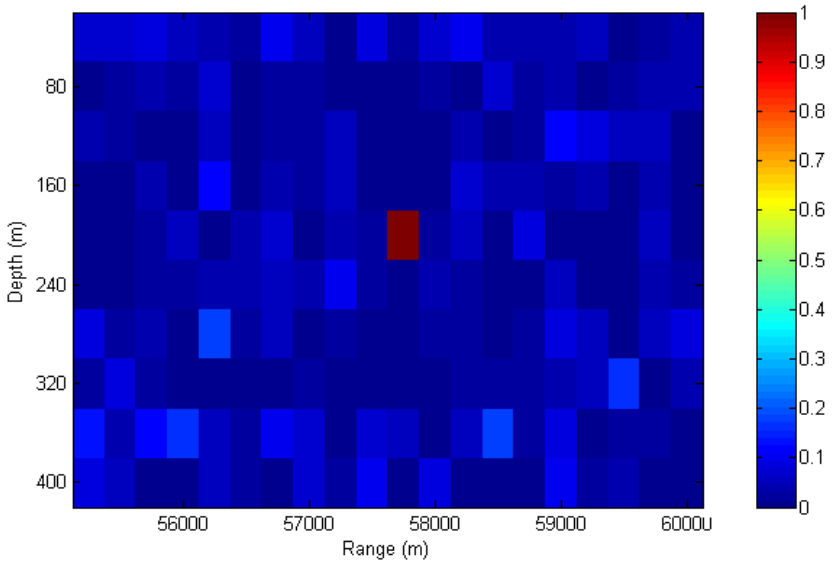

Figure 4.4: Ambiguity Surface for the Bartlett Coherent Processor for SNR=1 dB, no mismatch

First let us consider the case that sound speed profile is perfectly known, i.e. no mismatch case. In Figures 4.4 and 4.7, we see the coherent and incoherent Bartlett processors for high SNR case (SNR 1 dB). In Figure 4.4 we see that the Bartlett processor finds the correct position and there are some sidelobes which are almost inevident. In Figure 4.7, we see correct localization occurs again but sidelobes are getting more visible. For the same noise and no mismatch case, we see that coherent MVDR has almost no sidelobes (Figure 4.5) and has a perfect localization performance. On the other hand, for incoherent MVDR case (Figure 4.8) there is an increase in sidelobes but still it has a very good localization performance. The broadband MVDR-EPC has a sidelobe suppression performance similar to coherent MVDR, and it achives localization (Figure 4.6).

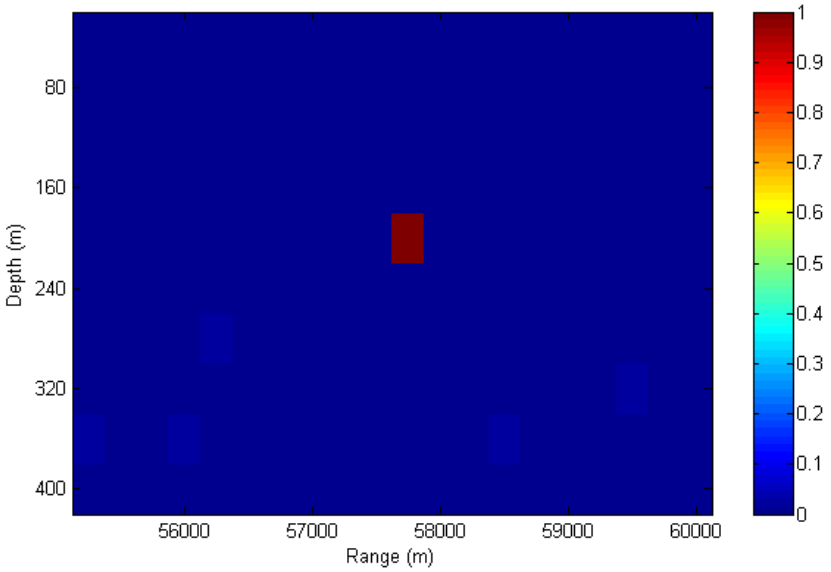

Figure 4.5: Ambiguity Surface for the MVDR Coherent Processor for SNR=1 dB, no mismatch

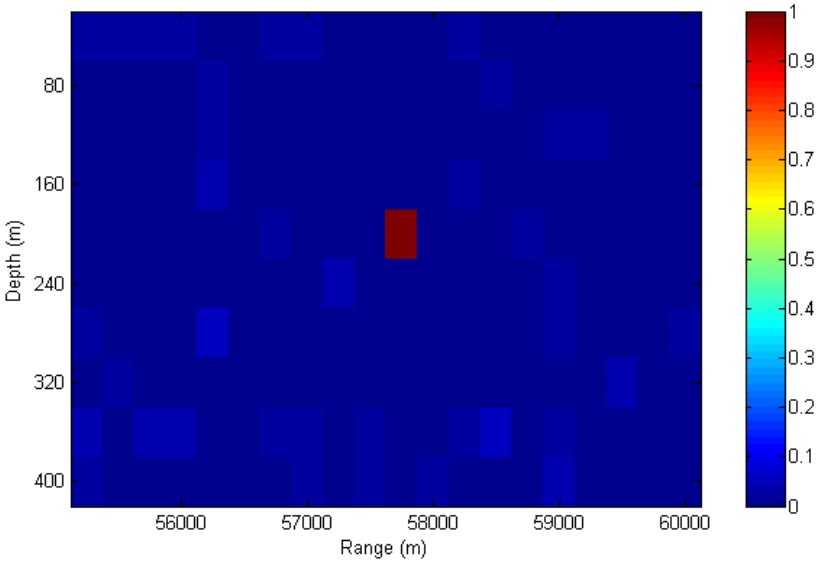

Figure 4.6: Ambiguity Surface for the Broadband MVDR-EPC Processor for SNR=1 dB, no mismatch

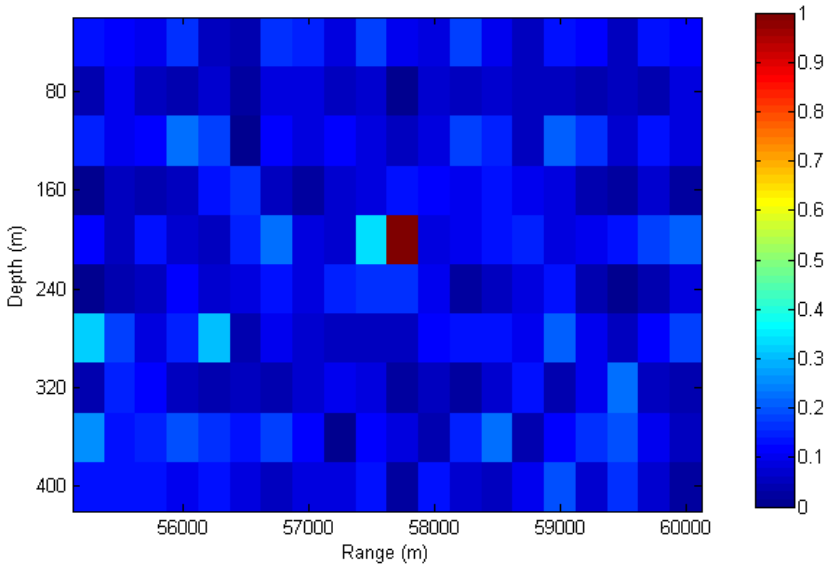

Figure 4.7: Ambiguity Surface for the Bartlett Incoherent Processor for SNR=1 dB, no mismatch

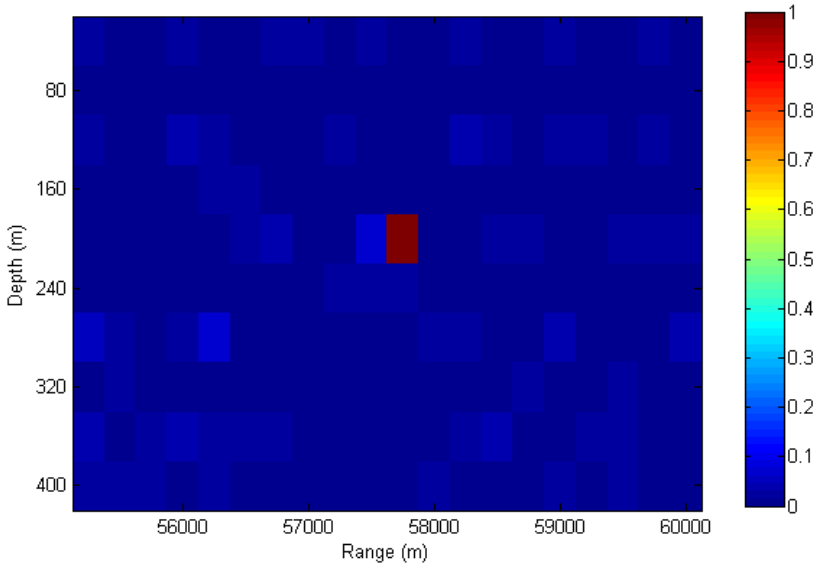

Figure 4.8: Ambiguity Surface for the MVDR Incoherent Processor for SNR=1 dB, no mismatch

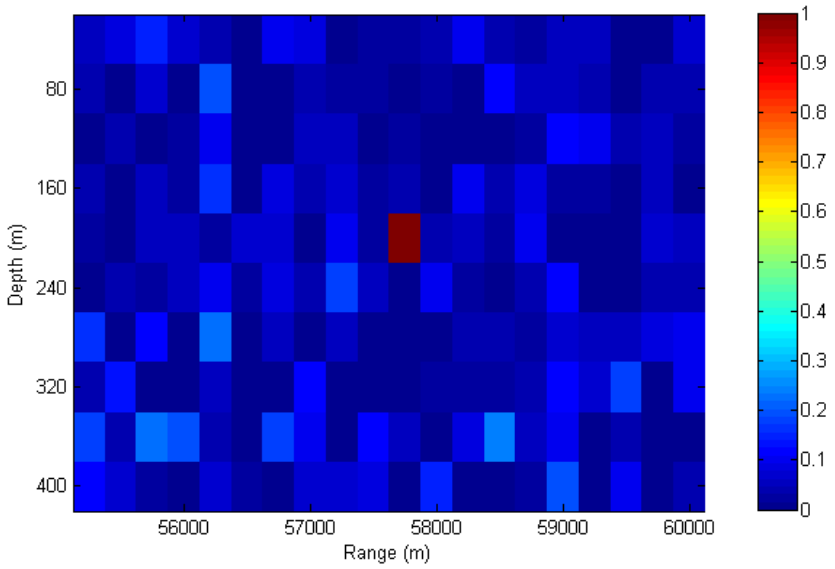

Figure 4.9: Ambiguity Surface for the Bartlett Coherent Processor for SNR=-6 dB, no mismatch

If we decrease the signal-to-noise ratio level to -6 dB, we see that there is an increase in sidelobes for both Bartlett coherent and incoherent processors. However, coherent Bartlett has a better sidelobe suppression (Figure 4.9) compared to the incoherent Bartlett processor (Figure 4.12.) The situation is similar for the MVDR case. The coherent MVDR still has a very good sidelobe suppression and sidelobes are barely visible (Figure 4.10). For the incoherent MVDR as seen in Figure 4.13, the sidelobes are becoming clearer compared to coherent MVDR case . The broadband MVDR-EPC has a sidelobe suppression between coherent Bartlett and MVDR as expected (Figure 4.11).

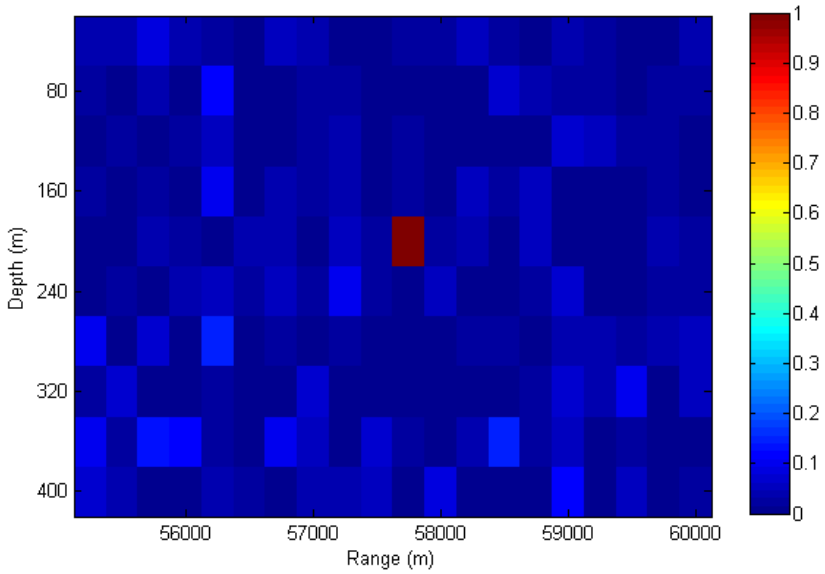

Figure 4.10: Ambiguity Surface for the MVDR Coherent Processor for SNR=-6 dB, no mismatch

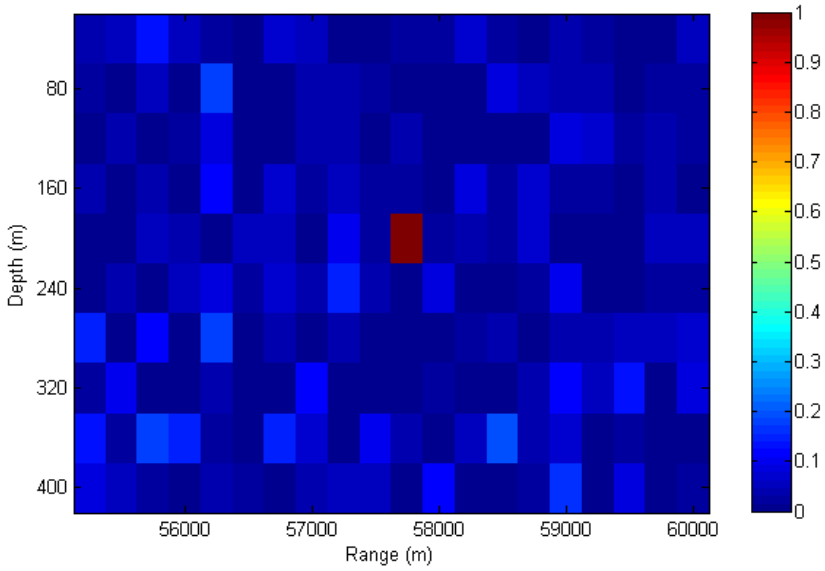

Figure 4.11: Ambiguity Surface for the Broadband MVDR-EPC Processor for SNR=-6 dB, no mismatch

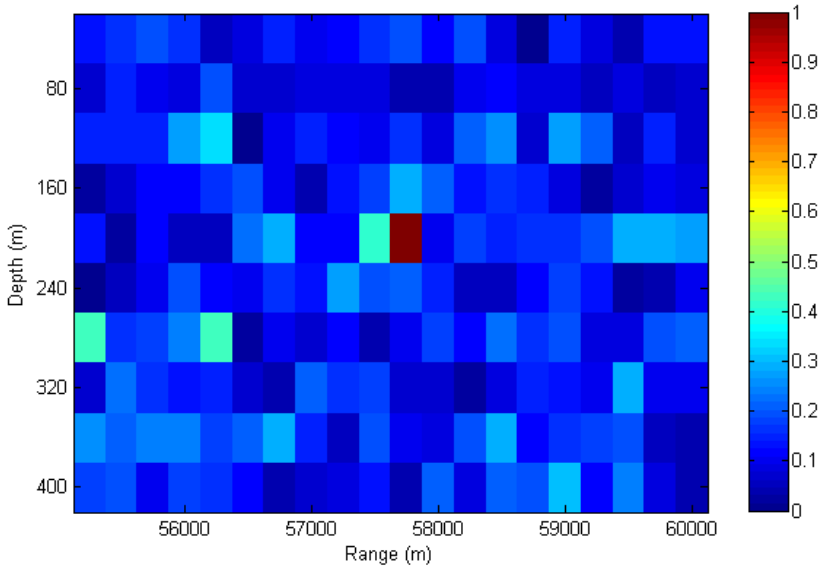

Figure 4.12: Ambiguity Surface for the Bartlett Incoherent Processor for SNR=-6 dB, no mismatch

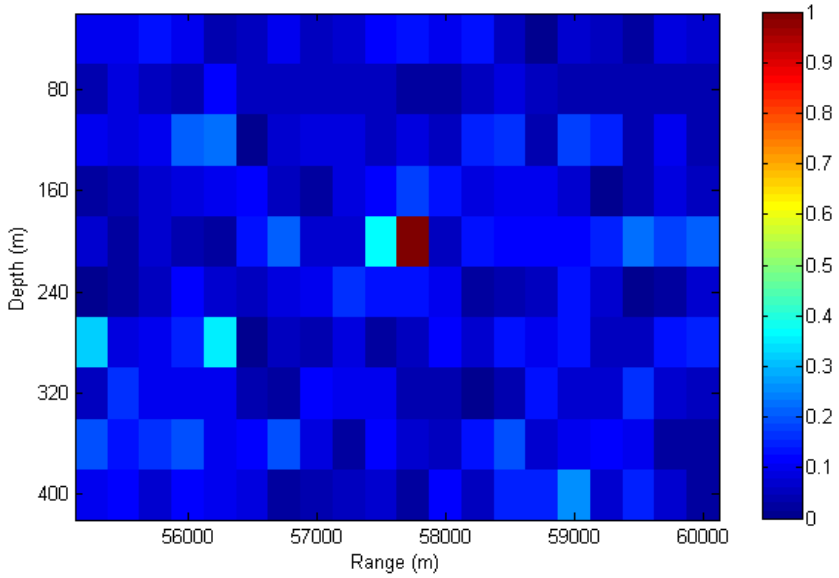

Figure 4.13: Ambiguity Surface for the MVDR Incoherent Processor for SNR=-6 dB, no mismatch

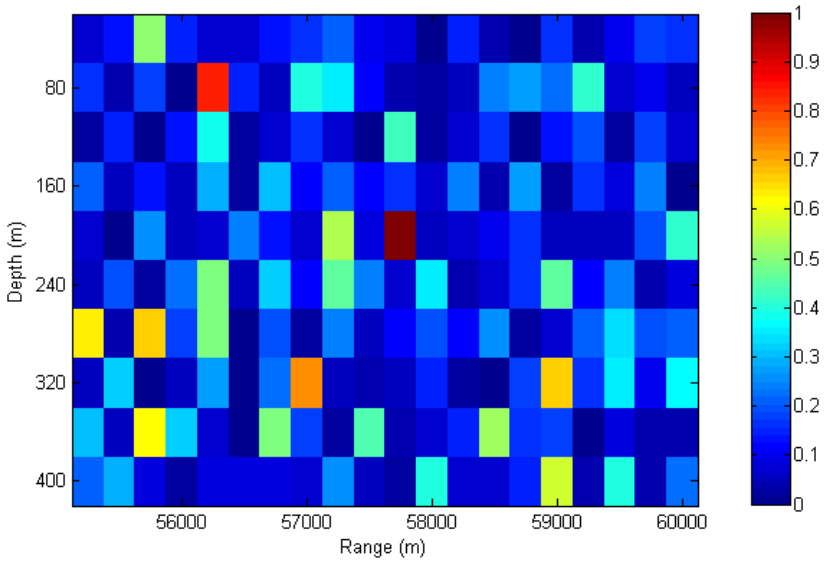

Figure 4.14: Ambiguity Surface for the Bartlett Coherent Processor for SNR=-12 dB, no mismatch

If we further decrease the signal-to-noise ratio (SNR=-12 dB), we see that coherent Bartlett still localizes the source but sidelobes are very evident now (Figure 4.14). On the other hand, as can be seen in Figure 4.17 incoherent Barlett now localizes the source incorrectly due to the sidelobe having a higher processor power that the correct location. For MVDR, we see that coherent MVDR suppresses sidelobes and has correct localization (Figure 4.15). However, although it has lower sidelobes than the incoherent Bartlett, the incoherent MVDR has incorrect localization too (Figure 4.18). Broadband MVDR-EPC has also correct localization in this case (Figure 4.16).

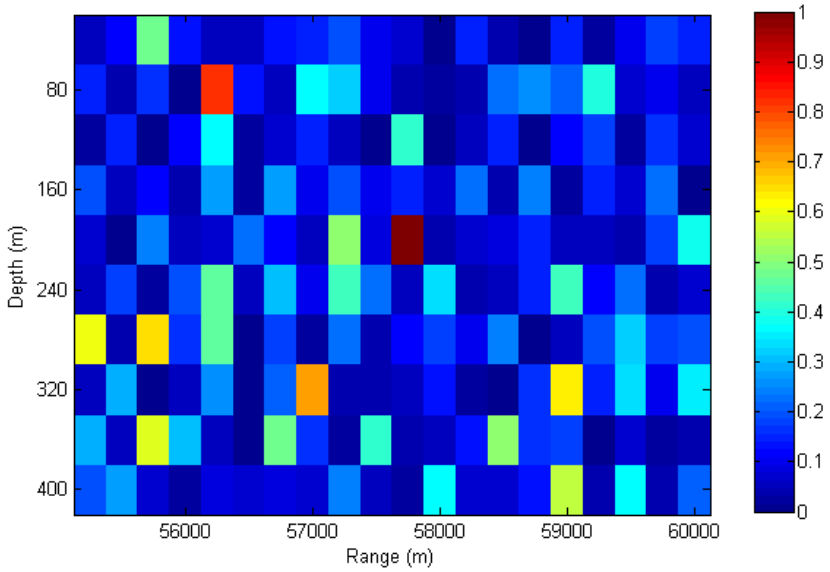

Figure 4.15: Ambiguity Surface for the MVDR Coherent Processor for SNR=-12 dB, no mismatch

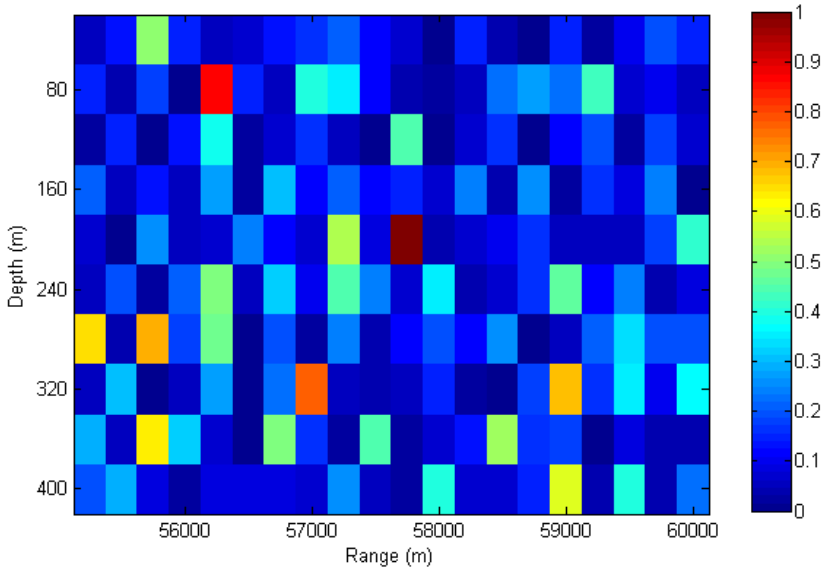

Figure 4.16: Ambiguity Surface for the Broadband MVDR-EPC Processor for SNR=-12 dB, no mismatch

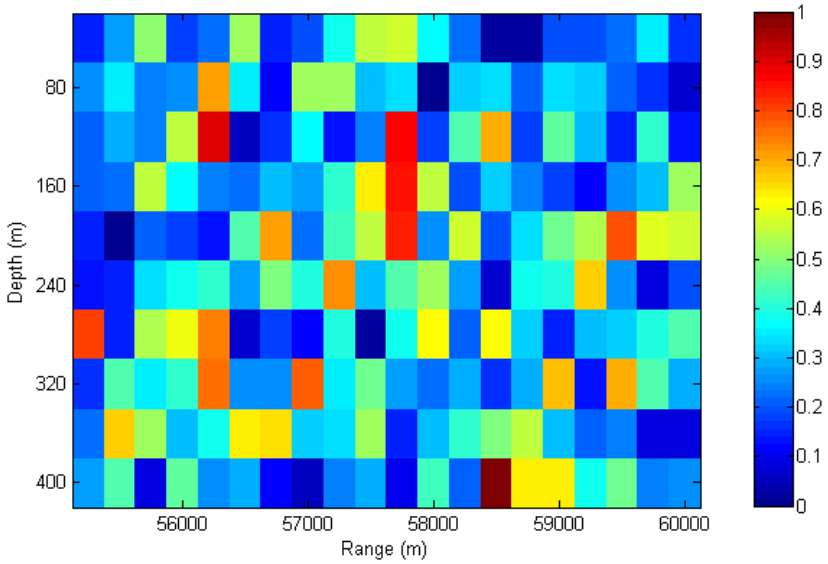

Figure 4.17: Ambiguity Surface for the Bartlett Incoherent Processor for SNR=-12 dB, no mismatch

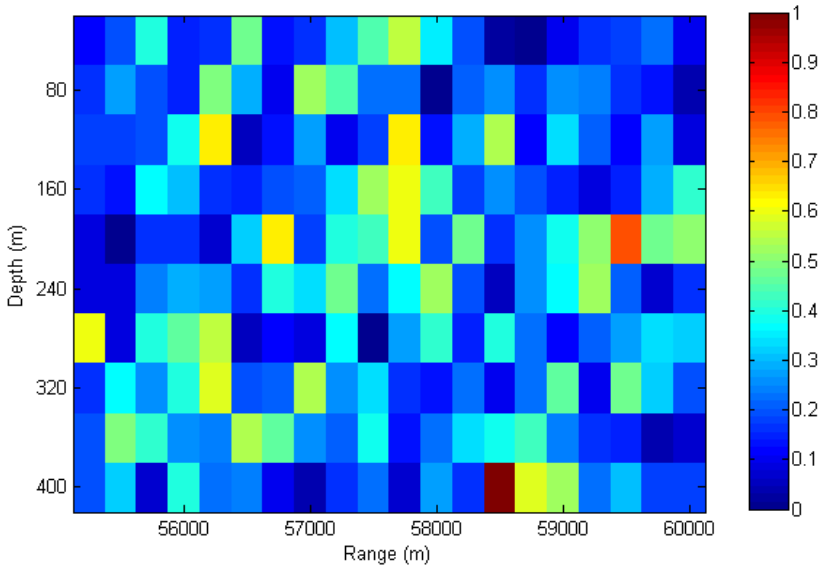

Figure 4.18: Ambiguity Surface for the MVDR Incoherent Processor for SNR=-12 dB, no mismatch

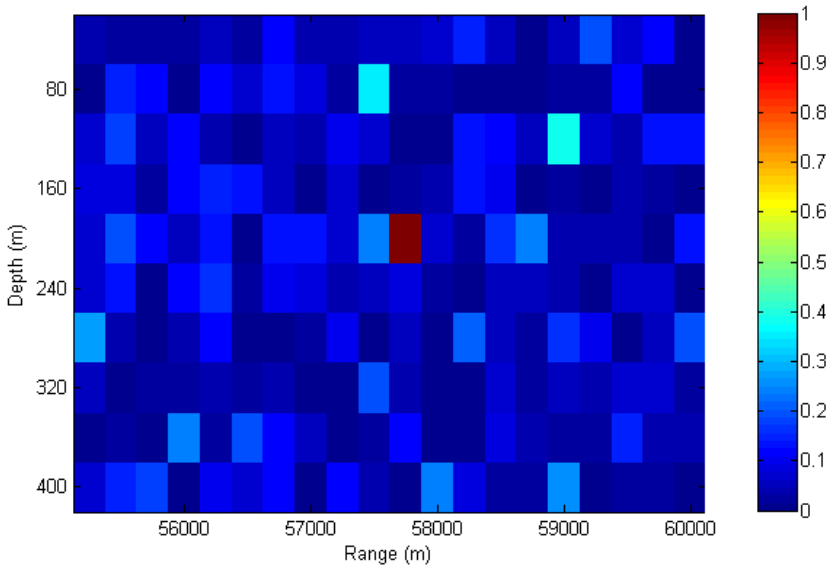

Figure 4.19: Ambiguity Surface for the Bartlett Coherent Processor for SNR=1 dB, under mismatch

Next we consider the case where the sound speed profile is not perfectly known, i.e. mismatch case. The sound speed perturbation model we use is the same as used in narrowband case.

For low noise case (SNR=1 dB), Figures 4.19 and 4.22, we see that both coherent and incoherent Bartlett processors has higher sidelobes compared to the no mismatch case. However, it still achieves correct localization for both incoherent and coherent Bartlett processors. MVDR under mismatch has also a higher sidelobe compared to MVDR working under a perfectly known channel for both coherent and incoherent cases (Figures 4.20 and 4.23). For both Bartlett and MVDR we see that coherent processors has a better sidelobe suppression compared to incoherent ones. The broadband MVDR-EPC has a better sidelobe suppression compared to coherent MVDR as expected because it takes environmental effects into account (Figure 4.21) .

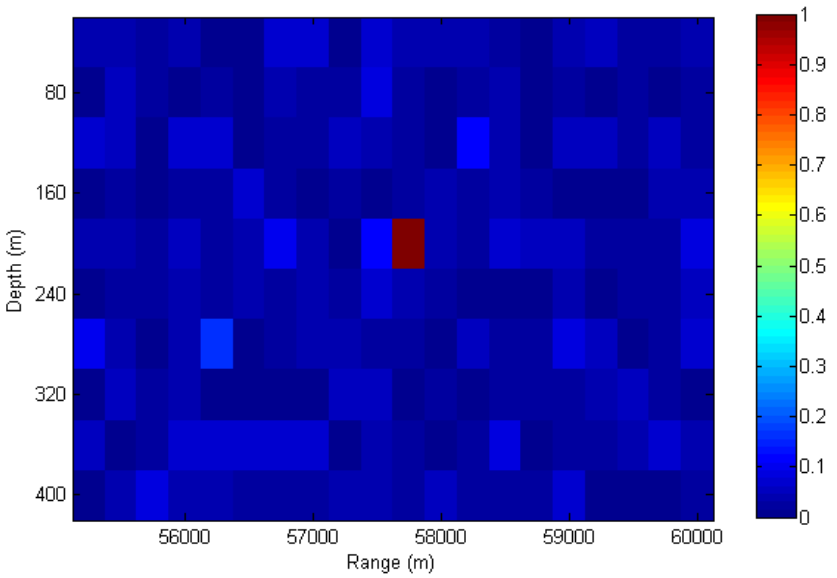

Figure 4.20: Ambiguity Surface for the MVDR Coherent Processor for SNR=1 dB, under mismatch

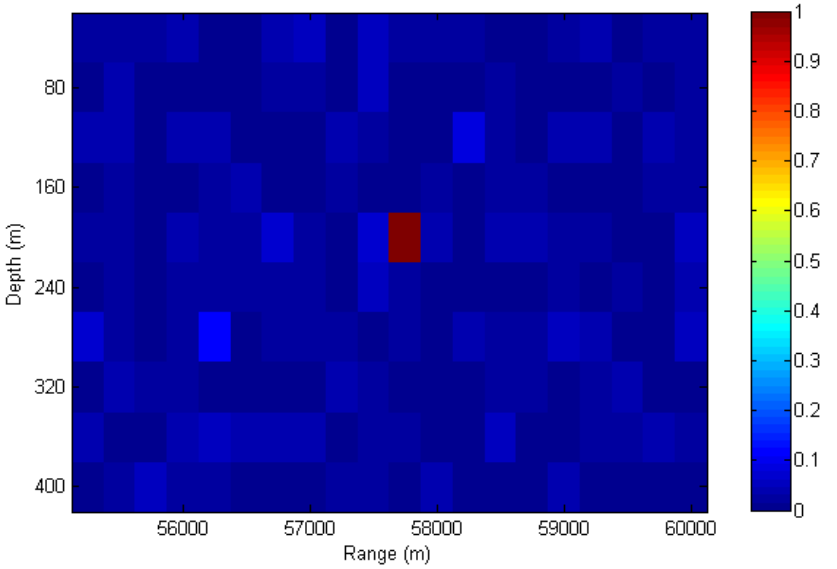

Figure 4.21: Ambiguity Surface for the Broadband MVDR-EPC Processor for SNR=1 dB, under mismatch

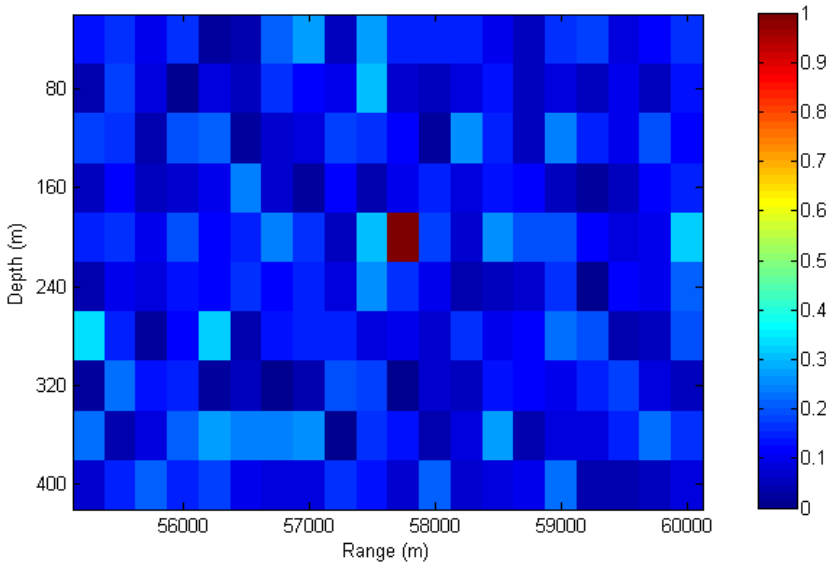

Figure 4.22: Ambiguity Surface for the Bartlett Incoherent Processor for SNR=1 dB, under mismatch

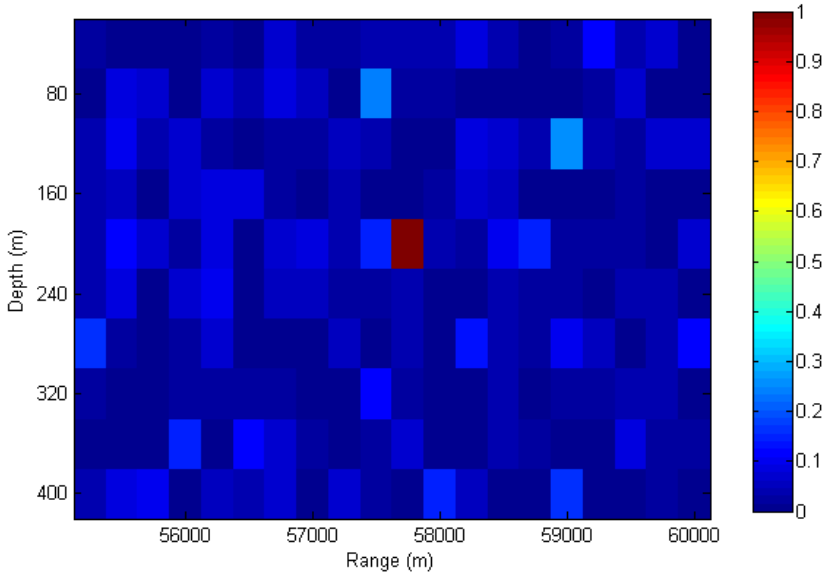

Figure 4.23: Ambiguity Surface for the MVDR Incoherent Processor for SNR=1 dB, under mismatch

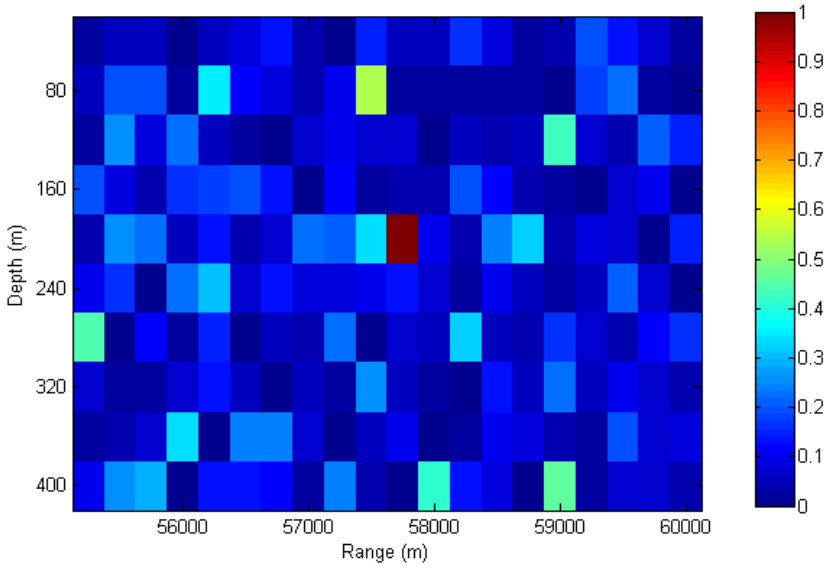

Figure 4.24: Ambiguity Surface for the Bartlett Coherent Processor for SNR=-6 dB, under mismatch

If we increase noise further (SNR=-12 dB), we see that the mismatch causes higher sidelobes for both Bartlett and MVDR processors compared to no mismatch case. And under high noise, we see that neither coherent Bartlett(Figure 4.29) nor incoherent Bartlett(Figure 4.32) processors have correct localization. The sidelobes are very high due to noise and mismatch. It is also the same for coherent MVDR(Figure 4.30) and incoherent MVDR(Figure 4.33) processors under mismatch too. We see that although it has better sidelobe suppression than coherent MVDR, broadband MVDR-EPC fails to localize correctly for this case (Figure 4.31). From the example ambiguity surfaces, we can understand that coherent processors have better sidelobe suppression compared to incoherent processors under both no mismatch and mismatch case. The mismatch causes a higher sidelobe for both coherent and incoherent processors, and causes degradation in processor performance.

The comparison of the correct localization performances of processors under no mismatch and under mismatch cases can also be seen in Tables 4.1 and 4.2 and Figures 4.5 and 4.35.

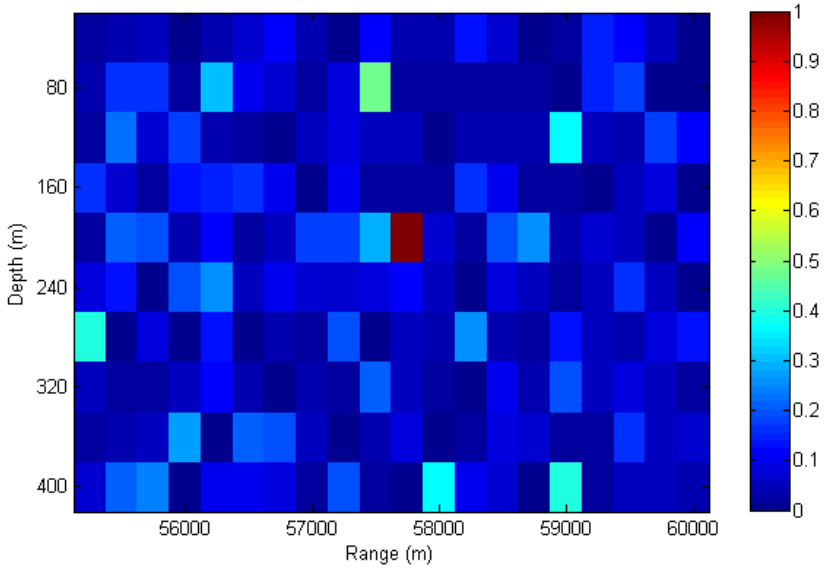

Figure 4.25: Ambiguity Surface for the MVDR Coherent Processor for SNR=-6 dB, under mismatch

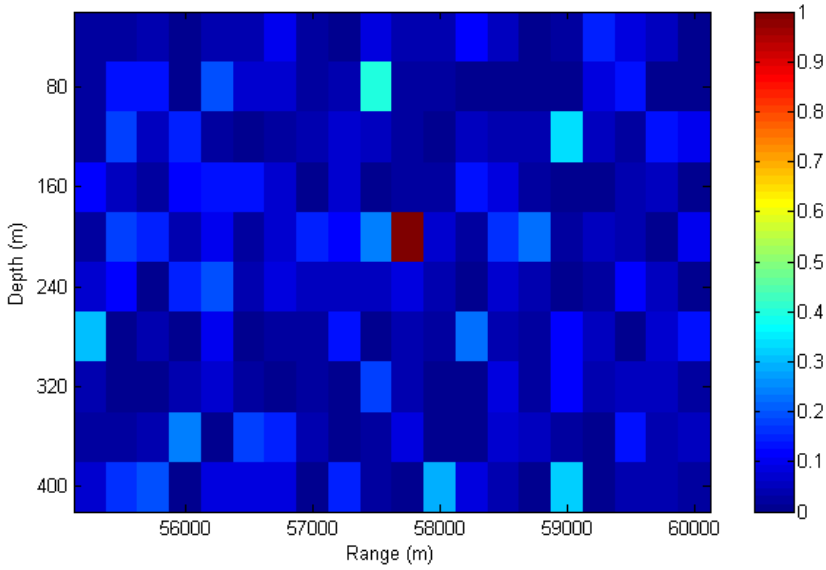

Figure 4.26: Ambiguity Surface for the Broadband MVDR-EPC Processor for SNR=-6 dB, under mismatch

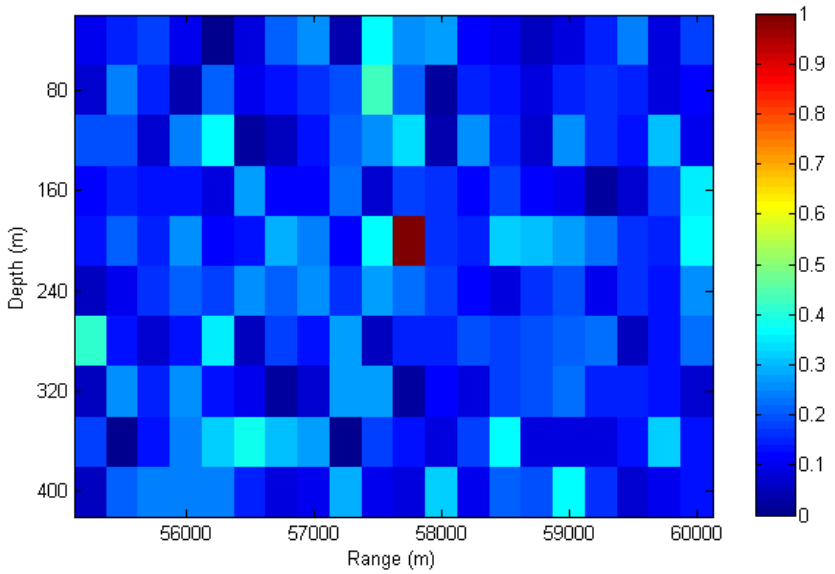

Figure 4.27: Ambiguity Surface for the Bartlett Incoherent Processor for SNR=-6 dB, under mismatch

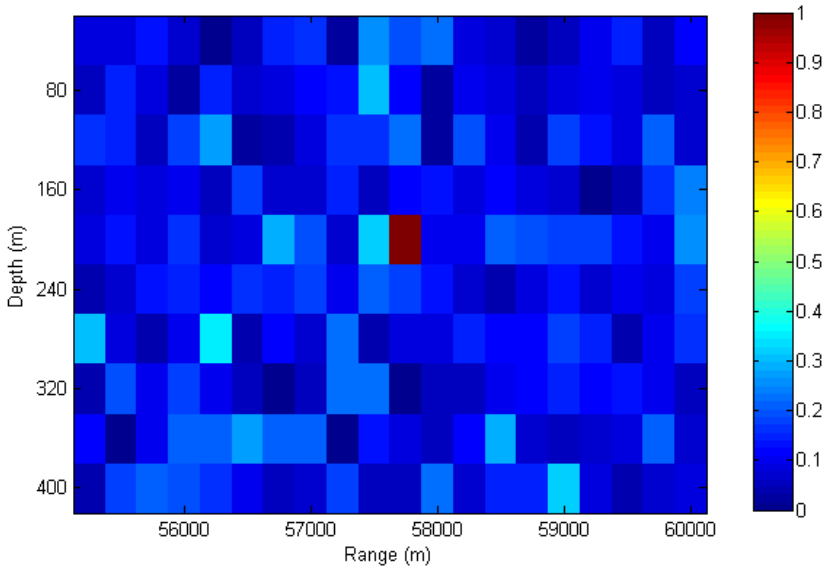

Figure 4.28: Ambiguity Surface for the MVDR Incoherent Processor for SNR=-6 dB, under mismatch

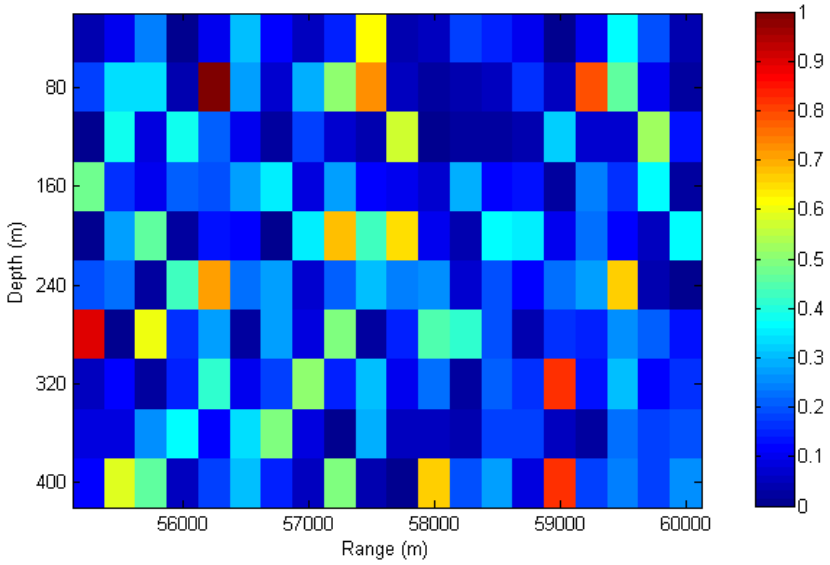

Figure 4.29: Ambiguity Surface for the Bartlett Coherent Processor for SNR=-12 dB, under mismatch

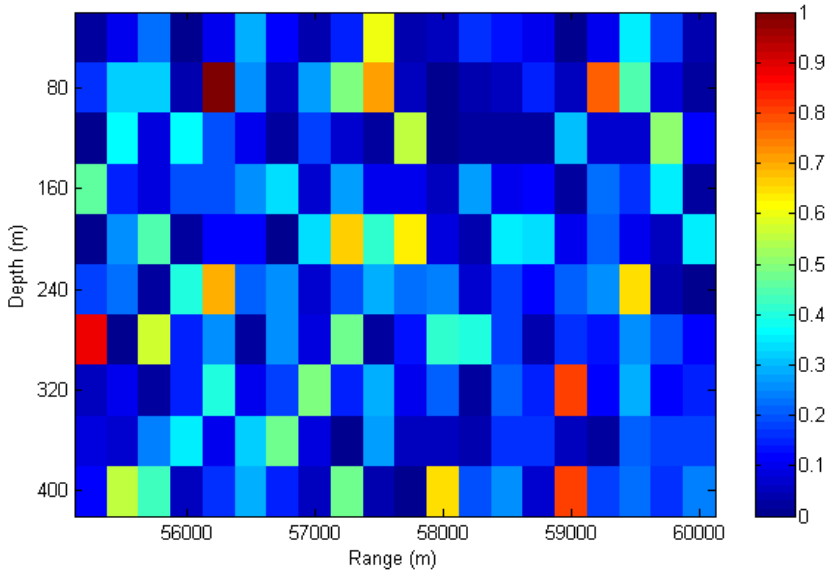

Figure 4.30: Ambiguity Surface for the MVDR Coherent Processor for SNR=-12 dB, under mismatch

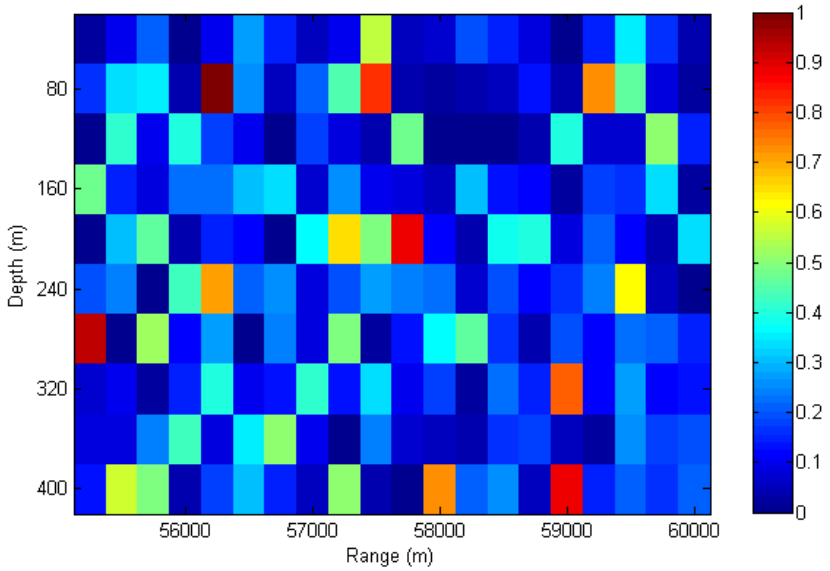

Figure 4.31: Ambiguity Surface for the Broadband MVDR-EPC Processor for SNR=-12 dB, under mismatch

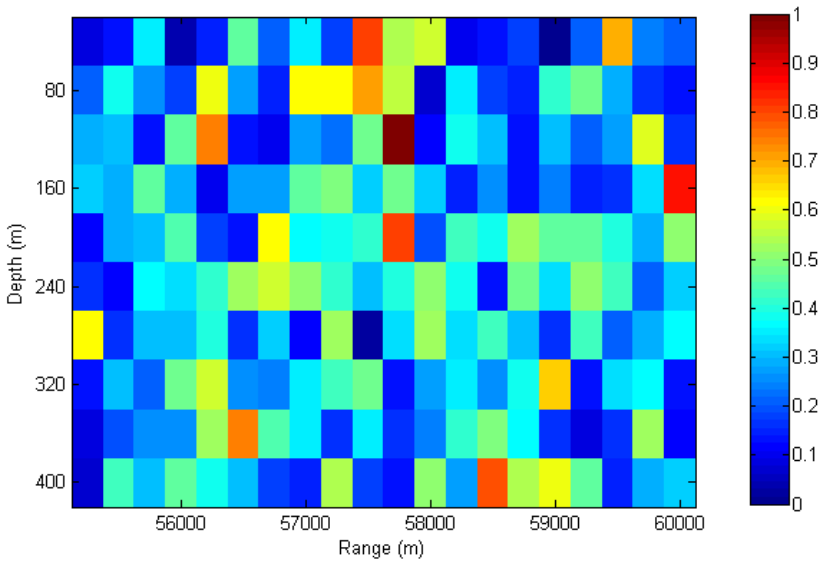

Figure 4.32: Ambiguity Surface for the Bartlett Incoherent Processor for SNR=-12 dB, under mismatch

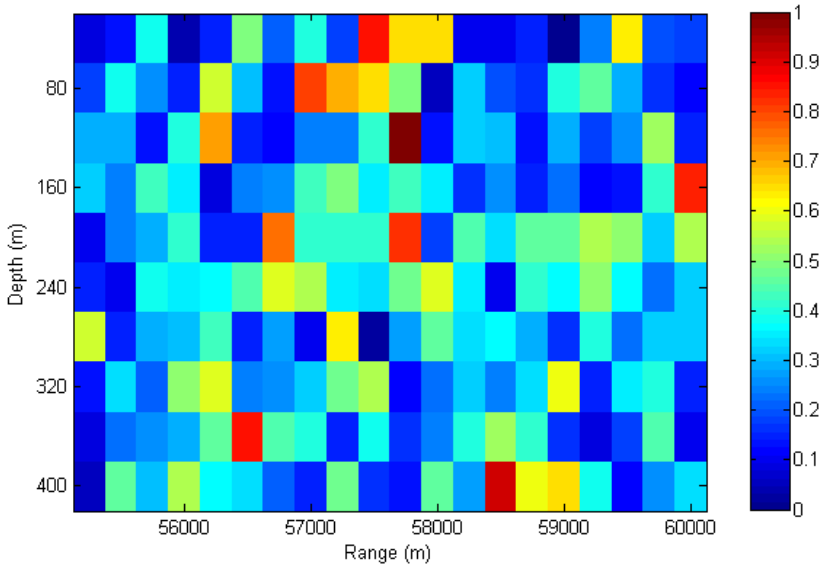

Figure 4.33: Ambiguity Surface for the MVDR Incoherent Processor for SNR=-12 dB, under mismatch

Table 4.1: The probability of correct localizations for Bartlett Incoherent, MVDR Incoherent, Bartlett Coherent, MVDR Coherent and broadband MVDR-EPC processors for the no mismatch case

SNR	$BartlettC.$	$MVDRC.$	$MVDR-EPC$	$BartlettI.$	$MVDRI.$
1	99.8	99.9	99.9	98.0	98.9
-1	98.4	99.6	99.4	91.2	93.4
-3	91.8	95.6	95.2	72.9	80.0
-6	83.5	88.3	87.9	59.8	65.2
-7	70.5	75.2	74.6	45.4	47.2
-9	57.3	61.5	59.9	33.9	33.5
-10	46.6	48.8	48.1	27.5	29.1
-11	38.3	40.8	39.7	23.1	22.0
-11.5	31.3	32.5	31.9	17.0	16.4
-12	24.7	25.9	25.1	12.7	12.5
-12.5	23.4	24.4	24.1	12.7	13.4
-13	18.5	18.8	18.6	12.6	11.6

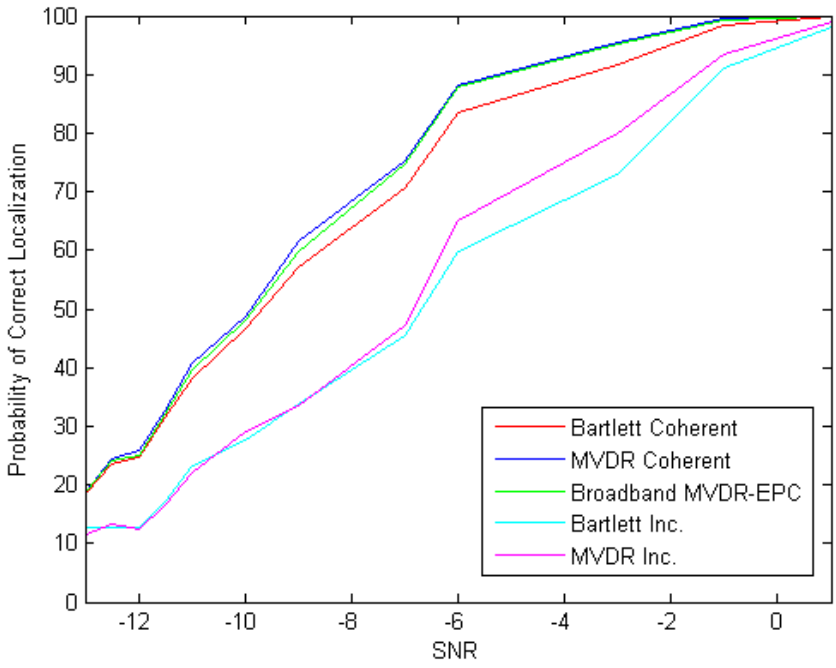

Figure 4.34: The probability of correct localizations for Bartlett Incoherent, MVDR Incoherent, Bartlett Coherent, MVDR Coherent and broadband MVDR-EPC processors for the no mismatch case

Table 4.2: The probability of correct localizations for Bartlett Incoherent, MVDR Incoherent, Bartlett Coherent, MVDR Coherent and broadband MVDR-EPC processors under mismatch

SNR	$BartlettC.$	$MVDRC.$	$MVDR-EPC$	$BartlettI.$	$MVDRI.$
1	82.7	85.5	88.1	81.3	84.8
-1	70.2	75.2	78.8	68.7	72.9
-3	56.9	60.3	62.1	50.8	52.2
-6	48.8	49.1	49.4	39.5	40.1
-7	33.3	36.1	36.7	27.5	28.8
-9	27.5	29.2	29.8	19.7	21.8
-10	21.5	22.2	22.6	17.2	17.7
-11	19.8	19.1	19.6	14.8	14.9
-11.5	16.2	17.6	17.6	12.9	12.8
-12	14.5	13.7	13.8	9.7	9.6
-12.5	14.9	10.7	11.2	9.5	9.2
-13	13.5	10.1	10.6	9.9	9.1

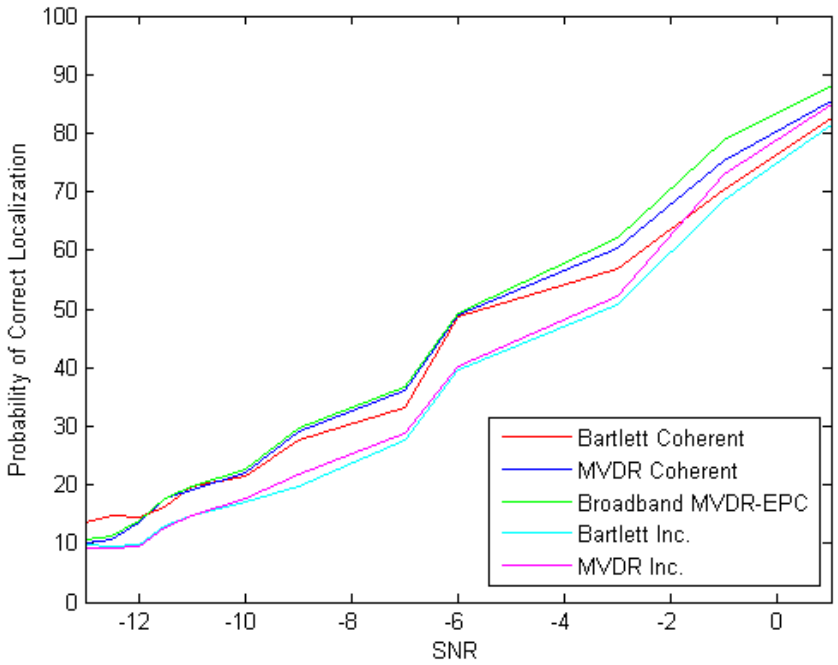

Figure 4.35: The probability of correct localizations for Bartlett Incoherent, MVDR Incoherent, Bartlett Coherent, MVDR Coherent and broadband MVDR-EPC processors under mismatch

CHAPTER 5

WEIGHTING APPROACH TO BROADBAND MATCHED FIELD PROCESSING

5.1 Introduction to Weighting Approach

As we have seen in previous section, there are two main approaches to the Broadband Matched Field Processing methods. These are incoherent and coherent approaches. Incoherent broadband processing was introduced by Baggeroer et al. [8]. In incoherent broadband processing, ambiguity surfaces for different frequencies are generated and then these ambiguity surfaces are averaged in a linear or logarithmic fashion. The coherent broadband processing dealt in this section was initially introduced by Tolstoy [13] and later extended by Michalopoulou [14]. In coherent broadband processing, sensor data for different frequencies are merged in supervectors and these supervectors are used to generate an ambiguity surface. It was shown that by making use of cross frequency information significant gain in correct localization probability can be achieved.

In this chapter, we consider both of these approaches and we develop a weighting approach considering the fact that information from different frequencies may have different reliability depending on the environmental conditions. We develop weighting approaches for both incoherent and coherent cases and search for weights that makes the probability of correct localization maximum. The work described here is based on [19].

This chapter is organized as follows: In Problem Statement section, we define the optimization problem to be solved. In Weighting Approach to Incoherent Case section,

we express the heuristic solution model used. In Weighting Approach to Coherent Case section, the same heuristic model is applied to coherent approach. In Simulation Results section, we give the results of our simulations.

5.2 Problem Statement

Recall that our problem is locating a radiating underwater source using m passive hydrophones which form a vertical linear array. An acoustic wave field emanating from the source is sampled in both space and time by the array. Our aim is to combine the spatial and temporal signal information at the array in such a way that we can predict the location of the source accurately.

We assume that we sense the acoustic field by the hydrophone array. Let $\mathbf{s}(t) = \mathbf{x}(t) + \mathbf{n}(t)$ be the signal vector sensed by the hydrophone array as a summation of source signal and noise. Let $\mathbf{S}(f)$ be the frequency domain representation of the received signal vector for frequency f. Let us also assume that source signal has N discrete frequency components, so we are only interested in these frequency components (multi-tonal source).

Let us first recall the matched field processing method known as Bartlett linear processor [2]. In this case, the measured acoustic signal and replicas generated for candidate source locations are correlated and the correlation results are used to form an ambiguity surface. In more formal terms, the ambiguity surface for frequency f is calculated as:

$$P_{bartlett}(\hat{\mathbf{p}}, f) = \mathbf{w}^*(\hat{\mathbf{p}}, f)\mathbf{R}(\mathbf{p}, f)\mathbf{w}(\hat{\mathbf{p}}, f) \tag{5.1}$$

where $\mathbf{R}(\mathbf{p}, f)$ is an estimate of the cross-spectral density matrix for signal $\mathbf{S}(\mathbf{p}, f)$ and $\mathbf{w}(\hat{\mathbf{p}}, f)$ is the replica signal vector for a candidate source location $\hat{\mathbf{p}}$. The source location estimate of the matched field processor is the $\hat{\mathbf{p}}$ point that creates the maximum $P_{bartlett}(\hat{\mathbf{p}}, f)$ value for the frequency of interest.

The broadband incoherent matched field processing first generates the ambiguity surfaces for different frequencies and then averages these surfaces in a linear or logarithmic fashion. For example, in the case of linear averaging, the output of incoherent matched

field processing can be expressed as:

$$P_{inc.broadband}(\hat{\mathbf{p}}, f) = \sum_{f=1}^{K} \mathbf{w}^{+}(\hat{\mathbf{p}}, f)\mathbf{R}(\mathbf{p}, f)\mathbf{w}(\hat{\mathbf{p}}, f) \tag{5.2}$$

where K is the total number of tonal frequency components of the broadband signal.

We introduce another approach to incoherent broadband matched field processing such as we use a different weight for each ambiguity surface when doing the averaging. The modified weighted incoherent broadband processor can be given as:

$$P_{mod.inc.broadband}(\hat{\mathbf{p}}, f) = \sum_{f=1}^{N} \alpha_f \mathbf{w}^{*}(\hat{\mathbf{p}}, f)\mathbf{R}(\mathbf{p}, f)\mathbf{w}(\hat{\mathbf{p}}, f) \tag{5.3}$$

The problem here is to find $\alpha_f, f = 1...N$ values such that the probability of correct localization is improved.

Next we recall the Michalopoulo's coherent broadband processor [14]. The cross-spectral matrix for the coherent broadband processor is formed by using supervectors such that $\mathbf{S}_{super}(\mathbf{p}) = [\mathbf{S}(\mathbf{p}, 1)...\mathbf{S}(\mathbf{p}, K)]$. The cross-spectral matrix is estimated using $\mathbf{S}_{super}(\mathbf{p})$ and it is correlated with the supervector generated for the candidate locations $\mathbf{w}_{super}(\hat{\mathbf{p}}, f) = [\mathbf{w}(\hat{\mathbf{p}}, 1)...\mathbf{w}(\hat{\mathbf{p}}, K)]$. In more formal terms:

$$P_{coh.broadband}(\hat{\mathbf{p}}) = \mathbf{w}^{+}_{super}(\hat{\mathbf{p}})\mathbf{R}_{super}(\mathbf{p}, f)\mathbf{w}_{super}(\hat{\mathbf{p}}) \tag{5.4}$$

In this way, cross coherent frequency information is also taken into account.

Similar to incoherent case, for coherent broadband processor we are looking for an optimal weighting such that we form $\mathbf{S}_{modifiedsuper} = [\alpha_1 S(\mathbf{p}, 1)..\alpha_K S(\mathbf{p}, K)]$ and find the modified cross-spectral matrix. Then the new modified coherent ambiguity surface can be found as:

$$P_{mod.coh.broadband}(\hat{\mathbf{p}}) = \mathbf{w}^{+}_{super}(\hat{\mathbf{p}})\mathbf{R}_{modifiedsuper}(\mathbf{p})\mathbf{w}_{super}(\hat{\mathbf{p}}) \tag{5.5}$$

The problem is to find the optimal $\alpha_f, f = 1...N$, values, if they exist, such that the probability of correct localization is improved compared to equation 5.4.

5.3 Weighting Approach to Incoherent Case

The weighted incoherent broadband processor can be expressed as the following sum:

$$\sum_{f=1}^{N} \alpha_f (\sum_{j=1}^{M} \sum_{k=1}^{M} w_j^*(\hat{\mathbf{p}}, f) s_j(\mathbf{p}, f) s_k^*(\mathbf{p}, f) w_k(\hat{\mathbf{p}}, f)) \tag{5.6}$$

where:

- α_f is the weight for the ambiguity surface generated for frequency f, $f = 1, ..., N$.
- $w_j(\hat{\mathbf{p}}, f)$ is the modeled (replica) acoustic field vector for candidate source location ($\hat{\mathbf{p}}$) and frequency f as sensed by hydrophone j.
- $s_j(\mathbf{p}, f)$ is the measured acoustic field vector at frequency f as sensed by hydrophone j.

A heuristic approach is to search over different weight values to find optimal α vector that makes the probability of correct localization optimum. In simulation results section we search over for different α values and we show that for some α values different than $\alpha_1 = ... = \alpha_N$ the probability of correct localization can be improved.

5.4 Weighting Approach to Coherent Case

The weighted coherent broadband processor can be expressed as the following sum:

$$\sum_{f=1}^{N} \sum_{g=1}^{N} \sum_{j=1}^{M} \sum_{k=1}^{M} \alpha_f w_j^*(\hat{\mathbf{p}}, f) s_j(\mathbf{p}, f) s_k^*(\mathbf{p}, g) w_k(\hat{\mathbf{p}}, g) \alpha_g \tag{5.7}$$

where:

- α_f is the weight for the measured signal for the frequency f, $f = 1, ..., N$.
- $w_j(\hat{\mathbf{p}}, f)$ and $s_j(\mathbf{p}, g)$ are defined same as in the case of incoherent case.

Note that the extra cross frequency terms make this sum different then the incoherent sum. Similar to incoherent case, a heuristic approach is to search over different weight values to find α values that makes the probability of correct localization maximum.

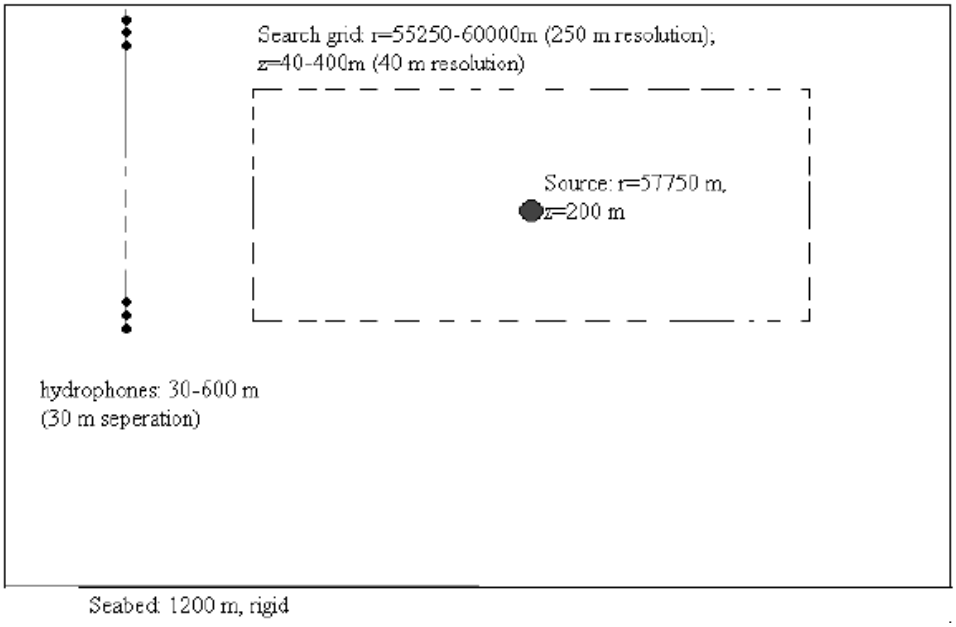

Figure 5.1: The scenario considered for the examples

5.5 Simulation Results

Let us assume the scenario that there is a vertical array with 20 hydrophones which are located from 30 m to 600 m and there is a source with two frequencies: 10 and 20 Hz. The source is located at 57750 km range and 200 m depth. The matched field processor search region is from 55250 m to 60000 m in range with a resolution of 250 m and from 40 m to 400 m in depth with a resolution of 40 m. The seabed depth is 1200m. The scenario is depicted in Figure 5.1.

The sound speed profile is the chosen as the well known Munk profile which is given as $c(z) = 1500[1+\epsilon(\bar{z}-1+e^{-\bar{z}})]$ where $\epsilon = 0.00737$ and the scaled depth $\bar{z} = \frac{2(z-1300)}{1300}$ [4].

For different SNR's the performances of incoherent broadband matched field processor and modified incoherent matched field processor are compared. The performance criteria considered is the probability of correct localization under the given scenario.

In order to compare performances of two broadband incoherent processors, the α values that maximizes probability of correct localization are searched for different

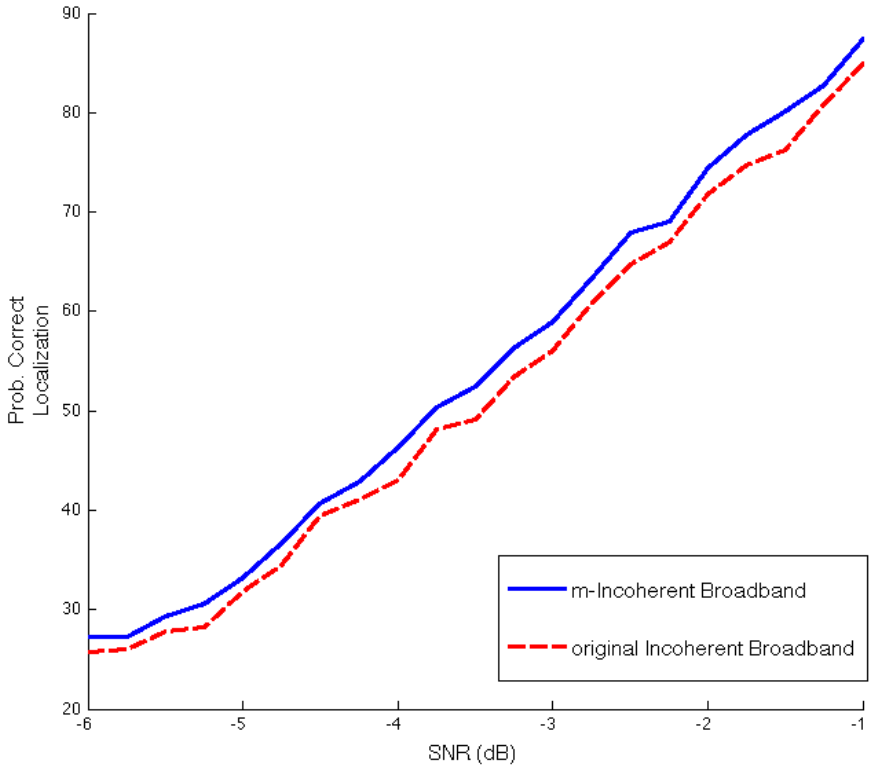

Figure 5.2: Comparison of Correct Localization Performances of the original Incoherent Broadband Processor and the modified Incoherent Broadband Processor

SNR scenarios. Note that for the modified incoherent case with 2 frequency component source it is sufficient to consider $\gamma = \frac{\alpha_2}{\alpha_1}$. For the example considered α_1 corresponds to the weighting for 10 Hz whereas α_2 corresponds to weighting for 20 Hz. As can be seen in the Table 5.1 and Figure 5.2, it is shown by simulation that the modified incoherent matched field processing improves the probability of correct localization in the SNR region considered.

The change of γ values with SNR is found to be non-uniform as can be seen in Table 5.2. For different SNR values, different γ values gives the maximum correct localization performance.

We also consider the change of correct localization performance with γ for a specific SNR (-3.5 dB). As can be seen in Figure 5.3, we notice that the correct localization performance is also not uniformly changing by γ.

Table 5.1: The probability of correct localizations for Modified Incoherent and Original Incoherent Broadband Processors

SNR	Modified Incoherent (%)	Original Incoherent (%)
-6	27.3	25.8
-5.5	29.4	27.8
-5	33.2	31.8
-4.5	40.7	39.4
-4	46.3	43.0
-3.75	50.3	48.1
-3.5	52.4	49.1
-3.25	56.3	53.4
-3	58.9	56.1
-2.75	63.3	60.8
-2.5	68.0	64.7
-2.25	69.0	67.0
-2	74.4	71.8
-1.75	77.7	74.7
-1.5	80.1	76.2
-1.25	82.7	80.8
-1	87.5	84.9

Table 5.2: The γ values maximizing the probability of correct localization for different SNRs (incoherent case)

SNR (dB)	$\gamma = \frac{\alpha_2}{\alpha_1}$
-6	1.27
-5.5	1.20
-5	1.48
-4.5	1.28
-4	1.40
-3.75	1.46
-3.5	1.47
-3.25	1.52
-3	1.33
-2.75	1.59
-2.5	1.48
-2.25	1.27
-2	1.34
-1.75	1.43
-1.5	1.45
-1.25	1.36
-1	1.3

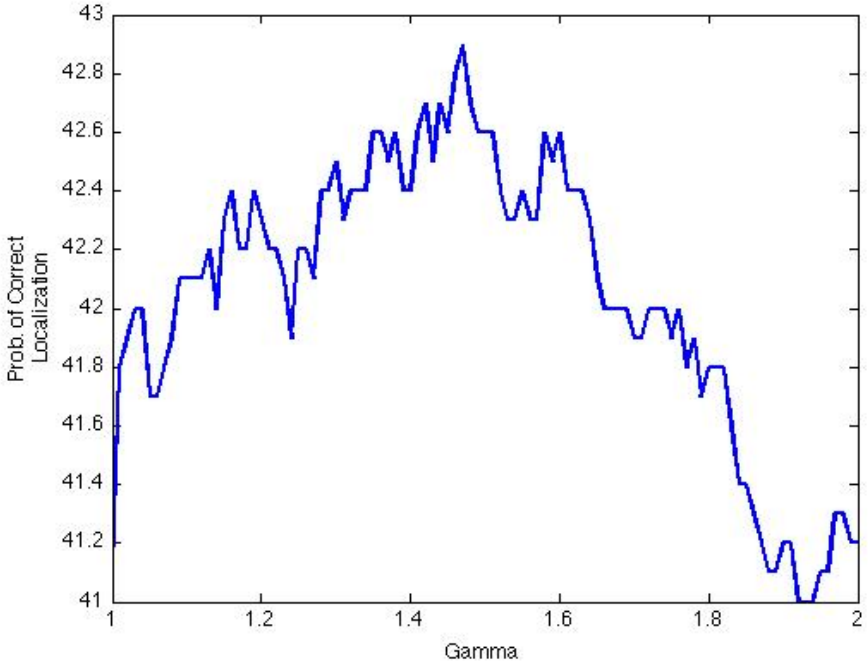

Figure 5.3: Change of Correct Localization Probability with Different γs (Incoherent Case)

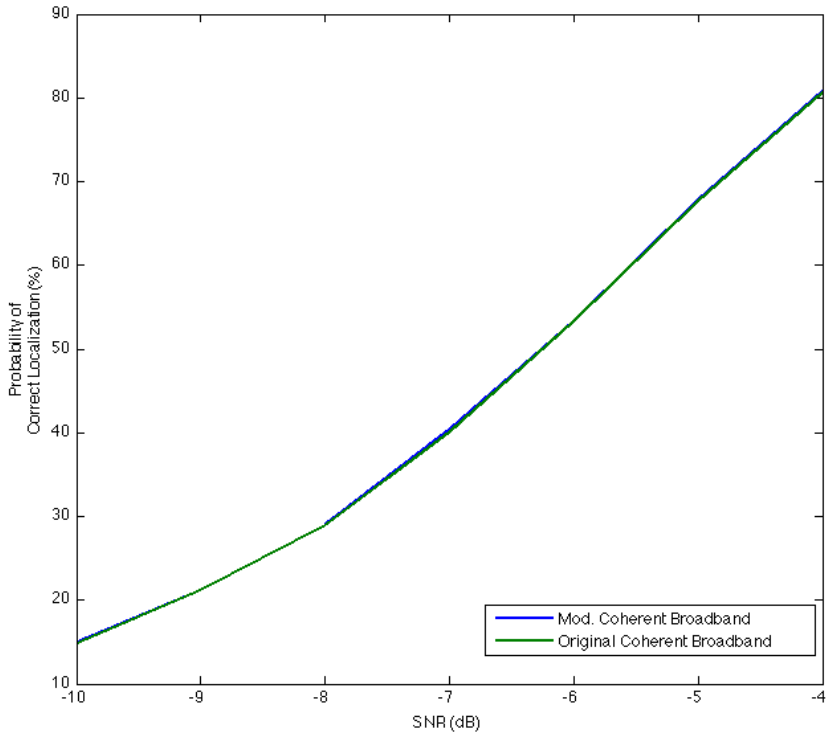

Figure 5.4: Comparison of the Correct Localization Performances of the original Coherent Broadband Processor and the modified Coherent Broadband Processor

Next we consider the coherent case. Similar to the incoherent case, we search for the optimal α values that makes probability of localization maximum. Note that this time α values are the weightings for the sensor inputs, contrary to the incoherent case where α values are weightings for the ambiguity surfaces. We compare coherent broadband matched field processing and modified coherent matched field processing outputs. Similar to the modified incoherent case with 2 frequency component source it is sufficient to consider the ratio $\gamma = \frac{\alpha_2}{\alpha_1}$.

As it was done in incoherent case, the γ values that maximizes the probability of correct localization are searched for different SNR scenarios. It can observed from Figure 5.4 and Table 5.3 that by using a weighted combination of cross-frequency data, only a slight performance gain can be achieved.

Similar to incoherent case, we give the γ values that makes the probability of correct localization maximum in Table 5.4. Also the change of correct localization perfor-

Table 5.3: The probability of correct localizations for Modified Coherent and Original Coherent Broadband Processors

SNR	Modified Coherent	Original Coherent
-10	15.0	14.8
-9	21.3	21.2
-8	29.1	28.9
-7	40.5	40.1
-6	53.3	53.3
-5	67.8	67.7
-4	80.9	80.7

Table 5.4: The γ values maximizing the probability of correct localization for different SNRs (coherent case)

SNR	γ
-10	1.07
-9	1.03
-8	1.04
-7	1.13
-6	1
-5	1.03
-4	1.14

mance with gamma values for a specific SNR (-7 dB) is given in Figure 5.5.

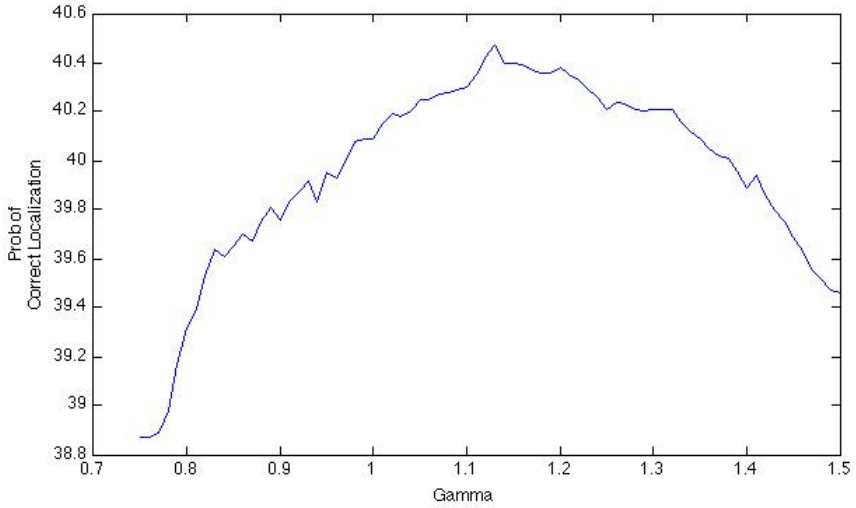

Figure 5.5: Change of Correct Localization Probability with Different γs (Coherent Case)

CHAPTER 6

CONCLUSION

In this thesis, we have dealt with the problem of localization of the underwater sound sources using matched field processing.

We have first given a comparative analysis of narrowband matched field processors. The four main processors: Bartlett processor, Minimum Variance Distortionless Response (MVDR) processor, MVDR with neighboring location constraints and MVDR with environmental perturbation constraints are compared in terms of their probability of correct localization under no mismatch and mismatch cases. We have given sample ambiguity surfaces and performance comparison tables for these processors. We have seen that under no mismatch MVDR has the best localization performance, whereas under mismatch MVDR with environmental perturbation constraints has the best performance.

A performance assesment for the most common broadband matched field processors is also made. The correct localization performances for incoherent broadband matched field processor, Tolstoy/Michalopoulo's coherent matched field processor and broadband matched field processor with environmental perturbation constraints is given for no mismatch and under mismatch cases. We have seen that coherent MVDR has the best localization performance for no mismatch case whereas broadband MVDR with environmental perturbation constraints has the best performance for mismatch case.

In last part, we have introduced a new weighting approach to combine data for broadband matched field processing. We have considered the fact that information from different frequencies may have different reliability depending on the environmental

conditions to develop a weighting scheme. We have shown that a performance gain compared to existing processors can be achieved by using the weighting scheme.

As future work, we would like to develop a method to search for optimal weights instead of the direct search method used in this thesis. For this purpose, we plan to elaborate more in underlying physical phenomena that causes sidelobes.

In the examples in this thesis, we have used synthetic data to generate the measured signals for the simulations. In future, we would like to work with real measured data that will be gathered in sea experiments. We believe that gathering real data via sea experiments in Turkish coastal areas would be very useful for researchers working in underwater acoustics area and infrastructure and resources should be created for this purpose.

REFERENCES

[1] P. Stoica and R. Moses, *Introduction to Spectral Analysis*, Prentice Hall, 1997

[2] A. Tolstoy, *Matched Field Processing for Underwater Acoustics*, World Scientific, 1993.

[3] M. Porter, *The KRAKEN normal-mode program*, SACLANT, 1991.

[4] F. Jensen, W. Kuperman, M. Porter, and H. Schmidt, *Computational Ocean Acoustics*, Springer, New York, NY, 2000.

[5] I. Stakgold, *Green's Functions and Boundary Value Problems*, Wiley, New York, 1979.

[6] M. J. Hinich, "Maximum likelihood signal processing for a vertical array", J. Acoust. Soc. Am. 54, 499-503 (1973).

[7] H. P. Bucker, "Use of calculated sound fields and matched field detection to locate sound sources in shallow water", J. Acoust. Soc. Am. 59, 368-373 (1976).

[8] A. B. Baggeroer, W. A. Kuperman, and H. Schmidt,"Matched field processing: Source localization in correlated noise as an optimum parameter estimation problem", J. Acoust. Soc. Am. 83, 571-587 (1988).

[9] H.Schmidt, A. B. Baggeroer, W. A. Kuperman and E.K. Sheer, "Environmentally tolerant beamforming for high-resolution matched field processing: Deterministic mismatch", J. Acoust.Soc.Am. 88, 1802-1810 (1990).

[10] L. R. LeBlanc and F. H. Middleton, "An underwater acoustic sound velocity data model", J. Acoust.Soc.Am. 67, 2055-2062 (1980).

[11] B.M. Howe, P.F. Worcester and R.C. Spindel, "Ocean acoustic tomography. mesoscale velocity", J . Geophys Res. 92, 3785-3805 (1987).

[12] L. Brekhovskikh and Y. Lysanov, *Fundamentals of Ocean Acoustics*, Springer-Verlag, Berlin, 1982.

[13] A. Tolstoy, *Computational aspects of matched field processing in underwater acoustics*, Computational Acoustics,Amsterdam, 1990.

[14] Z.-H. Michalopoulou, "Robust multi-tonal matched-field inversion: a coherent approach", J. Acoust. Soc. America, 104, pp. 163-170, (1998).

[15] M. B. Porter and Z. H. Michalopoulou, "A coherent approach to broadband matched-field processing: Application in the Hudson Canyon", Proc. of the IEEE ICASSP-96, (1996).

[16] J. L. Krolik, “Matched-field minimum variance beamforming in a random ocean channel”, J. Acoust. Soc. Am. 92, 1408-1419 (1992).

[17] S.P. Czenszak and J.L. Krolik, “Robust wideband matched-field processing with a short vertical array”, J. Acoust. Soc. Am., vol. 101(2), pp.749-759, (1997).

[18] A. B. Baggeroer, W. A. Kuperman, and P. N. Mikhalevsky, “An overview of matched field methods in ocean acoustics”, IEEE J. Ocean. Eng. 18, 401-424 (1993).

[19] T. Sarıkaya, T. Çiloğlu, “An optimal weighting approach to combine data for broadband matched field processing”, *Proceedings of the 10th European Conference on Underwater Acoustics, Volume 1*, pp. 583-589, (2010).

APPENDIX A

ADIABATIC NORMAL MODE MODELING FOR RANGE DEPENDENT SOUND SPEED PROFILES

Here we review the adiabatic approach as explained in [12]. Recall that for a deterministic underwater acoustic medium, if the sound velocity $c(z)$ is range independent, the pressure can be expressed as

$$p(z, z_s, r_s) = a\sqrt{(2\pi)} \sum_{n=1}^{N} \frac{\psi_n(z)\psi_n(z_s)}{\sqrt{k_n r_s}} e^{jk_n r_s} \tag{A.1}$$

where $\varphi_n(z)$, $i = 1..N$ are modal eigenfunctions and k_n , $i = 1..N$ are horizontal wave numbers, for the depth of receiver z, and source locations specified by depth z_s, and range r_s. The modal eigenfunctions and horizontal wavenumbers can be found from the equation:

$$\frac{d^2\psi}{dz^2} + \{k(z)^2 - k_n^2\}\psi_{=}0 \tag{A.2}$$

where $k(z) = \frac{\omega}{c(z)}$.

Next we consider the case where sound speed depends on range as well as depth. So the sound speed, $c(z, r)$ is a function of range and depth. Then the Helmholtz equation takes the form:

$$\Delta p + k^2(z, r)p = 0 \tag{A.3}$$

where

$$k(z, r) = \frac{\omega}{c(z, r)} \tag{A.4}$$

Therefore the pressure now can be expressed as a sum of r dependent term and a depth dependent term for a fixed r:

$$p(z, r) = \sum_{l} \phi_l(r)\psi_l(z, r) \tag{A.5}$$

From the adiabatic approximation as explained in [12], we get:

$$\frac{1}{r}\frac{\delta}{\delta r}(r\frac{\delta\phi_m}{\delta r}) + \xi_m^2(r)\phi_m = 0 \tag{A.6}$$

If a new function $F_m(r) = r^{1/2}\phi_m(r)$ is introduced which satisfies $F_m^{''} = -(\xi_m^2 + \frac{1}{4r^2})F_m$, and if the assumption is made that $\xi_m r >> 1$ then we get

$$F_m^{''} = -\xi_m^2 F_m \tag{A.7}$$

The solution to this equation can be given as in [12]:

$$F_m(r) = A_m\psi_m(z,r)(\xi(r)^{\frac{-1}{2}}exp(i\int_0^r \xi_l dr) \tag{A.8}$$

This yields:

$$p(z,r) = \sum_l A_l\psi_l(z,r)(\xi r)^{\frac{-1}{2}}exp(i\int_0^r \xi_l dr) \tag{A.9}$$

A_l can be obtained as [12]:

$$\sqrt{\frac{2}{\pi}}exp(\frac{-i\pi}{4})\psi_l(z,0) \tag{A.10}$$

where $\psi_l(z,0)$ is the depth dependent eigenfunction at source range. This results the signal wavefront for the random channel as:

$$p(z;r_s,z_s) = a\sqrt{(2\pi)}\sum_{n=1}^{N}\frac{\psi_n(z;0)\psi_n(z_s;r_s)}{\sqrt{k_n(r_s)r_s}}exp(j\int_0^{r_s} k_n(r)dr) \tag{A.11}$$